Downscaled climate change data from the HADCM3 and ECHAM5 models on precipitation and temperature for Ethiopia and Kenya

Philip Ward

Ralph Lasage

Report W-09/05

June 16, 2009

This report was commissioned by: Cordaid (Gijs Aarts)

IVM

Institute for Environmental Studies
Vrije Universiteit
De Boelelaan 1087
1081 HV Amsterdam
The Netherlands

Tel. ++31-20-5989 555
Fax. ++31-20-5989 553
E-mail: info@ivm.vu.nl

Contents

Summary

The main aim of this study is to provide a large dataset showing the possible changes in climate that can be expected in Ethiopia and Kenya during the 21st Century. This dataset can be used with and by regional and local stakeholders in the assessment of adaptation requirements and possible adaptation strategies. The research goals are: (a) to provide maps and graphs showing the possible short and medium-term changes in annual and monthly precipitation and temperature in the study region; (b) to assess the possible impacts of climate change on the occurrence of drought events, and the incidence of high temperatures; and (c) to assess the effects of these climate changes on the discharge of the Omo River.

The results of two General Circulation Models (GCMs) (HADCM3 and ECHAM5) are downscaled to a resolution suitable for regional climate impact assessment (10' x 10'). Downscaled climate data are provided for a number of future greenhouse gas emission scenarios (B1, A2, A1B), and for two time horizons, namely 2006-2035 (short-term) and 2036-2065 (medium-term). A hydrological model (STREAM) is used to simulate the monthly discharge of the Omo River; the model is driven by the downscaled climate data from both the HADCM3 and ECHAM5 models.

In the appendices, large datasets are provided showing the downscaled results of these models for the study region. Maps are provided showing the change in mean annual precipitation and temperature over the entire study region (Ethiopia and Kenya), and graphs are shown giving more detailed assessments of the change in mean monthly and annual precipitation and temperature for 10 case study locations, namely Moyale, Mandera, Marsabit, Maralal, Isiolo, Nairobi, Awasa, Kelem, Asayita, and Addis Ababa.

There are a number of similarities and differences in the climate results of the two GCMs. Firstly, the expected changes in the temperature regimes across the region are very similar according to both HADCM3 and ECHAM5. Both models show very clear trends at all locations towards warmer conditions in the future, with greater increases in mean temperature by 2050 compared to 2020, and greater increases for the 'A' scenarios compared to the B1 scenario.

In terms of the variability of annual rainfall totals, the results of the two GCMs are also in good agreement. Both show that in general there will be no significant increase in the variability of annual rainfall, between the baseline period and the future scenarios. Exceptions are noted in the northern half of the study area for both GCMs. A large increase in the variability of annual rainfall is simulated for the most northerly location of Asayita by both models. Increases in variability are also noted in both models for the northern locations of Addis Ababa and Awasa under some combinations of scenario and/or time period, though the trend is less clear than for Asayita.

However, in terms of mean annual precipitation, the results of the two GCMs show numerous differences. In general, the ECHAM5 model shows a trend towards wetter annual conditions over most parts of Ethiopia and Kenya. Though this is also the case for large parts of northern Ethiopia according to HADCM3, the latter model simulates generally drier conditions over large parts of southern Kenya, especially in the south-western section. Furthermore, changes in the monthly rainfall regime were not consistent between the two models. The results of HADCM3 suggest that those areas af-

fected by a main rainy season from March to May will experience an increase in precipitation in March and April, but a decrease in May. Furthermore, these locations will experience a decrease in precipitation during their secondary precipitation peak in October-November. This pattern is not reproduced by ECHAM5, which shows overall a more general tendency towards wetter conditions throughout the year, with relatively large positive anomalies in the second half of the year (especially during the rainy season of October-November).

Datasets and assessment are also given of changes in the frequency of dry months, and for changes in the frequency of months with high temperatures. For the future scenarios, both models simulate large increases in mean annual temperature and the frequency of very warm months (indicative of increased heat stress) for the entire region, including those areas already affected by adverse heat waves in the current period. Even in the short-term, and under the most optimistic of the emission scenarios used (B1), the increase is very large, and suggests that increased heat wave frequency and heat stress will become a much more severe problem than at present in the near future. The clear signal presented by both models, for all scenarios and locations, suggests that urgent measures may be needed to ensure that various activities and sectors (e.g. crop growth, livestock rearing, health care, irrigation, energy supply) can adapt to these changes. Changes in the number of dry months can be indicative of changes in the occurrence of dry (or drought) periods. However, the signals of change associated with the two GCMs are not in agreement.

The river discharge results for the Omo River show little coherency between the two GCMs in terms of changes in the annual hydrograph. The HADCM3-driven model shows very little change in discharge during the long dry season (December-June), followed by a decrease in discharge during the main discharge period between July and November. In contrast, the ECHAM5-driven model shows a large increase in discharge during the first months of the year (especially January to March), and a further large increase during the peak of the high discharge season (August-September).

This study provides a large dataset of downscaled climate data for temperature and precipitation in the region, in both the short and medium-term. Thus, the data presented in this report can assist local stakeholders and decision-makers in assessing the expected physical effects of climate change, and therefore the need (or otherwise) for adaptive measures. Whilst this study does not provide an assessment of the impacts of these changes in various sectors (e.g. agriculture, health, energy), it does provide a wealth of climate data tailored to the regional situation which can subsequently be used as input into specific impact models for those sectors, or to develop short and medium-term plans via expert judgement and stakeholder dialogue.

There are large discrepancies between the results of the two models for the future scenarios in terms of changes in mean precipitation and the frequency of droughts and intense wet months. Clearly, the signal of change in future precipitation is very uncertain. This has a number of implications. The first implications are with regards to the methods used to predict future changes in precipitation. It is well known that precipitation is much more difficult to simulate than temperature. At present, GCMs cannot accurately represent all of the physical atmospheric processes involved in the generation of precipitation. A larger number of GCMs could be used in order to compare their results for the future. However, there is no way to assess in advance which of the models will perform most accurately for the future period. Using a larger number of GCMs would also mean using models which have been proven to perform less well for the study region during the baseline period. A second implication

related to the use of climate models is the need for more regional climate model (RCM) simulation results for the study region. Such models are capable of resolving regional climatology more accurately than GCMs, but are computationally very demanding. Nevertheless, the development of RCMs, or making public the results of existing RCMs, could lead to a decrease in the uncertainty in predictions of future precipitation, and could therefore assist greatly in climate impact assessment.

A further implication of the high uncertainty of the precipitation data, is with regards to the response of stakeholders and decision-makers to that uncertainty. A possible reaction to the existing uncertainty is the tendency to 'wait and see', in which stakeholders and decision-makers delay developing plans until more clear information is available. However, the possible impacts associated with the potential changes in climate (e.g. increased droughts, flash floods, etc.) are so detrimental that early planning is still preferable under the precautionary principle. Furthermore, adaptation measures can be sought which provide benefits under a wide range of future scenarios. For example, more efficient irrigation techniques to reduce evaporative water losses may be essential if the frequency of droughts increases in areas such as the southern Ethiopian lowlands. However, such schemes can be designed in ways that they also provide benefits even if such an increase in drought frequency should not materialise (e.g. more availability of water for drinking, increased yields, reduced water costs, etc.). Therefore, the results of this study show that stakeholders and decision-makers need to consider robust management options to tackle both increasing drought frequency, and an increasing frequency of high rainfall events.

Given the uncertainties surrounding the changes in precipitation, a useful recommendation for regional adaptation is to provide long-range seasonal weather forecasts, and to promote the dissemination of such information. A long-range seasonal weather forecast allows farmers to make informed decisions on which crops and/or species to plant in the forthcoming growing season, and can allow health sector workers to anticipate climate-related health problems (and therefore the treatments required) prior to onset of problems. Furthermore, medium-term river discharge projections could then be made which would allow for early warning systems in the event of flooding, and better forward planning of reservoir levels for electricity generation.

1. Introduction

1.1 Background

Climate change is expected to have major impacts on semi-arid areas around the world and on the people living in these areas. Their livelihoods are strongly connected to the climatic conditions, and especially to the amount of precipitation received during the rainy seasons. In East Africa, Cordaid is active in trying to improve people's livelihoods and make them less vulnerable to variations in precipitation, through drought management projects. Currently, Cordaid is evaluating its activities and projects in preparation for drafting a strategy for the region for the period 2010-2015. Part of this evaluation is to assess the potential impacts of climate change on their projects and to develop, if necessary, adaptive measures. At the same time, IVM is involved in a case study on climate change impacts in Ethiopia, and on which adaptation measures are possible in water management, as part of the ADAPTS project.

Together, Cordaid and IVM decided to start a project on assessing the impacts of climate change on Ethiopia and Kenya. The major activity is to downscale information from global climate models to regional information and to assess the changes in temperature and precipitation for some areas. It is necessary to first have insights in the predicted changes in the area, before adaptive measures can be developed. The information becoming available through this project will be used by Cordaid for the development of their strategy and by IVM for the ADAPTS project. The information will also be shared with several partners from the region.

It is a first activity for both institutes to assess climate change on development projects, and one of the goals is to see whether the information from climate models is relevant for development NGOs like Cordaid.

1.2 Regional setting

The project covers Kenya and Ethiopia, with special focus on southern Ethiopia and northern Kenya (see Figure 1.1). This area was chosen because Cordaid is working with local NGOs (AfD, PISP, CISP, etc) in these areas. The areas are fairly similar; they are semi-arid lowlands with two rainy periods, from March to May and from September to November. The region is hit by droughts once every 5 years on average. The region has a semi-arid savannah landscape. The landscape exists of gently sloping lowlands and floodplains vegetated predominantly with grass and bush land. The geology is composed of a crystalline basement with overlying sedimentary and volcanic deposits. There are no perennial rivers and rainfall varies highly, both spatially and temporally. People are predominantly involved in small-scale subsistence agriculture production and livestock husbandry (Lasage and de Vries, 2008). To assess the impacts on river discharge and water availability, we chose the Omo River as a case study. This is the nearest perennial river in a comparable climatic region.

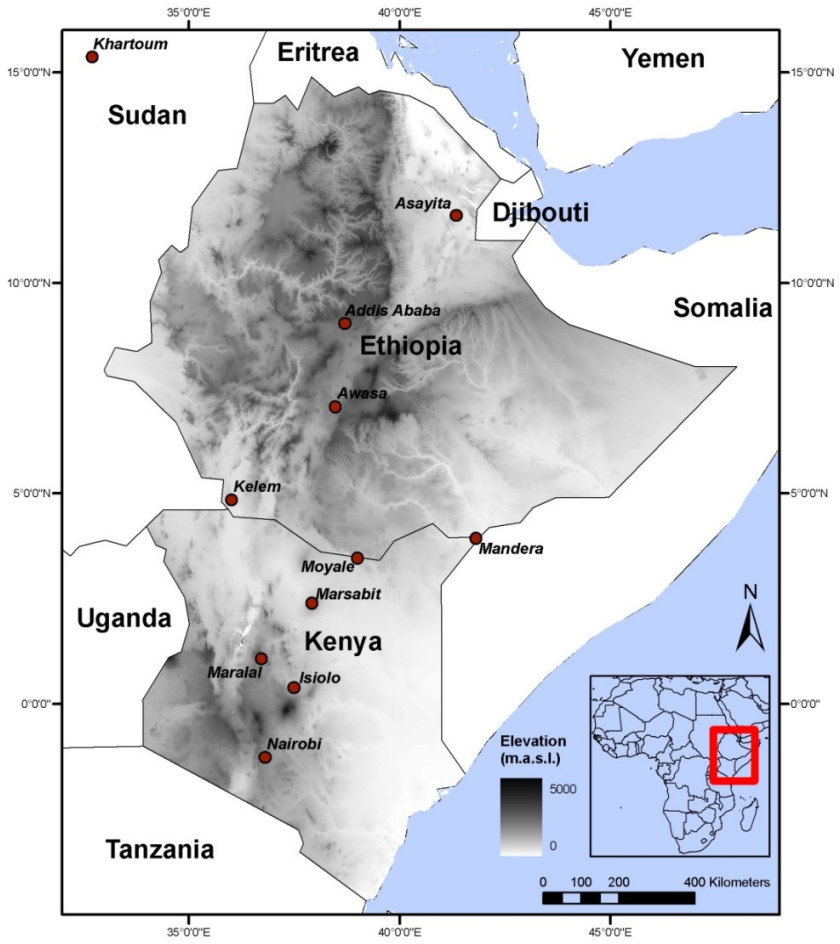

Figure 1.1 Map of Kenya and Ethiopia, showing the elevation (m.a.s.l.), the locations used in this study, and the discharge measuring station of the Blue Nile at Khartoum (Sudan).

1.3 Aims and objectives

The main aim of this study is to provide a large dataset showing the possible changes in climate that can be expected in Ethiopia and Kenya during the 21st Century. This dataset can be used with and by regional and local stakeholders in the assessment of adaptation requirements and possible adaptation strategies. This main aim is subdivided into the following objectives:

- To provide maps and graphs showing the possible short and medium-term changes in annual and monthly precipitation and temperature in the study region;
- To assess the possible impacts of climate change on the occurrence of drought events, and the incidence of high temperatures;
- To assess the effects of these climate changes on the discharge of the Omo River.

1.4 Structure of this report

The remainder of this report is set up as follows. In Section 2, the methods and models used to assess the changes in climate and discharge are thoroughly described and discussed. In Section 3, the main results are described. The results are firstly described for the region as a whole, with reference to the large datasets (maps, graphs, tables) on regional and local climate change which can be found in the appendices. Then, the results are described in more detail for the case study location of Moyale, and for the Omo River. The results are summarised, together with a concise outline of implications, in Section 4. The main corpus of data can be found in the appendices.

2. Methods

In order to assess the possible changes in regional climate in the 21st Century we used the results of two GCMs (HADCM3 and ECHAM5). The GCM results were first statistically downscaled so as to increase the spatial resolution, thus making the data more appropriate for a regional assessment. The downscaled data were then analysed to assess how precipitation and temperature are projected to change under a number of future scenarios, compared to the baseline period 1961-1990. These downscaled climate data were then used as input in a hydrological model, in order to simulate changes in the discharge of the Omo River in the 21st Century in response to the modelled changes in climate. In this section we describe the climate data and scenarios used, the methods used to downscale the data to the regional level, and the methods and data used to simulate changes in the discharge of the Omo River.

2.1 Climate change scenarios

The climate change scenario data used in this study are based on simulations carried out using General Circulation Models (GCMs) for the Fourth Assessment Report (AR4) of the Intergovernmental Panel on Climate Change (IPCC, 2007). For our assessment we used simulations of monthly temperature and precipitation over the period 1901-2100 carried using the climate models ECHAM5[1] and HADCM3[1,2]. These models were selected since they have the highest 'skill scores' for both precipitation and temperature of all the models used for the AR4 in the region of study (Cai et al, 2009). The raw data were downloaded from the website of IPCC Data Distribution Centre (http://www.mad.zmaw.de/IPCC_DDC/html/SRES_AR4/index.html).

In order to analyse the changes in climate simulated by these models, we compared the simulated values for the baseline period 1961-1990 with the values for two dates in the future: 2020 and 2050 AD. We used these to correspond to short-term and medium-term climate change respectively. Note that in keeping with standard methods in climatological studies, these two dates are defined as the means of 30-yr periods, so that 2020 refers to the period 2006-2035, and 2050 refers to the period 2036-2065. Also note that since the modelled baseline data for the period 1961-1990 are derived from two different climate models, the baselines differ between the HADCM3 and ECHAM5 results. For the 20th Century we used simulations forced using the scenario 20C3M, which prescribes greenhouse gases and aerosols on an annual basis according to observed values throughout the 20th Century. For the 21st Century we used simulation results forced using SRES scenarios B1, A1B, and A2

---

[1] We acknowledge the international modelling groups for providing their data for analysis, the Program for Climate Model Diagnosis and Intercomparison (PCMDI) for collecting and archiving the model data, the JSC/CLIVAR Working Group on Coupled Modelling (WGCM) and their Coupled Model Intercomparison Project (CMIP) and Climate Simulation Panel for organising the model data analysis activity, and the IPCC WG1 TSU for technical support. This work, including access to the data and technical assistance, is provided by the Model and Data Group (M&D) at the Max-Planck-Institute for Meteorology, with funding from the Federal Ministry for Education and Research and by the German Climate Computing Centre (DKRZ).

[2] © Crown copyright 2005, Data provided by the Met Office Hadley Centre.

(IPCC, 2000), and non-SRES scenario COMMIT. These scenarios are described in the following paragraphs.

SRES Scenarios B1, A1B, and A2

These scenarios were developed for and described in the IPCC Special Report on Emission Scenarios (SRES) (IPCC, 2000). The SRES describes 40 different emission scenarios, each making different assumptions about future emissions of greenhouse gases, land use, and other driving forces. The B1, A1B, and A2 scenarios lie towards the lower, middle, and upper section of the full spectrum of IPCC scenarios respectively (in terms of projected temperature change by the end of the 21st Century), and can therefore be used to assess climate change under a broad range of possible futures.

The B1 scenario describes a convergent world with the same global population by 2100 AD (compared to 1990 AD), peaking in the mid 21st Century and declining thereafter. The scenario assumes rapid change in economic structures towards a service and information economy, with reductions in material intensity and the introduction of clean and resource-efficient technologies. The emphasis is on global solutions to economic, social, and environmental sustainability, but without additional climate incentives. Compared to the baseline concentration of atmospheric CO_2 in 1990 AD (ca. 367 ppm), the B1 scenario prescribes an increase to ca. 540 ppm by 2100 AD (according to the Bern model).

The A1B scenario describes a world of very rapid economic growth, global population that peaks in the mid 21st Century and declines thereafter, and the rapid introduction of new and more efficient technologies. The major underlying themes are convergence among regions, capacity building, and increased cultural and social interactions, with a substantial reduction in regional differences in per capita income. This scenario assumes a balance across fossil intensive and non-fossil energy sources. Compared to the baseline concentration of atmospheric CO_2 in 1990 AD (ca. 367 ppm), the A1B scenario prescribes an increase to ca. 703 ppm in 2100 AD (according to the Bern model).

The A2 scenario describes a very heterogeneous world. The underlying theme is one of self-reliance and the preservation of local identities. Fertility patterns across regions converge very slowly, resulting in continuously increasing population. Economic development is mainly regionally oriented, and per capita economic growth and technological change are more fragmented and slower than in other storylines and scenarios. Compared to the baseline concentration of atmospheric CO_2 in 1990 AD (ca. 367 ppm), the A2 scenario prescribes an increase to ca. 836 ppm by 2100 AD (according to the Bern model).

COMMIT scenario

This scenario is not included in the SRES (IPCC, 2000), but was used in the AR4 (IPCC, 2007). It is an idealised scenario in which the atmospheric burdens of long-lived greenhouse gasses in the 20th Century are held fixed at the same levels as in 2000 AD. Hence, it can be used as a reference against which the effects of the SRES scenarios can be assessed.

2.2 Climate change scenarios

The raw data from the HADCM3 and ECHAM5 models were imported for the scenarios described above. HADCM3 has an equidistant grid with a spatial resolution of 3.75° in longitude and 2.5° in

latitude. ECHAM5 has a spatial resolution of 1.875° in longitude and ca. 1.875° in latitude. These resolutions are rather coarse for use in regional impact assessment studies (Arnell et al., 1996; Bouwer et al., 2004; Kleinn et al., 2005; Wood et al., 2002, 2004). Hence, the data were downscaled to a higher spatial resolution. Bouwer et al. (2004) identify two main approaches to downscale climate data for use in regional impact assessments: statistical methods which transform the data in such a way as to match the main statistical properties of modelled and observed climate data sets (e.g. Bouwer et al., 2004; Wilby and Wigley, 1997; Wilby et al., 1998; Wood et al., 2002); and dynamical approaches which use finer resolution regional circulation models (RCMs) nested within coarser GCMs (e.g. Cocke and LaRow, 2000; Kim et al., 2000; Murphy, 2000; Wood et al., 2002; Yarnal et al., 2000). The results of these two approaches have been found to have similar levels of skill, with different methods performing better or worse dependent on the region of study (Wilby et al., 2000; Wood et al., 2004), but dynamical methods are computationally far more demanding (Bouwer et al., 2004). Hence, in this study we chose to use a statistical downscaling technique.

Statistical downscaling involves the use of correction factors (for temperature additive and for precipitation multiplicative) which are applied to the low resolution model data so as to preserve the statistical properties of a higher resolution observed (baseline) dataset. In this study the spatially explicit correction method based on monthly averages as described by Bouwer et al. (2004) was used. For the observed baseline datasets of precipitation and temperature, the Climate Research Unit (CRU) CL 2.0 dataset (New et al., 2002) was used. This dataset shows climatology for the period 1961-1990 for the whole world with a spatial resolution of 10' x 10', and is available at http://www.cru.uea.ac.uk/cru/data/hrg.htm. No correction was made to preserve the variance of the downscaled data, since observed temperature and precipitation time-series data were not available at the 10' x 10' resolution.

The downscaling involves two steps. The first step is a spatial downscaling procedure (Bouwer et al., 2004), whereby the values from the low resolution GCM are simply resampled onto a grid of 10' x 10'; this resolution was selected as it is the same resolution as the CRU climate data. In the study region of this project, a resolution of 10' x 10' corresponds to ca. 18.4 km x 18.4 km. The spatially downscaled GCM data are then statistically downscaled using the following formulae:

$$p'_{GCM(m,i)} = p_{GCM(m,i)} \times \left(\frac{\overline{p}_{CRU(m,i)}}{\overline{p}_{GCM(m,i)}} \right) \tag{2.1}$$

where $p'_{GCM(m,i)}$ is the statistically downscaled GCM precipitation for a particular month, m, and cell, i, $p_{GCM(m,i)}$ is the spatially downscaled raw GCM precipitation data for a particular month, m, and cell, i, $\overline{p}_{CRU(m,i)}$ is the observed (CRU) average monthly precipitation for a particular month, m, and cell, i, and $\overline{p}_{GCM(m,i)}$ is the spatially downscaled raw GCM mean monthly precipitation for a particular month, m, and cell, i.

$$t'_{GCM(m,i)} = t_{GCM(m,i)} + (\overline{t}_{CRU(m,ii)} - \overline{t}_{GCM(m,i)}) \tag{2.2}$$

where $t'_{GCM(m,i)}$ is the statistically downscaled GCM temperature for a particular month, m, and cell, i, $t_{GCM(m,i)}$ is the spatially downscaled raw GCM temperature for a particular month, m, and cell, i, $\overline{t}_{CRU(m,i)}$ is the observed (CRU) average monthly temperature for a particular month, m, and cell, i,

and $\bar{t}_{GCM(m,i)}$ is the spatially downscaled raw GCM mean monthly temperature for a particular month, *m*, and cell, *i*.

2.3 Validation of downscaled climate data

In order to validate the downscaled climate data, they were compared with observed climate data from weather stations. Comparisons were made for weather stations located in regions of Ethiopia and Kenya that were indicated as regions of interest by Cordaid. The weather station data were taken from the KNMI climate explorer (www.climexp.knmi.nl), which provides a repository of global climate data.

Observed data were taken for the baseline period 1961-1990, and compared to the downscaled climate data for the same period. For precipitation, observed climate data were available for: Moyale (Kenya), Mandera (Kenya), and Addis Ababa (Ethiopia).

In Figures 2.1a – 2.1f, the monthly observed precipitation values are compared to the downscaled GCM data. Also shown is the correlation of the monthly means between the two datasets; in all cases r^2 is at least 0.98. In Table 2.1, mean annual observed and simulated precipitation are shown. Also shown are the results of the t-test to establish whether there is a statistical difference between the annual means of the two datasets, and the F-test to establish whether there is a statistical difference between the variability of annual observed and modelled precipitation. For these locations there was no statistical difference between the mean or variability of the observed and simulated annual precipitation datasets.

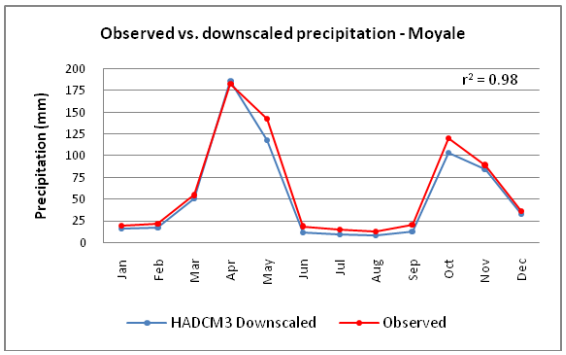

2.1a

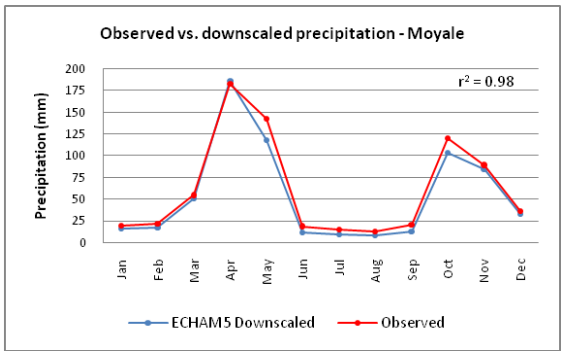

2.1b

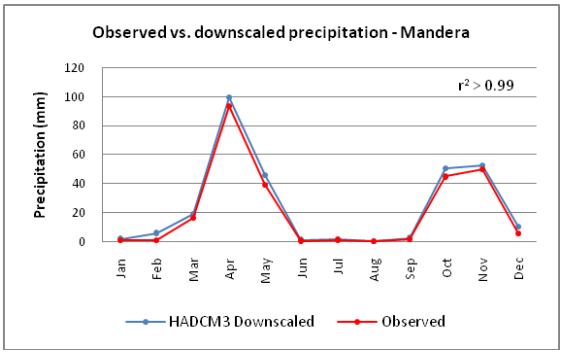

2.1c

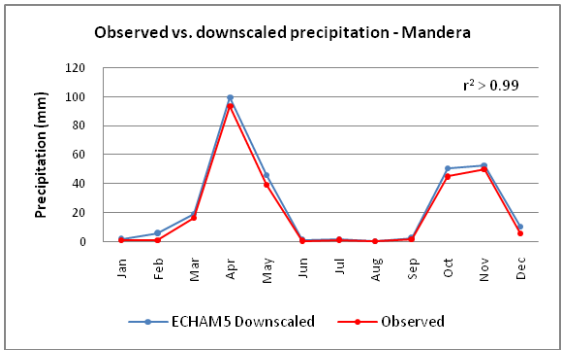

2.1d

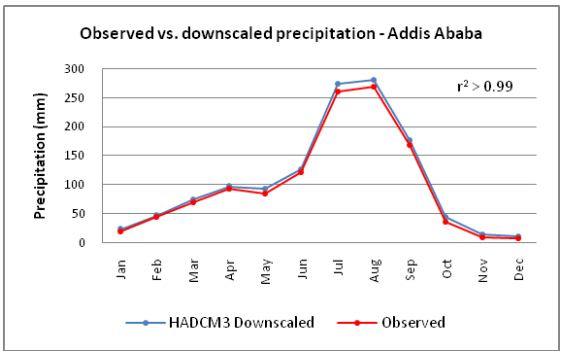

2.1e

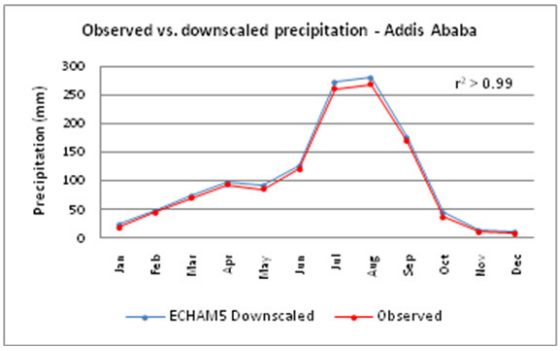

2.1f

Figure 2.1 Correlation between mean monthly observed and downscaled GCM data for precipitation in the baseline period 1961-1990 at: (a) Moyale (HADCM3); (b) Moyale (ECHAM5); (c) Mandera (HADCM3); (d) Mandera (ECHAM5); (e) Addis Ababa (HADCM3); and (f) Addis Ababa (ECHAM5).

Table 2.1 Comparison of observed and downscaled-GCM precipitation data for the periods 1961-1990. Also shown are the probabilities (p) associated with the t-test and F-test. In this case these tests show no statistically significant difference in mean or variance between the observed and modelled annual precipitation datasets (2-tailed test, $\alpha = 0.05$).

Station	Mean annual observed precipitation (mm)	Mean annual modelled precipitation (mm)	t-test (p)	F-test (p)
HADCM3				
Moyale	735.0	650.6	0.234	0.249
Mandera	257.5	290.4	0.163	0.351
Addis Ababa	1185.7	1258.8	0.056	0.108
ECHAM5				
Moyale	735.0	650.6	0.279	0.987
Mandera	257.5	290.4	0.190	0.891
Addis Ababa	1185.7	1258.8	0.063	0.581

For temperature, the only station in the data repository is Nairobi, and hence this was used for validation. Reference to Figures 2.2a and 2.2b shows that the downscaled model data slightly overestimate the temperature in Nairobi. The observed temperature for the baseline period 1961-1990 is 18.97°C, compared to 17.82°C for the downscaled GCM data for both HADCM3 and ECHAM5. In both cases the difference is statistically significant (t-test, $p < 0.001$). However, this can be related to the size of the grid cells to which the downscaling takes place. The grid cells of the CRU data have a resolution of 10' x 10' (ca. 18.4 km x 18.4 km), whilst the observed temperature data refer to a specific point. This leads to an underestimation of temperature in Nairobi for two reasons. Firstly, the CRU grid cell which contains Nairobi city also includes the higher area to the west of the city (parts of the Ngong Hills), where temperature is lower due to altitudinal effects. Secondly, observed point temperature measurements in cities tend to be higher than surrounding areas, due to the so-called urban heat island effect, whereby cities are generally warmer than the surrounding area. Reference to Figures 2.2a and 2.2b shows that the monthly pattern of temperature is very well represented between the observed and model data ($r^2 > 0.99$ in both cases).

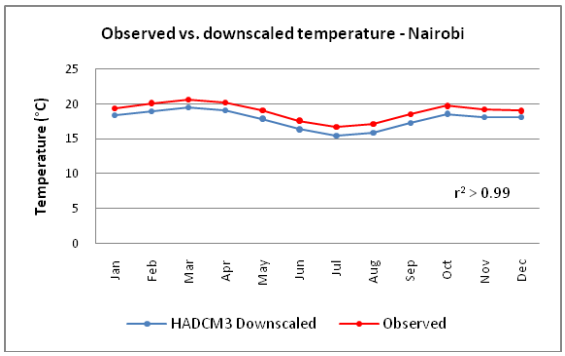

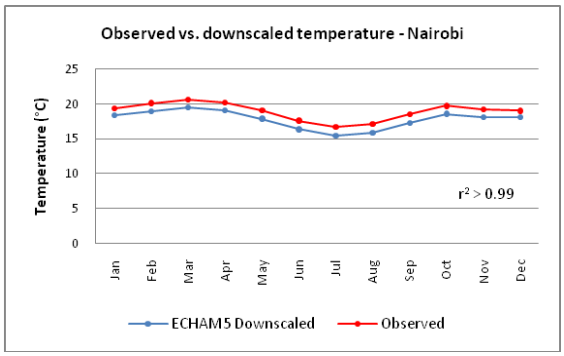

2.2a *2.2b*

Figure 2.2 *Correlation between mean monthly observed and downscaled GCM data for temperature in the baseline period 1961-1990 at Nairobi for: (a) HADCM3; and (b) ECHAM5.*

2.4 Hydrological modelling

Following consultations with Cordaid, it was decided to simulate the effects of future climate change on the discharge regime of the Omo River, which has its source in the southern Ethiopian Highlands, and empties into Lake Turkana at the border between Ethiopia and Kenya. For this purpose we used the STREAM hydrological model to simulate changes in monthly discharge under the climate scenarios described above.

STREAM is a grid-based spatially distributed water balance model that describes the hydrological cycle of a drainage basin as a series of storage compartments and flows (Aerts et al., 1999). It is based on the RHINEFLOW model of Kwadijk (1993), and uses a raster GIS database to calculate the water balance of each grid cell per month. The water balance is calculated using the Thornthwaite (1948) equations for potential evapotranspiration and the Thornthwaite and Mather (1957) equations for actual evapotranspiration; these equations use temperature and precipitation as the major input parameters. For each month, the model generates runoff, groundwater storage (shallow and deep), snow cover, and snow melt. The direction of water flow between cells is based on the steepest descent for the eight surrounding grid cells on a digital elevation model (DEM). The main flows and storage compartments used to calculate water availability per cell are shown in Figure 2.3. In this study the model was set up at a resolution of 10' x 10', since this is the resolution of the climate input data.

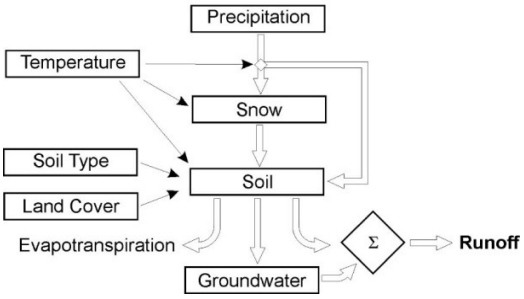

Figure 2.3 Flowchart showing the main storage compartments and flows of the STREAM model (Aerts et al., 1999).

STREAM (or its predecessor RHINEFLOW) has been successfully applied to numerous basins of varying sizes in different parts of the world for studies of the 20th and 21st Centuries, e.g. the Rhine in Europe (Van Deursen and Kwadijk, 1994a); the Ganges-Brahmaputra and Krishna in India (Bouwer et al., 2006; Van Deursen and Kwadijk, 1994b); the Yangtze in China (Van Deursen and Kwadijk, 1994b); and the Perfume River in Vietnam (Aerts and Bouwer, 2002a). Moreover, Aerts et al. (2006) and Ward et al. (2007) applied the model to numerous large basins around the globe (including the Congo, Nile, Volta, and Zambezi in Africa) to simulate changes in discharge over periods of thousands of years.

2.4.1 Model input data

To set up the model a GIS database of input maps was created, using the IDRISI Kilimanjaro software. The various input data files are described in this section; all input maps have a spatial resolution of 10' x 10'.

Climate data

Maps showing monthly precipitation (mm) and temperature (°C) were prepared for the entire study area (Ethiopia and Kenya) as described in Sections 2.1 to 2.3.

Land use data

For this study the land use map was taken from the USGS Earth Resources Observation and Science Center (EROS) Africa Land Cover Characteristic Database (http://edc2.usgs.gov/glcc/). We used the USGS Land Use/Land Cover System map. The data are available at a resolution of 1km x 1km, and were first reprojected onto the 10' x 10' grid used in this study.

The land use classes were then reclassed into so-called crop factors (CropF). A crop factor map is used in STREAM to calculate potential evapotranspiration (*PE*). The crop factor is a dimensionless factor by which the reference *PE* is multiplied in order to account for the difference in *PE* over different land use types. The land use classes were reclassed to crop factors based on values in Kwadijk (1993) and Aerts and Bouwer (2002b), as shown in Table 2.2.

Table 2.2 Land use classes and their associated crop factors, reclassed according to values in Kwadijk (1993) and Aerts and Bouwer (2002b).

Land use class	Crop factor (CropF)
Urban and built-up land	0.8
Dryland cropland and pasture	1.0
Cropland/grassland mosaic	0.9
Cropland/woodland mosaic	1.0
Grassland	0.8
Shrubland	0.8
Savannah	0.6
Forest	1.1
Water bodies	1.5
Wetlands	1.1
Barren or sparsely vegetated	0.5

Soil water holding capacity (WHC)

A map showing the maximum water holding capacity (WHC) of the soil (mm) is used in STREAM in the calculation of evapotranspiration, runoff, groundwater seepage, and base flow. For this project we used the *Assessment of Water Holding Capacity of Soils Map* of the United States Department of Agriculture (http://soils.usda.gov/use/worldsoils/mapindex/whc.html). The map is available at a spatial resolution of 0.5° x 0.5°, and resampled to the resolution of our STREAM model.

Digital Elevation Model (DEM)

A DEM is used in STREAM to route the flow of water through the basin; the direction of water flow between grid cells is based on the steepest descent for the eight surrounding grid cells. For this study we used the USGS GTOPO30 DEM (http://edc.usgs.gov/products/elevation/gtopo30/gtopo30.html. This DEM is available with a spatial resolution of 0.5° x 0.5°, and was taken for the area shown in Figure 1.1. The DEM was then resampled to the resolution of the STREAM model, and the drainage networks of East Africa were defined using the RUNOFF module of the IDRISI software.

2.4.2 Calibration and validation of the hydrological model

The STREAM model is calibrated by varying model parameters with the aim of reproducing annual and monthly discharge characteristics similar to those in the observed record. The parameters used for calibration are: CropF; WHC; HEAT (used in the Thornthwaite (1948) equation for calculating potential evapotranspiration); TOGW multiplier (determines the proportion of surplus water per grid cell that runs off directly or that seeps to the groundwater); and the C factor (determines the proportion of groundwater that contributes to base flow).

Measured discharge data are not available for the Omo River. Hence, it was necessary to select a neighbouring basin with similar hydrological characteristics which could be used for establishing the parameter set. This parameter set was then transferred to the Omo basin. This method is known as

model calibration on ungauged river basins (e.g. Bárdossy, 2007). For this study the most representative basin for which observed discharge data were available is the Blue Nile.

Observed discharge data for the Blue Nile (at Khartoum, Sudan, see Figure 1.1) were taken from the Global River Discharge database (RivDis) (Vörösmarty et al., 1998; http://daac.ornl.gov//RIVDIS/rivdis.html). Data are available for the period 1912-1982. Hence, two periods of 30-yr duration were chosen for calibration and validation. The calibration was carried out for the period 1951-1980, and the validation for the period 1921-1950. Calibration and validation were carried out separately for the models forced using each GCM (i.e. HADCM3 and ECHAM5). The downscaled GCM data were used as input for the calibration (as opposed to the CRU reanalysis ('observed') data, since the future runs were also carried out using downscaled GCM data. Hence, the simulated discharge time-series do not refer to specific months and years of the observed record. It was therefore only possible to compare the statistics of the simulated discharge time-series with the statistics of the observed discharge time-series over the calibration and validation periods, rather than comparing the paired values of individual months and years.

The agreement of mean monthly discharge for the calibration and validation periods can be seen visually in Figure 2.4. The figures show that the STREAM models driven by both HADCM3 and ECHAM5 data simulate the annual hydrograph well. This is confirmed by a number of statistical analyses shown in Table 2.3. The agreement of mean annual discharge was assessed by expressing mean annual simulated discharge as a percentage of mean observed discharge (%). As can be seen in Table 2.3 this agreement is very good for the calibration period for both models, and good for the validation period. The results of the t-test (Table 2.3) show that there is no significant difference between mean annual simulated and observed discharge for the calibration and validation periods for either GCM (2 tail, n=60, α=0.05). The correlation of mean monthly discharges was assessed using the correlation coefficient, r, and the Nash and Sutcliffe (N&S) efficiency coefficient (Nash and Sutcliffe, 1970); for all cases the correlation was high (Table 2.3).

However, the results of the F-test (Table 2.3) show that whilst there was no significant difference in the variance of annual discharge between the simulated and observed records for the STREAM model driven by downscaled HADCM3 data, there was a highly significant difference in variance for the model driven by downscaled ECHAM5 data for both the calibration and validation period. This can be explained by the fact that the variance of precipitation in the catchment area of the Blue Nile is greater in the downscaled ECHAM5 dataset than in reality. Hence, whilst the ECHAM5 data can be used to simulate changes in mean monthly and annual discharge, their application to changes in discharge variability is not reliable.

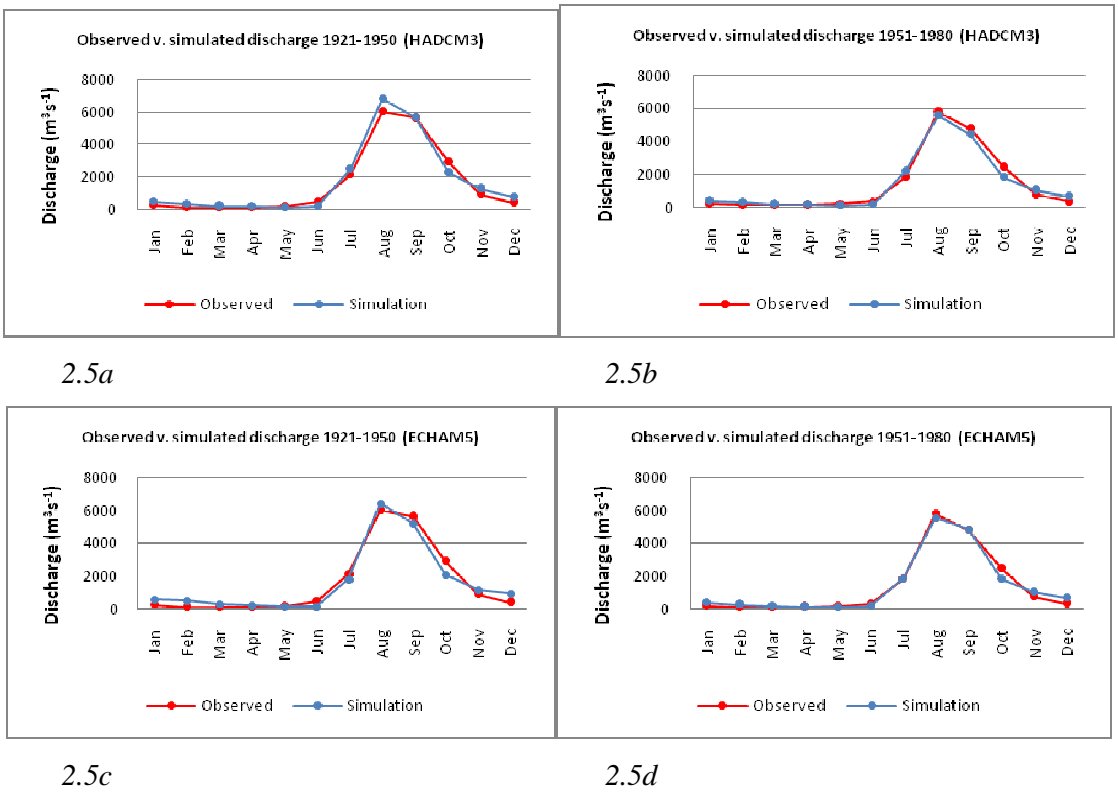

2.5a *2.5b*

2.5c *2.5d*

Figure 2.5 Hydrographs showing the agreement between mean monthly simulated and observed discharge at Khartoum (Blue Nile) for: (a) the validation period 1921-1950 (HADCM3)(b); the calibration period 1951-1980 (HADCM3)(c); the validation period 1921-1950 (EHCAM5); and (d) the calibration period 1951-1980 (ECHAM5).

Table 2.3 Results of statistical analyses comparing the simulated discharge series with the observed series. % refers to the annual mean simulated discharge as a percentage of the observed discharge. Also shown are the probabilities associated with the t-test and F-test of annual discharge, and the correlation coefficient (r) and N&S correlation coefficient between the mean monthly simulated and observed discharges.

Period	%	t-test (p)	F-test (p)	r	N&S
HADCM3					
1951-1980	99.9	0.998	0.414	0.991	0.979
1921-1950	107.8	0.090	0.077	0.998	0.968
ECHAM5					
1951-1980	100.4	0.972	<0.001	0.993	0.984
1921-1950	102.0	0.835	<0.001	0.982	0.964

In order to assess the skill of the hydrological models in simulating the frequency of high and low flow events, rather than just mean flows, we calculated the k^{th} percentiles of monthly discharge for the calibration period 1951-1980 from both the simulated and observed discharge time-series. The results (Table 2.4) show that both high and low flow frequencies are better simulated by the

HADCM3-driven model than by the ECHAM5-driven model. Again, this is likely to be related to the fact that the variability of the precipitation data in the catchment area in the downscaled ECHAM5 data is too high. For this reason, the analyses of changes in high and low flows will only be carried out for the HADCM3-driven model.

Table 2.4 Magnitudes of k^{th} percentiles of observed and simulated monthly discharge (Q_k, k = 1, 5, 10, 25, 75, 90, 95, and 99) at Khartoum (Blue Nile).

Period	Q_1	Q_5	Q_{10}	Q_{25}	Q_{75}	Q_{90}	Q_{95}	Q_{99}
HADCM3								
1951-1980 (observed)	67.5	102.0	122.0	176.0	1913.5	5253.9	5864.8	7073.5
1951-1980 (simulated)	80.0	98.4	120.0	194.1	1847.1	4612.5	5852.2	7918.7
ECHAM5								
1951-1980 (observed)	67.5	102.0	122.0	176.0	1913.5	5253.9	5864.8	7073.5
1951-1980 (simulated)	35.9	67.0	90.8	174.2	1712.2	4114.9	6054.5	10495.1

3. Results

The main objectives of this study are to provide maps and graphs showing the possible short and medium-term changes in annual and monthly precipitation and temperature in the study region; to assess the possible impacts of climate change on the occurrence of dry events and the incidence of high temperatures; and to assess the effects of these climate changes on the discharge of the Omo River. The main aim is to provide a large dataset showing the projected changes in climate, which can be used with and by regional and local stakeholders in the assessment of adaptation requirements and possible adaptation strategies. The most important results of the study are therefore the large dataset which can be found in the appendices. Based on these datasets, stakeholders and decision-makers in the region can make informed decisions on the need for adaptation measures to adapt to climate change.

All results are given for the following 10 locations (see Figure 1.1): Moyale, Mandera, Marsabit, Maralal, Isiolo, Nairobi, Awasa, Kelem, Asayita, and Addis Ababa. For all of the graphical results relating to the SRES emission scenarios (Appendices 1–4), we have used the same colour coding as adopted in the Fourth Assessment Report (AR4) of the IPCC (IPCC, 2007), i.e. B1 in green, A1B in red, and A2 in yellow. This allows for direct and easy comparison with other results to be found in the AR4 (and related studies).

The results section is set up as follows. In Section 3.1, a brief description is given of which results can be found in each appendix. In Section 3.2, a summary assessment is made of the regional patterns that can be found in those results. In Section 3.3, further demonstrative assessments and analyses are carried out for the case study location of Moyale. These relate specifically to changes in precipitation totals during the wet seasons, and changes in the frequency of months with very high temperatures. In Section 3.4, results are shown of the effects of climate change on the discharge of the Omo River.

3.1 Short guide to the datasets in the appendices

Appendix 1:

These maps show the spatial distribution of the mean annual values of the downscaled GCM data for precipitation (Appendix 1a) and temperature (Appendix 1b), at a spatial resolution of 10' x 10'. On the upper half, the results are shown for HADCM3, and the results for ECHAM5 are shown on the lower half. The results are shown for 2020 (2006-2035) and 2050 (2036-2065) for scenarios COMMIT, B1, A1B, and A2.

Appendix 2:

These maps show the spatial distribution of the anomaly in the mean annual precipitation (Appendix 2a) and temperature (Appendix 2b), between the future scenarios and the baseline period 1961-1990. The anomalies are calculated by subtracting the downscaled GCM data for the baseline period from the downscaled GCM data for the future scenarios. Hence, a positive anomaly means that precipitation or temperature will be higher in the future scenario compared to the baseline period, and a nega-

tive anomaly means that precipitation or temperature will be lower in the future scenario compared to the baseline period. The anomalies are shown at a spatial resolution of 10' x 10'. On the upper half, the results are shown for HADCM3, and the results for ECHAM5 are shown on the lower half. The results are shown for 2020 (2006-2035) and 2050 (2036-2065) for scenarios COMMIT, B1, A1B, and A2. On the maps are clear large 'blocks', with abrupt change in anomalies along the edges of these blocks. These blocks result from the original grid cells of the GCMs. Since GCMs have a coarse resolution, there can be large differences in the change in mean values between the baseline and future scenarios for two adjoining grid cells (especially for precipitation) in the raw (non-downscaled) data. For example, one GCM grid cell may show an increase in mean annual precipitation of 50 mm, whilst the adjoining cell may show zero change. Let us then assume for the sake of illustration that the correction factors used to downscale these two GCM grid cells to the higher resolution grid cells are equal (since the values of the two original GCM grid cells were equal in the baseline period, and both cells had the same climate in the observed dataset). Consequently, the downscaled anomaly values will show an abrupt change between the two GCM grid cells, since the anomaly of one cell will be 50 mm, whilst the anomaly of the other cell will be 0 mm.

Appendix 3:

Graphs are presented to show the changes in mean annual and monthly precipitation characteristics. For each location, the results of the two GCMs are shown on facing pages, to allow for easy comparison. For example, Appendix 3.1 shows the results for Moyale for the HADCM3 model, and Appendix 3.2 shows the results for Moyale for the ECHAM5 model. For each location and model the following graphs are shown: (a) mean monthly precipitation for 2020 (2006-2035) and the baseline period (1961-1990); (b) mean monthly precipitation for 2050 (2036-2065) and the baseline period (1961-1990); (c) mean monthly precipitation anomaly between the future scenarios in 2020 and the baseline period, calculated by subtracting the baseline period data from the scenario data; (d) mean monthly precipitation anomaly between the future scenarios in 2050 and the baseline period, calculated by subtracting the baseline period data from the scenario data; and (e) a graph showing the long term trends in mean annual precipitation (10-yr moving mean) between 1901 and 2100. The black line indicates the 20C3M scenario for the period 1901-2000, and the COMMIT scenario for the period 2001-2100. It should be noted that the black line indicating the trends in long term 20th Century mean annual precipitation are based on the downscaled climate model results, and not observed values. Hence, the values shown here cannot be compared with the observed data on a year to year basis, as climate models do not simulate actual weather in an observed year, but rather the average climate over a longer time-period. Similarly, the values shown here differ between the two climate models used, because the models give different variations over short periods. However, the mean annual values of precipitation for the period 1961-1990 are statistically similar, because observed data (CRU) for the period 1961-1990 were used to establish correction factors for the statistical downscaling of each of the climate models. Hence, the modelled and observed mean annual precipitation are statistically similar for that period (see Sections 2.2 and 2.3).

Appendix 4:

The same graphs are presented as in Appendix 3, but in this case for temperature. Again, it should be noted that the black line indicating the trends in long term 20th Century mean annual temperature are based on the downscaled climate model results, and not observed values. Hence, the values shown

here cannot be compared with the observed data on a year to year basis, as climate models do not simulate actual weather in an observed year, but rather the average climate over a longer time-period. Similarly, the values shown here differ between the two climate models used, because the models give different variations over short periods. However, the mean annual values of temperature for the period 1961-1990 are statistically similar, because observed data (CRU) for the period 1961-1990 were used to establish correction factors for the statistical downscaling of each of the climate models. Hence, the modelled and observed mean annual temperature are statistically similar for that period (see Sections 2.2 and 2.3).

Appendix 5:

Tables showing the percentage of months in which precipitation or temperature are above or below given thresholds. Appendix 5.1 shows the percentage of months in which the precipitation is less than the thresholds listed in the first column. All values are derived from the downscaled HADCM3 dataset, including those for 1961-1990 (i.e. the baseline period is the simulated data for 1961-1990, rather than the observed data). The use of different thresholds is useful since it allows local stakeholders to assess the changes associated with the thresholds which are important for their own livelihoods and activities. Appendix 5.2 is the same as Appendix 5.1, but refers to the ECHAM5 precipitation data. In Appendices 5.3 and 5.4, the percentage of months with precipitation above given thresholds (i.e. months with high rainfall) are shown for the HADCM3 and ECHAM5 data respectively. Finally, in Appendices 5.5 and 5.6, the percentage of months with temperature above given thresholds (i.e. months with intense heat) are shown for the HADCM3 and ECHAM5 data respectively.

3.2 Summary assessment of regional climate change results

The main aim and strength of this study is to provide a large dataset showing the projected changes in climate, which can be used with and by regional and local stakeholders in the assessment of adaptation requirements and possible adaptation strategies. Hence, the appendices form the most important part of the report, since the specific datasets can be referred to depending on the location of interest, or the issue to be addressed (heat, drought, intense rainfall, etc.). However, a summary assessment of the regional patterns that can be seen in the results provides added value, and is presented in the following sub-sections.

3.2.1 Changes in the overall spatial patterns of mean precipitation and temperature

Reference to the maps of spatially distributed mean annual precipitation (Appendix 1a) and mean annual temperature (Appendix 1b) show that the overall regional climate pattern is largely similar between the various scenarios and GCMs. However, the maps showing the anomalies of mean annual precipitation (Appendix 2a) and mean temperature (Appendix 2b) show that there are large regional and localised differences, especially between the results of the two GCMs.

Overall, the results of HADCM3 appear to show a tendency towards somewhat wetter conditions in large parts of the northern half of the study area (northern Ethiopia), but drier conditions in southern Kenya, especially in the south-western corner. Along the border region of Kenya and Ethiopia, there is no clear signal of change, with some periods or scenarios showing no or little change, and others showing either an increase or decrease in precipitation. In general the magnitude of change in this re-

gion is small. The results of the ECHAM5 model do not show the same overall pattern. The latter model shows a more clear regional signal towards wetter conditions, with larger anomalies towards the western part of the region (especially western Ethiopia). An exception to this is in the south-eastern tip of Kenya, where drier conditions are simulated by both GCMs (except HADCM3 for scenario A1B).

The regional anomaly pattern with regards to mean annual temperature is much more homogeneous. Positive anomalies (i.e. increased temperatures) are simulated for all parts of the region, and for all scenarios under both GCMs. As would be expected, the increases in temperature are clearly greater by 2050 than by 2020, and for the 'A' scenarios compared to the B1 scenario.

3.2.2 Regional and local patterns in precipitation change

A more detailed assessment of the regional and local changes in precipitation, with reference to the 10 case study locations, shows more complex patterns of change than those outlined above. These are discussed in this subsection.

Mean precipitation

In the HADCM3 results, a number of clear regional patterns can be distinguished. For those basins in which the main rainy season occurs between March and May, with a second peak in October and November (i.e. Moyale, Mandera, Marsabit, Isiolo, Kelem, and Nairobi), some similarities in the change in the annual cycle can be seen. Firstly, these locations show a tendency towards more rainfall in the early part of the first (main) rainy season in March and April, but in contrast a decrease in precipitation towards the latter part of this season (May). These changes are the most pronounced and consistent in those locations in the central part of the study area (i.e. Moyale, Mandera, Marsabit), and also Isiolo. In Kelem, the increase in precipitation between March and April can also be seen, though it is much less pronounced than in the former locations. Moreover, the decrease in May is absent in Kelem, where very little change is simulated in this month. Precipitation in Nairobi, on the other hand, does show a decrease in May, but little change in March and April. The other main characteristic change in this area of bi-annual rainfall maxima, is the decrease in total precipitation in the second rainy season, mainly in October, but to a lesser extent also in November. This change can be seen in all of the aforementioned locations, except for Kelem, where little or no change occurs in October, and a slight increase in November.

For the other locations (Maralal, Awasa, Asayita, and Addis Ababa) increases in March precipitation can also be seen. Hence, this seems to be a characteristic of the entire region, except for the southern area (Nairobi), and to a lesser extent the far western area (Kelem). In Maralal, which is characterised in the baseline period by tri-annual rainfall maxima (main rainy season from March to May, second in October and November, and a third lower peak in July and August), a clear decrease can be seen in the precipitation in October (as was the case for most of the bi-annual rainfall locations discussed previously).

To summarise, the main regional patterns that can be identified in the downscaled HADCM3 precipitation data, are an increase in precipitation in March in a large part of the region. For those areas with two rainfall peaks whereby the main one occurs between March to May, and the second one in October and November, this is generally accompanied by increased precipitation in April, but decreased

precipitation in May, and a decrease in total precipitation in the second rainy season (October-November).

For the results of the downscaled ECHAM5 data, fewer clear regional changes in the monthly precipitation regime can be identified, although there is a more clear tendency to overall (annual) wetter conditions in general. One of the most striking changes is the relatively large increase in August precipitation in Moyale, Marsabit, and Nairobi, which causes a small precipitation peak in August that is not present in the baseline period. As a result, the overall annual patterns for these locations resemble that of Maralal (which also shows a large positive anomaly in August precipitation). Overall, the results for most stations tend to show wetter conditions in the second half of the year, causing increased rainfall in the October-November rainy season in those locations where this is a characteristic.

Precipitation variability

Climate change can also affect the variability of annual rainfall; often such changes are more difficult to cope with than changes in mean precipitation, since an increase in variability can cause less predictability in the climate. Hence, we assessed the change in the variability of annual precipitation by carrying out the statistical F-test (2-tailed, n=60, α=0.05) on the annual precipitation totals for the baseline period, compared to the future scenarios. The F-test assesses whether there is a significant difference in variance between two samples. The results of this analysis showed that for the vast majority of locations and scenarios, there is no significant change in the variability of annual precipitation. The main exception is Asayita, where the results of both GCMs show a significant increase in the variability of annual precipitation under all SRES scenarios and for both periods 2020 and 2050. Significant increases in variability were also found for: Addis Ababa with the HADCM3 model for scenario A2 (2020 and 2050); and Awasa under the A2 scenario for 2020 (HADCM3 only) and 2050 (HADCM3 and ECHAM5). Hence, the results of both models suggest that increased precipitation variability can be expected in the more northern regions of Ethiopia, with the clearest increase in the far northern area (Asayita). For the SRES scenarios, no other significant changes in variability were detected.

Changes in the frequency of dry months

The tables in Appendices 5.1 and 5.2, showing the change in the percentage of months with precipitation below given thresholds (for HADCM3 and ECHAM5 respectively), also reveal a number of regional patterns, although again these are generally not consistent between the two GCMs.

The downscaled HADCM3 data generally show a decrease in the percentage of months with low precipitation totals for the three case study locations with the most northern location (i.e. Asayita, Addis Ababa, and Awasa), as well as the location with the most westerly location (Kelem). This finding is in line with the small increases in mean annual precipitation generally projected for these locations by HADCM3. On the other hand, the three most southern locations (Nairobi, Isiolo, and Maralal) show a tendency towards an increase in the percentage of months with low precipitation totals. For the neighbouring locations of Marsabit and Moyale, there is no clear signal of change, with increases in some scenarios and/or time periods, and decreases in others; in all cases the changes are relatively small for the latter locations. For Mandera, there appears to be an increase in the percent-

age of months in which total precipitation is less than 1 mm, although the opposite is the case for months with total precipitation less than 5 mm or 10 mm; these changes are of a relatively small magnitude.

For the downscaled ECHAM5 data the overall regional trend is towards a decrease in the number of dry months, which is in line with the previously mentioned regional trend towards wetter mean conditions. The most clear change towards fewer dry months occurs in the central locations of Moyale, Marsabit, and Kelem, where a decrease in the percentage of months under all given thresholds is simulated under all three SRES scenarios and for both 2020 and 2050. Maralal also shows a tendency towards a decrease in the number of arid months, although small increases in the percentage of months with less than 5 and 10 mm precipitation are simulated in 2050 for this location. For the three most northerly locations (Asayita, Addis Ababa, and Awasa), as well as the most southerly location (Nairobi), no clear signal can be found between scenarios. The same is the case in Mandera for 2020, although a clear tendency towards a decrease in the number of dry months can be seen by 2050.

A comparison of the results from the two models reveals a number of contrasting patterns. Whilst the northern region shows a general decrease in the number of dry months in HADCM3, no general pattern can be found in ECHAM5. For the southern region, HADCM3 tends to suggest an increase in the number of dry months, whilst ECHAM5 suggests a general decrease in Isiolo and Maralal, with an increase in Nairobi by 2050. Moyale and Marsabit show increases in the frequency of the driest months (precipitation less than 1, 5, and 10 mm), whereas ECHAM5 shows the opposite. Of the driest locations (Asayita, Kelem, and Mandera), the only one in which a clear signal can be noted is Kelem; for this location a decrease in the number of arid months is simulated under both models.

Changes in the frequency of wet months

Changes in the number of months with precipitation above a given threshold, in other words wet months, are also important when planning adaptation strategies. These changes are documented in the tables in Appendices 5.3 and 5.4. In the downscaled HADCM3 data, the three stations which are currently the most arid (Asayita, Kelem, and Mandera) show a general tendency towards an increase in the number of wet months. This is especially the case for Asayita, where no months received precipitation totals in excess of 200 mm for the baseline period, but all future scenarios returned months with precipitation in excess of 350 mm. For Kelem and Mandera, the increase was restricted to a fairly small increase in the number of months with precipitation in excess of 100 mm, whereas no months were simulated with precipitation in excess of 200 mm for Kelem, or 300 mm for Mandera, even under the future scenarios. Awasa also shows an increase in the number of months with precipitation above 100 mm, but a monthly precipitation total in excess of 200 mm was simulated just once, namely for the A2 scenario in 2050. The opposite signal can be seen for Nairobi, Addis Ababa, and Maralal, where the simulated number of wet months in 2020 and 2050 is generally less than in the baseline period. For Marsabit and Moyale, the results of HADCM3 suggest that the number of wet months (precipitation in excess of 200, 300, and 350 mm) will decrease by 2020, but increase by 2050.

In line with the general regional increase in mean annual precipitation simulated by ECHAM5, the number of wet months tends to increase under the SRES scenarios for that model. For months with precipitation in excess of 200, 300, and 350 mm, there are only a few scenario/period combinations in which this is not the case, and for those cases there is either no change or only a minor decrease.

For ECHAM5 there is a clear tendency towards an increase in the number of wet months. For HADCM3 there is no single pattern over the entire region, although an increase in the number of wet months is expected for the three driest locations (Asayita, Kelem, and Mandera), as well as for Awasa and Isiolo. For Moyale and Marsabit an increase is also simulated by HADCM3 in 2050, though not in 2020. On the other hand, HADCM3 simulated decreases in the number of wet months for Addis Ababa, Maralal, and Nairobi.

3.2.3 Regional and local patterns in temperature change

Mean temperature

The trend towards higher temperatures is clear for all parts of the study region and under all of the scenarios used. In all cases, the temperature increase by 2050 is greater than the increase by 2020. For the SRES scenarios, the increase in mean annual temperature by 2020 ranges amongst the 10 case study locations between: 0.81°C-1.29°C (HADCM3, B1); 0.90°C-1.37°C (HADCM3, A1B); 0.81°C-1.18°C (HADCM3, A2); 0.52°C-0.87°C (ECHAM5, B1); 0.84°C-1.17°C (ECHAM5, A1B); and 0.79°C-1.04°C (ECHAM5, A2). By 2050 mean annual temperature for the 10 case study locations ranges between: 1.53°C-1.99°C (HADCM3, B1); 2.04°C-2.65°C (HADCM3, A1B); 2.10°C-2.82°C (HADCM3; A2); 1.44°C-1.83°C (ECHAM5, B1); 1.97°C-2.39°C (ECHAM5, A1B); and 1.80°C-2.27°C (ECHAM5, A2).

It is clear that in the medium term (2050) the expected increases in temperature under the 'A' scenarios are greater than the increases under the B1 scenario. In the short term (2020), the increases in temperature are of a similar order of magnitude under all of the SRES scenarios.

Changes in the frequency of very warm months

An assessment was also carried out into the change in frequency of the percentage of months with temperatures above given thresholds (i.e. very warm months); the results can be found in Appendices 5.5 and 5.6. All case study locations for which monthly temperatures occur above the minimum threshold shown here (27°C) show an increase in the number of months over that threshold. Clearly, both models show that the frequency of very warm months will increase greatly in the future, which is indicative of an increase in the occurrence of heat waves. The simulated increases by 2050 are greater than those by 2020. Moreover, the increases under the 'A' scenarios are generally speaking greater than those under the B1 scenario, which is in line with projections of global temperature change. Nevertheless, it is clear that the increases are very large even in the short term (2020), and for the most modest SRES scenario (B1). This suggests that strategies to adapt to heat stress should be considered and evaluated as a matter of urgency.

Changes in 'drought' occurrence

In Moyale, there are two main rainy seasons. The main rainy season is from March to May inclusive, with a strong peak in April; the second is a smaller and shorter rainy season in October and November (see Appendix 3.1a, baseline). This pattern of bi-annual rainy seasons in these months can also be seen in the monthly precipitation regimes of Mandera, Marsabit, Isiolo, Kelem, and Nairobi. Droughts can occur when rainfall in these seasons fails, or where the rainfall total during the rainy season falls below given thresholds required for the growing of crops or the rearing of livestock. Such thresholds are not homogenous across regions, as they are dependent on numerous factors including the type of agricultural activity (pastoral, arable, etc.), the type and/or species of crop or livestock, local soil characteristics, local relief, etc. Hence, local knowledge is essential in defining the minimum thresholds required to facilitate adequate productivity in a given region or locality.

In order to account for this need, the results in Figures 3.1-3.4 are presented in such a way that the change in the frequency of rainy season precipitation under a given threshold can easily be calculated in a workshop setting for any required threshold. For example, Figure 3.1 shows the total precipitation (in mm) during the main rainy season (March to May inclusive) for each year in the study period, based on the downscaled HADCM3 data. In Figure 3.1a the results are given for the SRES scenarios for the period 2006-2035 (i.e. 2020), so that year 1 refers to 2006, year 2 to 2007 etc. Also shown are the annual values for the baseline period (1961-1990), whereby year 1 refers to 1961, and year 2 to 1962 etc. For each year and each scenario, the dot shows the total precipitation for that year during the main rainy season. Hence, it is possible to count the number of dots in each scenario for the 30-yr period, for any given precipitation threshold, removing the need to establish *a priori* thresholds which do not account for local conditions. It should be noted that dots are only shown for years in which the total precipitation in March to May was less than 350 mm. This value is approximately equal to the median annual main rainy season precipitation in the observed series for 1961-1990 of 359 mm. Therefore, values above this total are not relevant for the assessment of changes in dry period frequency.

Figure 3.2 is as per Figure 3.1, but refers to the downscaled ECHAM5 data. Figures 3.3 and 3.4 show the yearly precipitation totals during the second rainy season in October and November for HADCM3 and ECHAM5 respectively. Note that in these figures the yearly values (dots) are only shown for those years in which the total simulated precipitation in October and November is less than 180 mm. This value is approximately equal to the median annual second rainy season precipitation in the observed series for 1961-1990 of 186 mm.

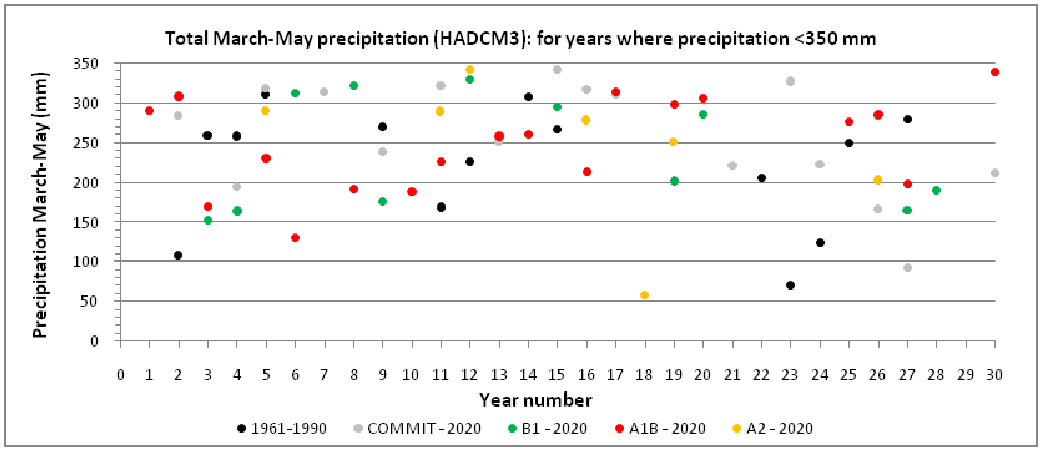

3.1a

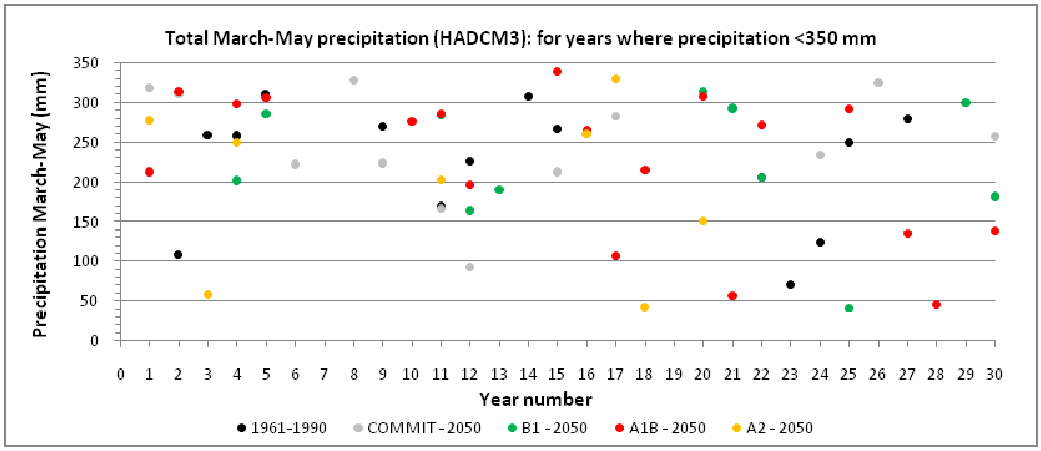

3.1b

Figure3.1 Scatter plots showing the total precipitation (mm) between March and May (MAM) inclusive based on the downscaled HADCM3 data. Fig. 6a shows the values for the period 2006-2035, and Fig. 6b shows the values for the period 2036-2065. The points show the total MAM precipitation per year, for each year in the 30-yr period (e.g. for the baseline period year 1 refers to 1961, and year 30 to 1990; and for the period 2020, year 1 refers to 2006, and year 30 to 2035, etc.). Scatter points are only shown for the years in which total MAM precipitation is less than 350 mm (which is approximately equal to the median precipitation of 359 mm in the observed records for the period 1961-1990).

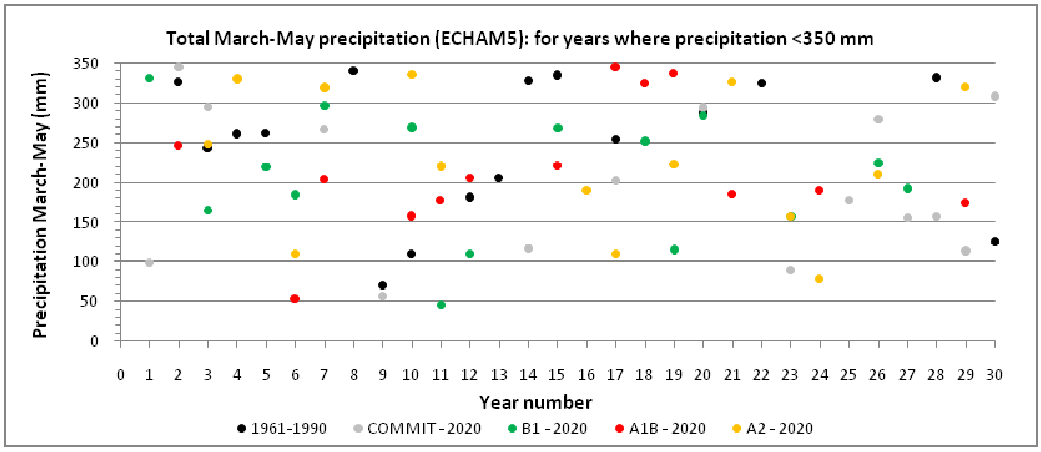

3.2a

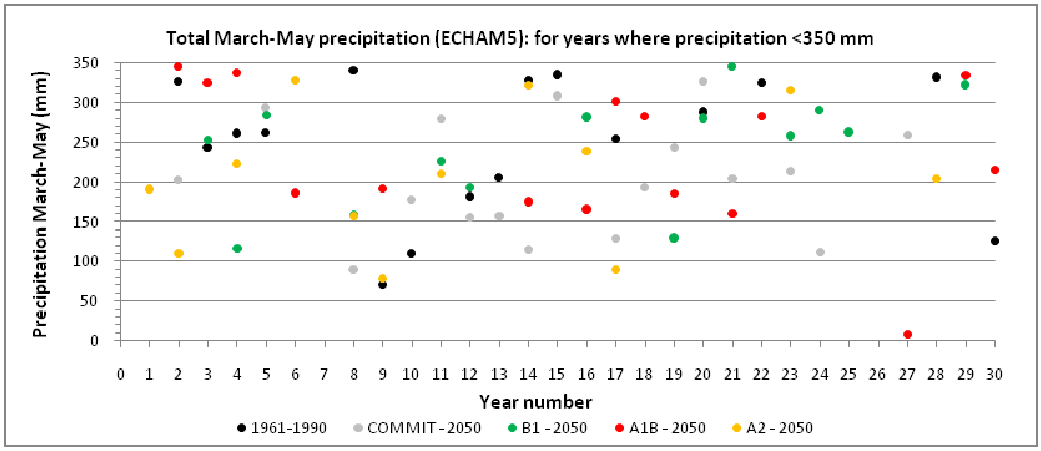

3.2b

Figure 3.2 Scatter plots showing the total precipitation (mm) between March and May (MAM) inclusive based on the downscaled ECHAM5 data. Fig. 7a shows the values for the period 2006-2035, and Fig. 7b shows the values for the period 2036-2065. The points show the total MAM precipitation per year, for each year in the 30-yr period (e.g. for the baseline period year 1 refers to 1961, and year 30 to 1990; and for the period 2020, year 1 refers to 2006, and year 30 to 2035, etc.). Scatter points are only shown for the years in which total MAM precipitation is less than 350 mm (which is approximately equal to the median precipitation of 359 mm in the observed records for the period 1961-1990).

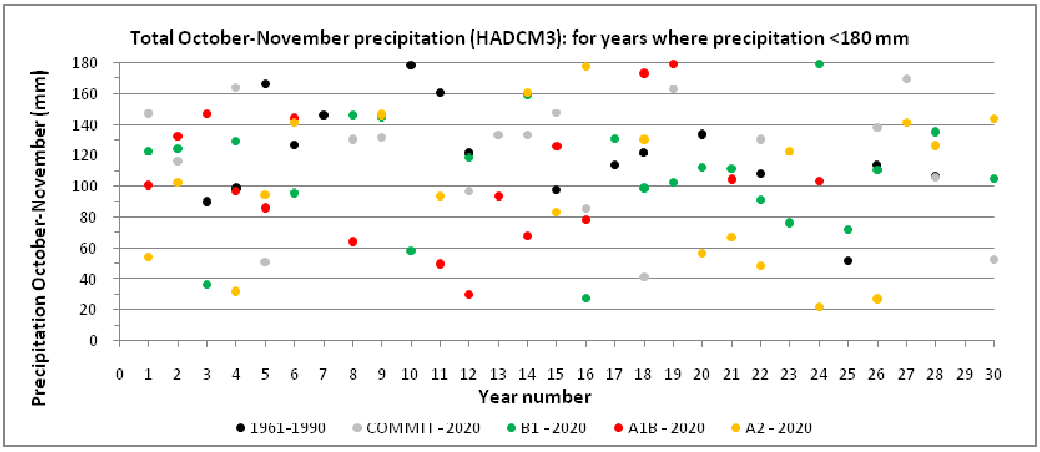

3.3a

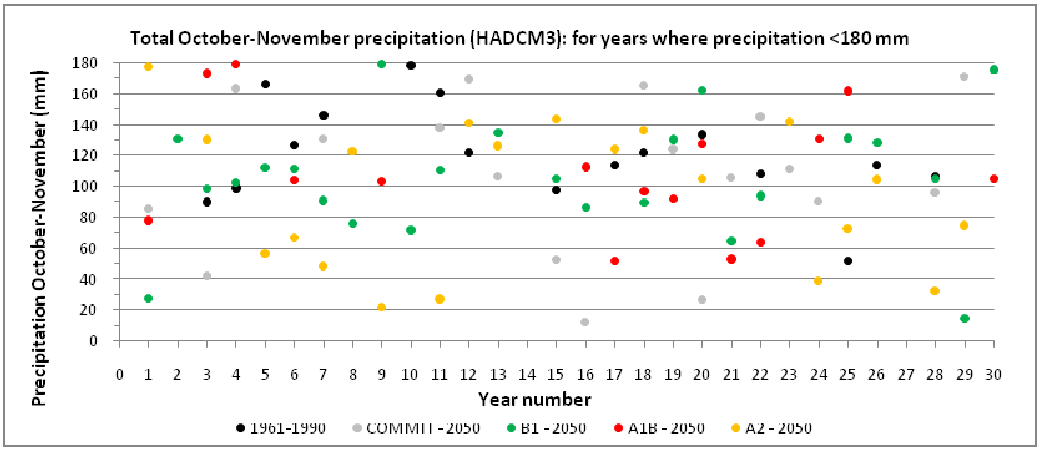

3.3b

Figure 3.3 Scatter plots showing the total precipitation (mm) in October and November (Oct-Nov) inclusive based on the downscaled HADCM3 data. Fig. 8a shows the values for the period 2006-2035, and Fig. 8b shows the values for the period 2036-2065. The points show the total Oct-Nov precipitation per year, for each year in the 30-yr period (e.g. for the baseline period year 1 refers to 1961, and year 30 to 1990; and for the period 2020, year 1 refers to 2006, and year 30 to 2035, etc.). Scatter points are only shown for the years in which total Oct-Nov precipitation is less than 180 mm (which is approximately equal to the median Oct-Nov precipitation of 186 mm in the observed records for the period 1961-1990).

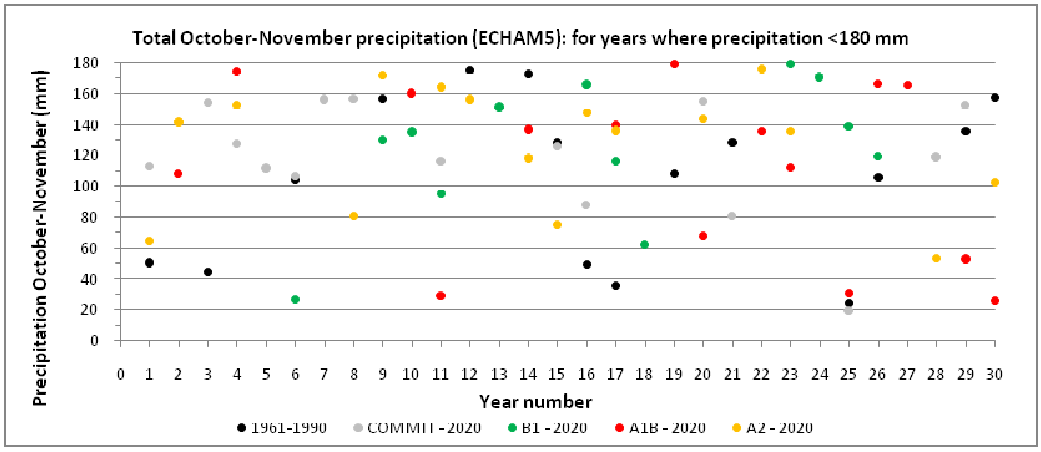

3.4a

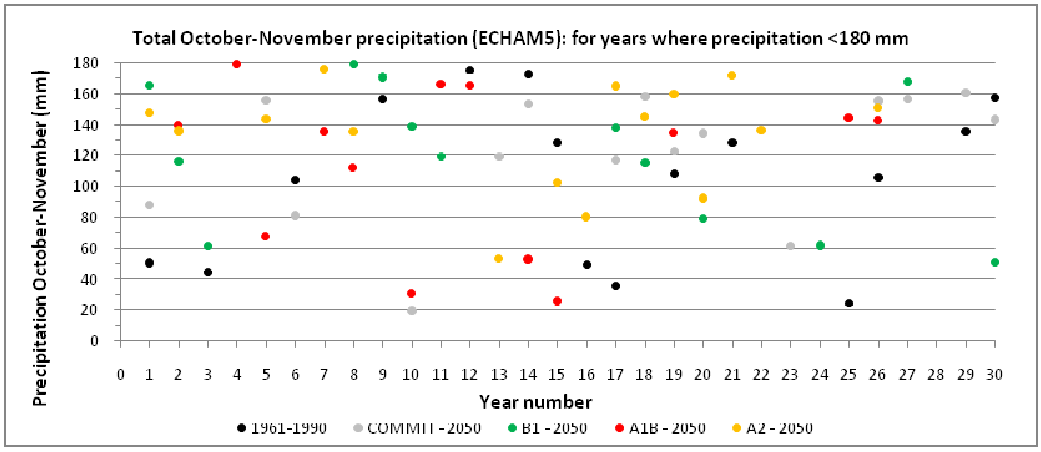

3.4b

Figure 3.4 Scatter plots showing the total precipitation (mm) in October and November (Oct-Nov) inclusive based on the downscaled ECHAM5 data. Fig. 9a shows the values for the period 2006-2035, and Fig. 9b shows the values for the period 2036-2065. The points show the total Oct-Nov precipitation per year, for each year in the 30-yr period (e.g. for the baseline period year 1 refers to 1961, and year 30 to 1990; and for the period 2020, year 1 refers to 2006, and year 30 to 2035, etc.). Scatter points are only shown for the years in which total Oct-Nov precipitation is less than 180 mm (which is approximately equal to the median Oct-Nov precipitation of 186 mm in the observed records for the period 1961-1990).

Although the main strength of the scatter plots in Figures 6-9 is that they can be used to assess changes in the occurrence of rainy season drought condition under any given threshold, an example is given in Table 5 for illustrative purposes. Here, the number of years is given in which the simulated precipitation during the rainy seasons is below the 10th percentile of the observed rainy season rainfall (based on the observed record for the period 1961-1990). For the main rainy season from March to May, ECHAM5 shows a clear increase in the number of years with precipitation above this threshold, thus indicating more rainfall in this growing season, and a lower incidence of drought conditions. For HADCM3 the results are not so clear cut. For SRES scenarios B1 and A2, decreases in the frequency of dry conditions are simulated for both 2020 and 2050, whilst the A1B scenario shows a small increase in the frequency of dry conditions. For the second rainy season (October and November), the results of the two GCMs clearly indicate the opposite signal of change. The results of HADCM3 suggest that low rainfall totals will occur more often during this rainy season in the future compared to the baseline period, whilst the results of ECHAM5 suggest that relatively dry rainy seasons will become less common.

Table 3.1 The number of years in which simulated wet season rainfall is below the 10th percentile of observed wet season rainfall (based on the observed record for Moyale for the period 1961-1990). On the left are shown the number of years in which simulated precipitation between March and May inclusive is below the observed 10th percentile for those months (253.4 mm). On the right are shown the number of years in which simulated precipitation in October and November is below the observed 10th percentile for those months (63.2 mm).

	Number of years with March-May precipitation < 253.4 mm		Number of years with October-November precipitation < 63.2 mm	
Scenario	HADCM3	ECHAM5	HADCM3	ECHAM5
20C3M (1961-1990)	7	6	1	5
COMMIT (2020)	8	9	3	1
B1 (2020)	6	10	3	2
A1B (2020)	8	10	2	4
A2 (2020)	3	9	6	1
COMMIT (2050)	6	12	4	2
B1 (2050)	6	6	2	3
A1B (2050)	8	8	2	3
A2 (2050)	5	9	6	1

Changes in the frequency of high temperatures

As discussed in Section 3.2.3, both the mean temperature and the frequency of months in which high temperatures occur are expected to increase in the future under all SRES scenarios according to the results of both GCMs. Such changes are important when considering the strategies required to adapt to climate change, since an increase in the number of very warm months may be indicative of an increase in heat wave occurrence. The increase in the number of months with very high temperatures at Moyale is large. Reference to 3.5 shows large increases in the number of months with temperatures over all of the given temperature thresholds according to both models, with huge increases in relative terms by 2050. For example, very hot months with an average temperature above 28°C are almost

non-existent in the simulation results for the baseline period. However, under the SRES scenarios for 2050, mean monthly temperatures of 28°C or more will occur between 12.5% and 21.1% of the time according to the HADCM3 model, and between 8.3% and 14.7% of the time according to the ECHAM5 model. Even in the short term (2020), the results of the two models agree that large increases in the number of very warm months will occur. Hence, it appears that urgent assessments are needed of the vulnerability of present-day systems to increased heat stress occurrence, as well as assessments of the adaption options available and their effectiveness in the local setting.

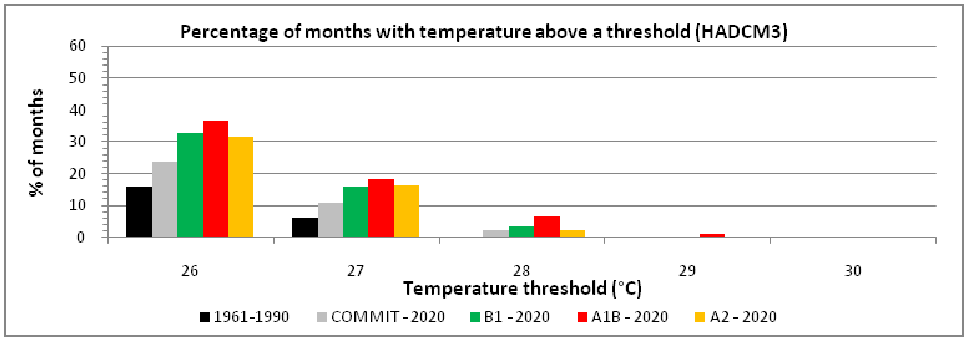

3.5a

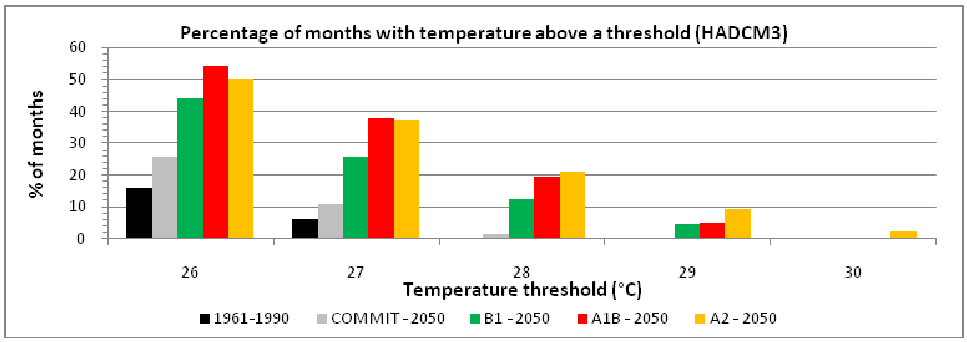

3.5b

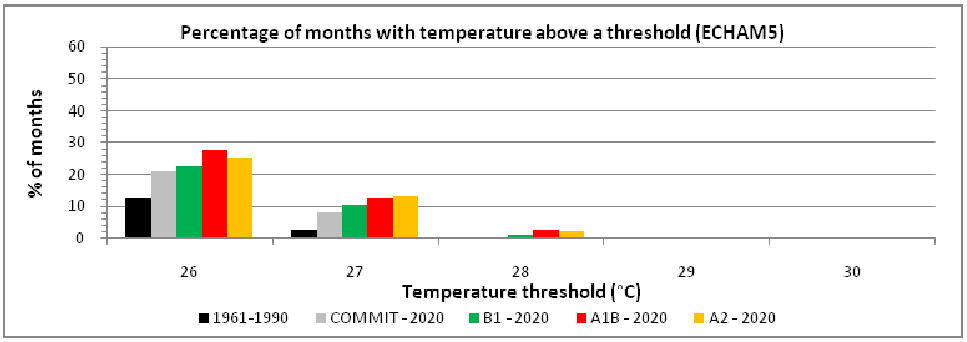

3.5c

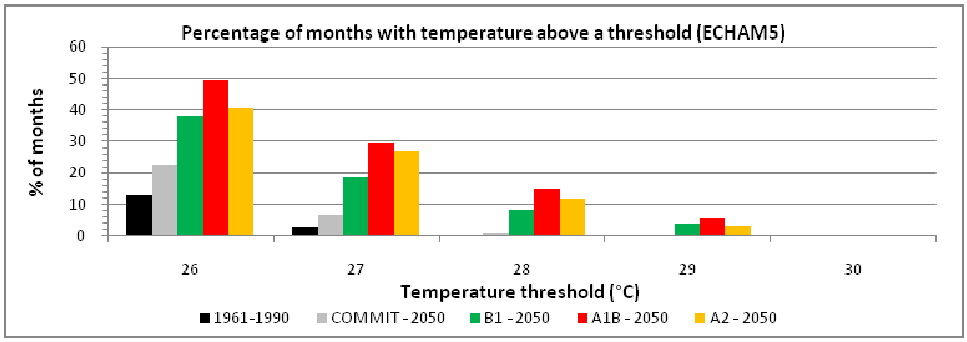

3.5d

Figure 3.5: Percentage of months with temperature above given thresholds (x-axis) for: (a) HADCM3 - 2020, (b) HADCM3 - 2050; (c) ECHAM5 - 2020; and (d) ECHAM5 - 2050.

3.4 Case study Omo River: changes in river discharge

Climate is one of the principal driving forces of hydrological systems, and even modest climate changes have the potential to causes significant changes in hydrological processes. Hence, a hydrological model (STREAM) was set up to examine the effects of climate change on the discharge of the Omo River. The setup and calibration of the model is described in Section 2.4. As discussed in Section 2.5, the model was calibrated twice, once for each GCM (i.e. separately for HADCM3 and ECHAM5). It was found that both STREAM models simulated mean annual and monthly discharge well in both the calibration and validation periods, but that the model forced using the downscaled ECHAM5 data led to significant differences in variability compared to the observed record. As a result, the results of both models are used in the assessment of changes in mean monthly discharge, but for the assessment of changes in high and low flows, only the results of the HADCM3-driven model are shown.

Changes in mean monthly discharge

Figure 3.6 shows the mean annual and monthly simulated discharge of the Omo River at Kelem (Figure 1) for the baseline period and the future scenarios. The hydrographs show that during the baseline period, monthly discharge is very low between January and June, before increasing to a peak in the months of August and September. This peak is followed by a fairly rapid recession in the months of October, November, and December.

Clear differences in the discharge anomalies associated with the two GCMs can be seen with reference to both Figures 3.6 and 3.7. According to the results of the HADCM3-driven model, discharge in the long dry season (December to June) remains very low. However, there is a negative discharge anomaly (i.e. lower discharge) in the period July to November. This pattern is not reproduced in the ECHAM5-driven model. In the latter, a large increase in discharge is simulated during the main discharge season (August-September), as well as early in the low discharge season (especially January to March). These changes are clear responses to simulated changes in precipitation in the South Omo region. With regards to the increase in discharge in the ECHAM5 model for the period January-March, this is related to a large precipitation anomaly in that model for the South Omo region in January and February.

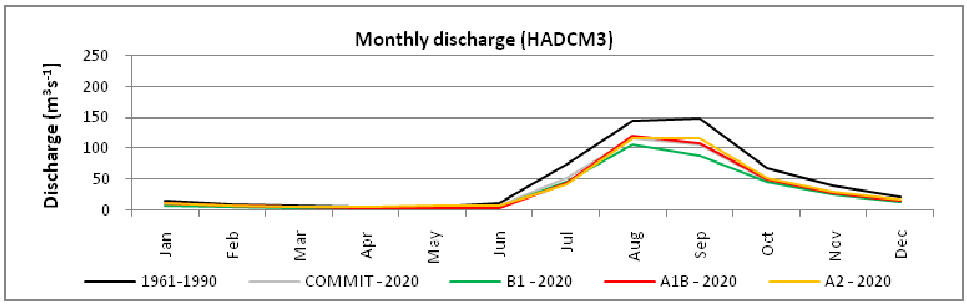

3.6a

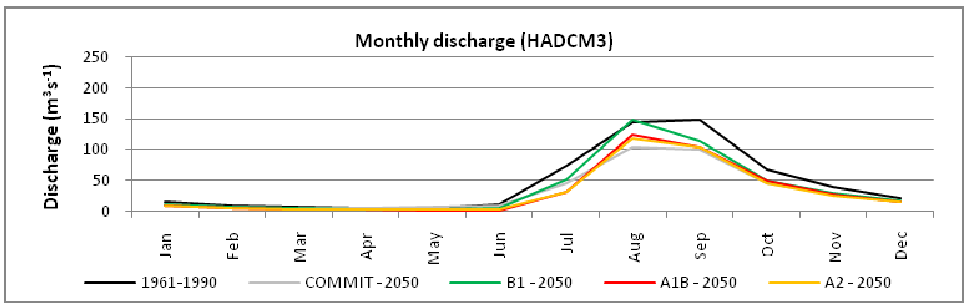

3.6b

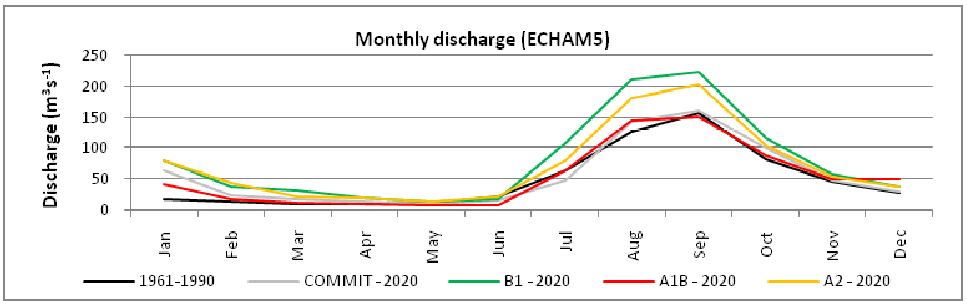

3.6c

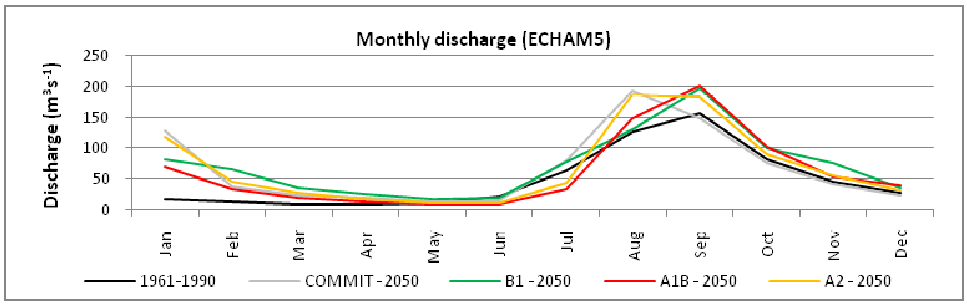

3.6d

Figure 3.6 Hydrographs showing the mean monthly discharge of the Omo River (near Kelem) for : (a) HADCM3 - 2020; (b) HADCM3 - 2050; (c) ECHAM5 - 2020; and (d) ECHAM5 - 2050.

3.7a

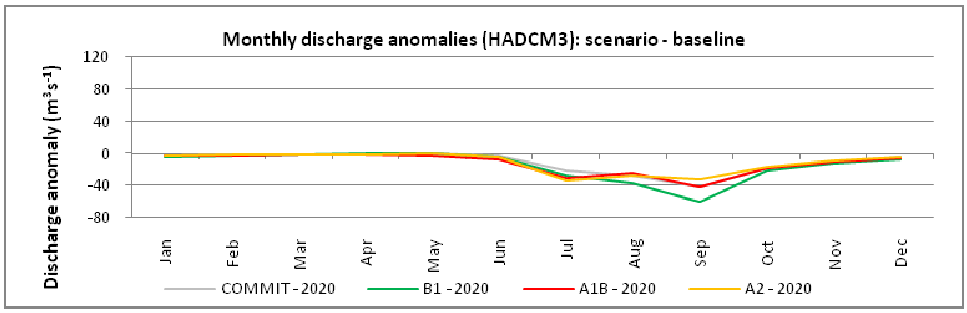

3.7b

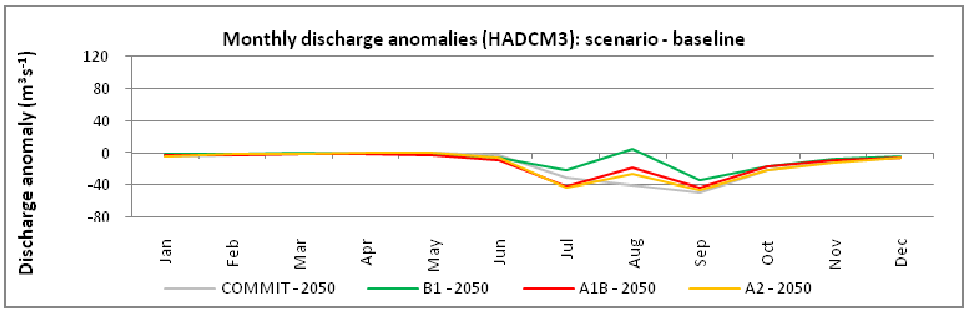

3.7c

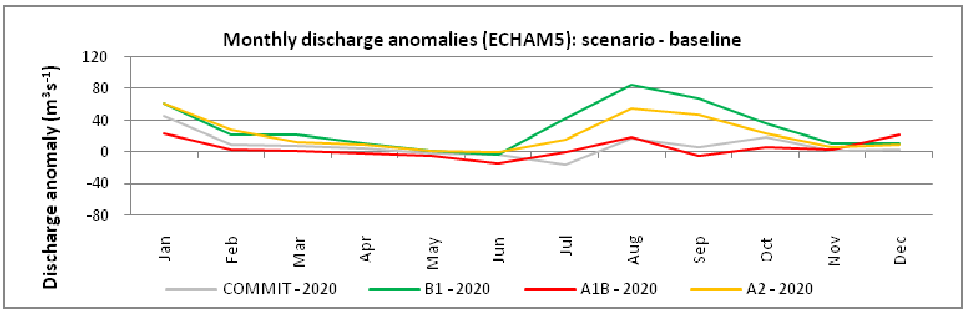

3.7d

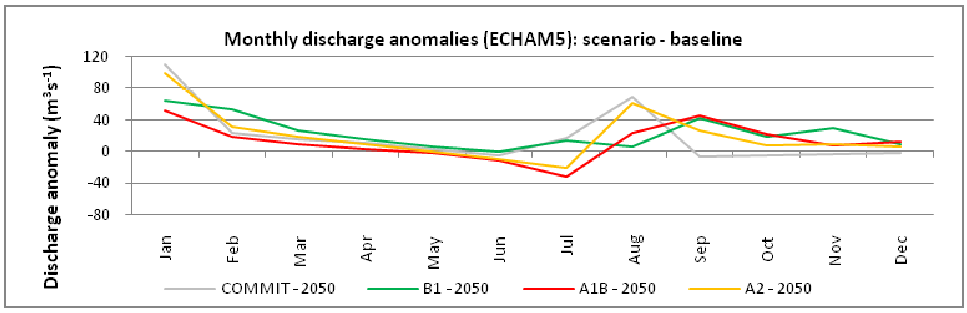

Figure 3.7 Mean monthly discharge anomalies of the Omo River (near Kelem) for : (a) HADCM3 – 2020; (b) HADCM3 - 2050; (c) ECHAM5 - 2020; and (d) ECHAM5 - 2050. The anomalies are calculated by subtracting the simulated values for the period 1961-1990 from the simulated values for the future scenario periods (i.e. scenario minus baseline).

In terms of the effects of the simulated climate changes on low flows, the graphs in Figure 3.8 show large increases in the percentage of months with mean discharge below the given thresholds for both 2020 and 2050, according to the results of the HADCM3-driven model. These changes are certainly not trivial, and are large even in the short term. For example, the percentage of months in which discharge falls below the very low level of 2 m^3s^{-1}, increases from just 3.3% in the baseline period to between 7.8 and 14.4% by 2020, and to between 11.7 and 19.7% by 2050 (dependent upon SRES scenario). These represent very large increases in the amount of time in which flows are extremely low. If these climate change driven changes do occur, effective adaptation measures will be essential, especially if water demand also increases in the future due to factors such as increased population, development, etc.

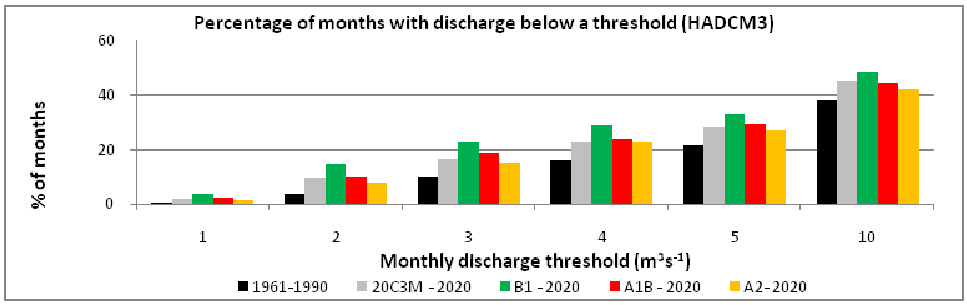

3.8a

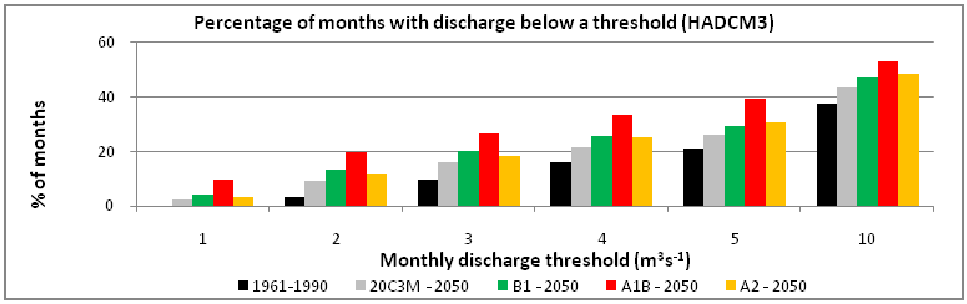

3.8b

Figure 3.8 Percentage of months with discharge below given thresholds (x-axis) for: (a) HADCM3 – 2020; and (b) HADCM3 – 2050.

Although the results of the HADCM3-driven STREAM model suggest that the frequency of months in which moderately high discharges (e.g. > 150 m^3s^{-1}, > 200 m^3s^{-1}, and > 350 m^3s^{-1}) occur may decrease in the future (Figure 14), an increase in the frequency of months with very high mean discharges (> 400 m^3s^{-1}) can be seen, especially by 2050. In many basins, mean monthly discharge shows a strong correlation with the magnitude of the maximum daily discharge in that month (e.g. Kwadijk, 1993). In such cases, an increase in the number of months with high discharges can be indicative of an increase in the frequency of high-flow events (i.e. floods). Unfortunately, since no observed data of Omo discharge are available, it is not possible to establish whether there is a correlation between mean monthly discharge and the magnitude of the maximum daily discharge in that month. However, the results displayed in 3.9 suggest that this is a real possibility, and hence precautionary measures should be considered to adapt to this future scenario.

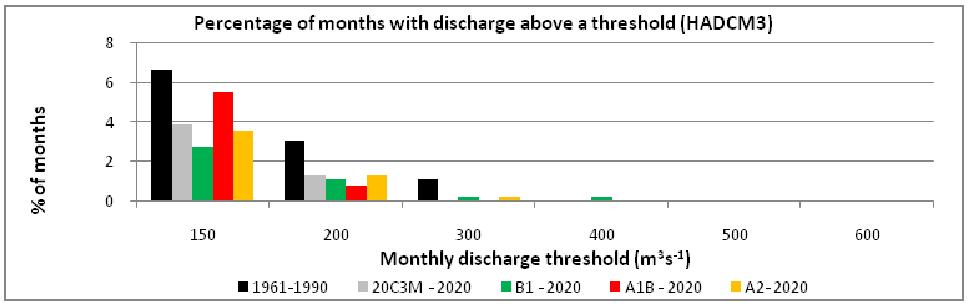
Percentage of months with discharge above a threshold (HADCM3)
% of months
0
2
4
6
8
150
200
300
400
500
600
Monthly discharge threshold (m³s⁻¹)
1961-1990
20C3M - 2020
B1 - 2020
A1B - 2020
A2-2020

3.9a

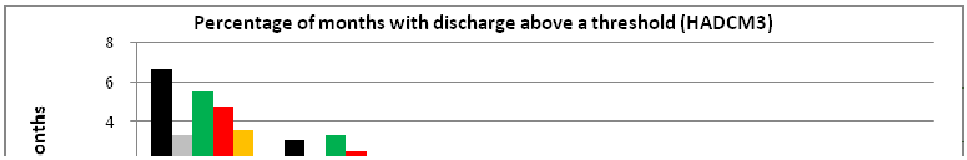
Percentage of months with discharge above a threshold (HADCM3)
8
6
4

3.9b

4. Summary, implications, and recommendations

The main aim of this study was to provide a large dataset showing the possible changes in climate that can be expected in Ethiopia and Kenya during the 21st Century. This dataset can be used with and by regional and local stakeholders in the assessment of adaptation requirements and possible adaptation strategies. This main aim was subdivided into the following objectives:

- To provide maps and graphs showing the possible short and medium-term changes in annual and monthly precipitation and temperature in the study region;
- To assess the possible impacts of climate change on the occurrence of drought events, and the incidence of high temperatures;
- To assess the effects of these climate changes on the discharge of the Omo River.

In this section a synthesis is provided of the results relating to these objectives. In addition, a short discussion is provided of some of the key implications of the results for climate change adaptation in Ethiopia and Kenya.

4.1 Dataset showing maps and graphs of possible short and medium-term changes in annual and monthly precipitation and temperature

The results of two GCMs (HADCM3 and ECHAM5) have been downscaled to a resolution suitable for regional climate impact assessment (10' x 10'). These models were chosen as they have the highest 'skill scores' for both precipitation and temperature of all the models used for the AR4 of the IPCC in the study region (Cai et al., 2009). In the appendices, a large dataset is provided showing the downscaled results of these models for the study region. Maps are provided in Appendices 1 and 2 showing the change in mean annual precipitation and temperature over the entire study region (Ethiopia and Kenya). Furthermore, the graphs in Appendices 3 and 4 show more detailed assessments of the change in mean monthly and annual precipitation and temperature for 10 case study locations, namely Moyale, Mandera, Marsabit, Maralal, Isiolo, Nairobi, Awasa, Kelem, Asayita, and Addis Ababa.

These datasets provide information than can be used by local and regional stakeholders to assess how climate is expected to change in the region in the short and medium-term (2020 and 2050 respectively). Moreover, based on this data, informed decisions can be made on the necessity for adaption to climate change, and the effectiveness of various adaptation strategies.

It should be noted that there are a number of similarities and differences in the results of the two GCMs. Firstly, the expected changes in the temperature regimes across the region are very similar according to both HADCM3 and ECHAM5. Both models show very clear trends at all locations towards warmer conditions in the future, with greater increases in mean temperature by 2050 compared to 2020, and greater increases for the 'A' scenarios compared to the B1 scenario.

In terms of the variability of annual rainfall totals, the results of the two GCMs are also in good agreement. Both show that in general there will be no significant increase in the variability of annual rainfall, between the baseline period and the future scenarios. Exceptions were noted in the northern half of the study area for both GCMs. A large increase in the variability of annual rainfall is simu-

lated for the most northerly location of Asayita by both HADCM3 and ECHAM5. Increases in variability were also noted in both models for the northern locations of Addis Ababa and Awasa under some combinations of scenario and/or time period, though the trend is less clear cut than for Asayita.

However, in terms of mean annual precipitation, the results of the two GCMs show numerous differences. In general, the ECHAM5 model shows a trend towards wetter annual conditions over most parts of Ethiopia and Kenya. Though this is also the case for large parts of northern Ethiopia according to HADCM3, the latter model simulates generally drier conditions over large parts of southern Kenya, especially in the south-western section. Furthermore, changes in the monthly rainfall regime were not consistent between the two models. The results of HADCM3 suggest that those areas affected by a main rainy season from March to May will experience an increase in precipitation in March and April, but a decrease in May. Furthermore, these locations will experience a decrease in precipitation during their secondary precipitation peak in October-November. This pattern is not reproduced by ECHAM5, which shows overall a more general tendency towards wetter conditions throughout the year, with relatively large positive anomalies in the second half of the year (especially during the rainy season of October-November).

4.2 Impacts of climate change on the occurrence of drought events, and high temperatures

Datasets are also provided for the assessment of changes in the frequency of dry months, and for changes in the frequency of months with high temperatures; these can be found in Appendix 5.

For the entire region, and for both models, there is a clear increase in the number of months with very high temperatures. The increase is greater for the 'A' scenarios than for the B1 scenario, and is greater by 2050 than by 2020. An increase in the number of months with very high temperatures is indicative that there may be an increase in heat stress in the region. In the short term (2020), the increases in the number of very warm days are large even for the most optimistic B1 scenario. This suggests that increased heat stress and adaptation strategies available to cope with this, need to be addressed as a matter of urgency (see Section 4.4).

Changes in the number of dry months (i.e. months with rainfall totals less than low threshold levels) can be indicative of changes in the occurrence of dry (or drought) periods. However, as with mean precipitation, the signals of change associated with the two GCMs are not in agreement. For example, HADCM3 shows a change towards fewer dry months in the northern part of the study region, but no such change is simulated by ECHAM5. Furthermore, HADCM3 simulates an increase in the frequency of dry months in the southern region, whilst ECHAM5 shows an increase in Isiolo and Maralal. Interestingly, neither model predicts an increase in the frequency of dry months for the three most arid locations (Asayita, Kelem, and Mandera); both models actually suggest a decrease in the number of dry months in Kelem.

4.3 Effects of climate change on the discharge of the Omo River

The STREAM model was used to simulate the monthly discharge of the Omo River. Two STREAM models were set up; the first was driven by the downscaled HADCM3 climate data, and the second one was driven by the downscaled ECHAM5 data. Due to the lack of observed discharge data for the

Omo River, the set up, calibration, and validation of the model is difficult. The model was calibrated for the neighbouring Blue Nile, and the calibration parameters were then transferred to the Omo River. Hence, a direct validation of the results for the baseline period was not possible, and the results of the Omo hydrological model should be considered as tentative assessments of the possible changes in discharge which could occur.

The discharge results show little coherency between the two GCMs in terms of changes in the annual hydrograph. The HADCM3-driven model shows very little change in discharge during the long dry season (December-June), followed by a decrease in discharge during the main discharge period between July and November. In contrast, the ECHAM5-driven model shows a large increase in discharge during the first months of the year (especially January to March), and a further large increase during the peak of the high discharge season (August-September).

4.4 Effects of climate change on over-water evaporation, water quality, and groundwater

Changes in climate are expected to have further effects on a myriad of hydrological parameters around the world, including evaporation over water bodies, water quality, and groundwater levels. These parameters have not been studied in this research exercise. Given the importance of regional and local geography on them, it is therefore not possible to provide detailed assessments of the effects of climate change on them in this report. Further research would be required to quantify the effects of climate change on these parameters. However, in the following paragraphs a short summary is given of the main expected effects of climate change on these parameters at the global scale, as described by the IPCC (2008).

Evaporative demand, or 'potential evaporation', is projected to increase in most regions of the world where atmospheric temperature increases, as is projected for Kenya and Ethiopia. This is because the water-holding capacity of the atmosphere increases with higher temperatures, whilst relative humidity is not projected to change markedly on a global scale (IPCC, 2008). As a result, the water vapour deficit of the atmosphere increases, as does the evaporation rate (Trenberth et al., 2003), and given a constant availability of water, actual evaporation over open water is also projected to increase (IPCC, 2008). Since atmospheric temperature is projected to rise in the study area, an increase in open water evaporation may also occur in the region. However, more specific analyses for Ethiopia and Kenya would need to examine the projected impacts of climate change on parameters such as relative humidity, wind speeds, and pressure in the region, which are also important factors in determining the rate of evaporation.

Globally, higher water temperatures, increased precipitation intensity, and longer periods of low flows are projected to exacerbate many forms of water pollution, including an increased presence of sediments, nutrients, dissolved organic carbon, pathogens, pesticides, and salt, as well as thermal pollution. Globally, higher temperatures are likely to lower water quality in lakes through increased thermal stability and altered mixing patterns, resulting in reduced oxygen concentrations and an increased release of phosphorus from sediments. More intense rainfall could lead to an increase in suspended solids in lakes and reservoirs due to fluvial soil erosion. Projected increases in precipitation intensity are expected to lead to deteriorations in water quality, as they result in the enhanced trans-

port of pathogens and other dissolved pollutants to surface waters, which leads to the mobilisation of adsorbed pollutants. Increased occurrences of low flows may cause decreased contaminant dilution capacity, and thus higher pollutant concentrations. In areas with overall decreased runoff (such as is projected in many semi-arid areas), water quality deterioration may be even worse. In semi-arid and arid areas, climate change is likely to increase salinisation of shallow groundwater due to increased evapotranspiration.

Climate change can affect groundwater recharge rates and depths of groundwater tables. However, to date knowledge of current recharge and levels is poor, and there has been very little research on the future impact of climate change on groundwater. As many ground waters both change into and are recharged from surface water, impacts of surface water flow regimes are expected to affect groundwater. In semi-arid and arid areas, however, increased precipitation variability may increase groundwater recharge, because only high-intensity rainfalls are able to infiltrate fast enough before evaporating, and alluvial aquifers are recharged mainly by inundations due to floods (IPCC, 2008).

4.5 Implications for adaptation and planning

Whilst many activities are being carried out in the region to examine the need for measures to adapt to possible climate change, there are few recent assessments of how the climate is likely to change at the regional level. Results of GCM simulations are publicly available for the entire globe, but first need to be downscaled if they are to be of use for regional and local impact assessments. This study provides a large dataset of downscaled climate data for temperature and precipitation in the region, in both the short and medium-term. Thus, the data presented in this report can assist local stakeholders and decision-makers in assessing the expected physical effects of climate change, and therefore the need (or otherwise) for adaptive measures. Whilst this study does not provide an assessment of the impacts of these changes in various sectors (e.g. agriculture, health, energy), it does provide a wealth of climate data tailored to the regional situation which can subsequently be used as input into specific impact models for those sectors, or to develop short and medium-term plans via expert judgement and stakeholder dialogue.

The two GCMs selected to carry out this research (HADCM3 and ECHAM5) were among the best two models for the study region among those used for the AR4 of IPCC, for both temperature and precipitation, according to the 'skill-score' maps for 1961-1990 of Cai et al. (2009). For the future scenarios, both models simulate large increases in mean annual temperature and the frequency of very warm months (indicative of increased heat stress) for the entire region, including those areas already affected by adverse heat waves in the current period. Even in the short term, and under the most optimistic of the emission scenarios used (B1), the increase is very large, and suggests that increased heat wave frequency and heat stress will become a much more severe problem than at present in the near future. The clear signal presented by both models, for all scenarios and locations, suggests that urgent measures may be needed to ensure that various activities and sectors (e.g. crop growth, livestock rearing, health care, irrigation, energy supply) can adapt to these changes.

Despite the fact that both GCMs simulated past regional precipitation well, there are still large discrepancies between the results of the two models for the future scenarios in terms of changes in mean precipitation and the frequency of droughts and intense wet months. Clearly, the signal of change in

future precipitation is very uncertain. This has a number of implications. The first implications are with regards to the methods used to predict future changes in precipitation. It is well known that precipitation is much more difficult to simulate than temperature. At present, GCMs cannot accurately represent all of the physical atmospheric processes involved in the generation of precipitation. A larger number of GCMs could be used in order to compare their results for the future. However, there is no way to assess in advance which of the models will perform most accurately for the future period. Using a larger number of GCMs would also mean using models which have been proven to perform less well for the study region during the period 1961-1990. A second implication related to the use of climate models is the need for more regional climate model (RCM) simulation results for the study region. Such models are capable of resolving regional climatology more accurately than GCMs, but are computationally very demanding. Nevertheless, the development of RCMs, or making public the results of existing RCMs, could lead to a decrease in the uncertainty in predictions of future precipitation, and could therefore assist greatly in climate impact assessment.

A further implication of the high uncertainty of the precipitation data, is with regards to the response of stakeholders and decision-makers to that uncertainty. A possible reaction to the existing uncertainty is the tendency to 'wait and see', in which stakeholders and decision-makers delay developing plans until more clear information is available. However, the possible impacts associated with the potential changes in climate (e.g. increased droughts, flash floods, etc.) are so detrimental that early planning is still preferable under the precautionary principle. Furthermore, adaptation measures can be sought which provide benefits under a wide range of future scenarios. For example, more efficient irrigation techniques to reduce evaporative water losses may be essential if the frequency of droughts increases in areas such as the southern Ethiopian lowlands. However, such schemes can be designed in ways that they also provide benefits even if such an increase in drought frequency should not materialise (e.g. more availability of water for drinking, increased yields, reduced water costs, etc.). Therefore, the results of this study show that stakeholders and decision-makers need to consider robust management options to tackle both increasing drought frequency, and an increasing frequency of high rainfall events.

Anticipating the effects of climate change on the discharge of the Omo River is particularly difficult. This is firstly, due to the uncertain projections of changes in precipitation, but also due to the lack of observed discharge data for that river. The uncertain projections of future precipitation change, render projections of Omo river discharge highly uncertain. Nevertheless, despite the fact that HADCM3 simulates hardly any change in mean dry season discharge, and a large decrease in mean wet season discharge, the same model does suggest that there will be more months with both low and high flows. This suggests that the extremes of river discharge may increase, necessitating measures to preserve minimum flows in the dry season and protect against flooding during the wet season. Moreover, in order to monitor changes in the discharge of the river over time, and to provide data which can be used to set up and validate new hydrological models, discharge gauging stations need to be set up to measure long term patterns and changes in discharge.

Finally, given the uncertainties surrounding the changes in precipitation, a useful recommendation for regional adaptation is to provide long-range seasonal weather forecasts, and to promote the dissemination of such information. A long-range seasonal weather forecast allows farmers to make informed decisions on which crops and/or species to plant in the forthcoming growing season, and can allow health sector workers to anticipate climate-related health problems (and therefore the treat-

ments required) prior to onset of problems. Furthermore, medium-term river discharge projections could then be made which would allow for early warning systems in the event of flooding, and better forward planning of reservoir levels for electricity generation.

References

Aerts, J.C.J.H. & Bouwer, L.M. (2002a). *STREAM Perfume Vietnam – Updates and analyses.* IVM Report (R-02/06). Amsterdam, The Netherlands, VU University, Institute for Environmental Studies.

Aerts, J.C.J.H. & Bouwer, L.M. (2002b). *STREAM Krishna. A hydrological model for the Krishna River in India.* The Hague, The Netherlands, RIKZ/Coastal Zone Management Centre.

Aerts, J.C.J.H., Kriek, M. & Schepel, M. (1999)**.** STREAM (Spatial Tools for River Basins and Environment and Analysis of Management Options): 'Set Up and Requirements'. *Physics and Chemistry of the Earth, Part B: Hydrology, Oceans and Atmosphere*, 24(6), 591-595, doi: 510.1016/S1464-1909(1099)00049-00040.

Aerts, J.C.J.H., Renssen, H., Ward, P.J., De Moel, H., Odada, E., Bouwer, L.M. & Goosse, H. (2006). Sensitivity of global river discharges under Holocene and future climate conditions. *Geophysical Research Letters, 33*, L19401, doi: 19410.11029/12006GL027493.

Arnell, N.W., Bates, B., Lang, H., Magnuson, J.J., Mulholland, P., Fisher, S., Liu, C., McKnight, D., Starosolszky, O., Taylor, M., Aquize, E., Arnott, S., Brakke, D., Braun, L., Chalise, S., Chen, C., Folt, C.L., Gafny, S., Hanaki, K., Hecky, R., Leavesley, G.H., Lins, H., Nemec, J., Ramasastri, K.S., Somlyódy, L. & Stakhiv, E., 1996. Hydrology and freshwater ecology. In: Watson, R.T., Zinyowera, M.C., Moss, R.H. (Eds.), *Climate Change 1995: Impacts, Adaptations and Mitigation of Climate Change: Scientific-Technical Analyses. Contribution of Working Group II to the Second Assessment Report of the Intergovernmental Panel on Climate Change* (pp. 325-363) Cambridge, U.K , Cambridge University Press.

Bárdossy, A., 2007. Calibration of hydrological model parameters for ungauged catchments. *Hydrology and Earth System Science*s, 11, 703-710, www.hydrol-earth-syst-sci.net/11/703/2007/.

Bouwer, L.M., Aerts, J.C.J.H., Droogers, P. & Dolman, A.J. (2006). Detecting the long-term impacts from climate variability and increasing water consumption on runoff in the Krishna river basin (India). *Hydrology and Earth System Sciences, 10*, 703-713, www.hydrol-earth-syst-sci.net/710/703/2006/.

Bouwer, L.M., Aerts, J.C.J.H., Coterlet, G.M. van de, Giesen, N. van de, Gieske, A. & Mannaerts, C. (2004). Evaluating downscaling methods for preparing Global Circulation Model (GCM) data for hydrological impact modelling. In Aerts, J.C.J.H. & Droogers, P. (Eds.), *Climate Change in Contrasting River Basins. Adaptation Strategies for Water, Food and Environment* (pp. 25-27). Wallingford, U.K., CABI Publishing.

Cai, X., Wang, D., Zhu, T. & Ringler, C. (2009). Assessing the regional variability of GCM simulations. *Geophysical Research Letters, 36*, L02706, doi: 10.1029/2008GL036443.

Cocke, S. & LaRow, T.E. (2000). Seasonal predictions using a regional spectral model embedded within a coupled ocean-atmosphere model. *Monthly Weather Review*, *128*(3), 689-708.

IPCC (2000). *Special Report on Emission Scenarios.* New York, U.S.A.: Cambridge University Press.

IPCC (2007). Climate Change 2007. *The Physical Science Basis. Contribution of Working Group I to the Fourth Assessment Report of the Intergovernmental Panel on Climate Change.* New York, U.S.A: Cambridge University Press.

IPCC (2008). *Climate Change and Water. Technical Paper of the Intergovernmental Panel on Climate Change.* Geneva, Switzerland, IPCC Secretariat, 210 pp.

Kim, J., Miller, N.L., Farrara, J.D. & Hong, S.-Y. (2000). A seasonal precipitation and stream flow hindcast and prediction study in the western United States during the 1997/98 winter season using a dynamic downscaling system. *Journal of Hydrometeorology*, 1(4), 311-329, doi: 310.1175/1525-7541(2000)1001<0311:ASPASF>1172.1170.CO;1172.

Kleinn, J., Frei, C., Gurtz, J., Lüthi, D., Vidale, P.L. & Schär, C. (2005). Hydrologic simulations in the Rhine basin driven by a regional climate model. *Journal of Geophysical Research, 110*, D04102, doi: 04110.01029/02004JD005143.

Kwadijk, J.C.J. (1993). *The impact of climate change on the discharge of the River Rhine*. Ph.D. thesis, Utrecht, The Netherlands, Utrecht University, 201 pp.

Lasage, R. and Vries & A. de (2008) *Mission report Ethiopie: Borona Zone – ADAPTS inception phase.* IVM Report (W08-26). Amsterdam, The Netherlands, VU University, Institute for Environmental Studies.

Mitchell, T.D. & Jones, P.D. (2005). An improved method of constructing a database of monthly climate observations and associated high-resolution grids. *International Journal of Climatology, 25*, 693-712, doi: 610.1002/joc.1181.

Murphy, J. (2000). Predictions of climate change over Europe using statistical and dynamical downscaling techniques. *International Journal of Climatology, 20*(5), 489-501, doi: 410.1002/(SICI)1097-0088(200004)200020:200005<200489::AID-JOC200484>200003.200000.CO;200002-200006.

Nash, J.E. & Sutcliffe, J.V. (1970). River flow forecasting through conceptual models part I - A discussion of principles. *Journal of Hydrology, 10*(3), 282-290, doi: 210.1016/0022-1694(1070)90255-90256.

New, M., Lister, D., Hulme, M. & Makin, I. (2002). A high-resolution data set of surface climate over global land areas. *Climate Research, 21*, 1-25.

Thornthwaite, C.W. (1948). An approach toward a rational classification of climate. *Geographical Review, 38*(1), 55-94.

Thornthwaite, C.W. & Mather, J.R. (1957). Instructions and tables for computing potential evapotranspiration and the water balance. Publications in *Climatology*, 10, 183-243.

Trenberth, K.E., Dai, A.G., Rasmussen, R.M. & Parsons, D.B. (2003). The changing character of precipitation. *Bulletin of the American Meteorological Society, 84*, 1205-1217.

Van Deursen, W.P.A. & Kwadijk, J.C.J. (1994a). In Kovar, K. & Nachtnebel, H.P. (Eds.), *RHINEFLOW: an integrated GIS water balance model for the River Rhine* (pp. 507-519). Paper presented at the Application of Geographic Information Systems in Hydrology and Water Resources Management. Proceedings of the conference HYDROGIS '93. IHAS publication no. 211, Vienna, Austri.

Van Deursen, W.P.A. & Kwadijk, J.C.J. (1994b). *The impacts of climate change on the water balance of the Ganges-Brahmaputra and Yangtze basin*. Report number RA/94-160. Delft, The Netherlands, Resource Analysis.

Vörösmarty, C.J., Fekete, B.M. & Tucker, B.A. (1998). *Global River Discharge, 1807-1991, V[ersion] 1.1 (RivDis).* Oak Ridge, Tennessee, U.S.A, Oak Ridge National Laboratory Distributed Active Archive Center.

Ward, P.J., Aerts, J.C.J.H., De Moel, H., Renssen, H. (2007). Verification of a coupled climate-hydrological model against Holocene palaeohydrological records. *Global and Planetary Change, 57*(3-4), 283-300, doi: 210.1016/j.gloplacha.2006.1012.1002.

Wilby, R.L., Hay, L.E., Gutowski Jr., W.J., Arritt, R.W., Takle, E.S., Pan, Z., Leavesley, G.H. & Clark, M.P. (2000). Hydrological responses to dynamically and statistically downscaled climate model output. *Geophysical Research Letters, 27*(8), 1199-1202.

Wilby, R.L. & Wigley, T.M.L. (1997). Downscaling general circulation model output: a review of methods and limitations. *Progress in Physical Geography*, 21(4), 530-548, doi:510.1177/030913339702100403.

Wilby, R.L., Wigley, T.M.L., Conway, D., Jones, P.D., Hewitson, B.C., Main, J. & Wilks, D.S. (1998). Statistical downscaling of general circulation model output: A comparison of methods. *Water Resources Research, 34*(11), 2995-3008.

Wood, A.W., Leung, L.R., Sridhar, V. & Lettenmaier, D.P. (2004). Hydrologic implications of dynamical and statistical approaches to downscaling climate model outputs. *Climatic Change, 62*(1-3), 189-216, doi: 110.1023/B:CLIM.0000013685.0000099609.0000013689e.

Wood, A.W., Maurer, E.P., Kumar, A. & Lettenmaier, D.P. (2002). Long-range experimental hydrologic forecasting for the eastern United States. *Journal of Geophysical Research, 107*(D20), 4429, doi: 4410.1029/2001JD000659.

Yarnal, B., Lakhtakia, M.N., Yu, Z., White, R.A., Pollard, D., Miller, D.A. & Lapenta, W.M. (2000). A linked meteorological and hydrological model system: The Susquehanna River Basin Experiment (SRBEX). *Global and Planetary Change, 25*(1-2), 149-161, doi: 110.1016/S0921-8181(1000)00026-00026.

Appendices

Appendix 1: Maps showing mean annual precipitation and temperature for the periods 2020 and 2050

Appendix 1a Spatially distributed mean annual precipitation (mm)

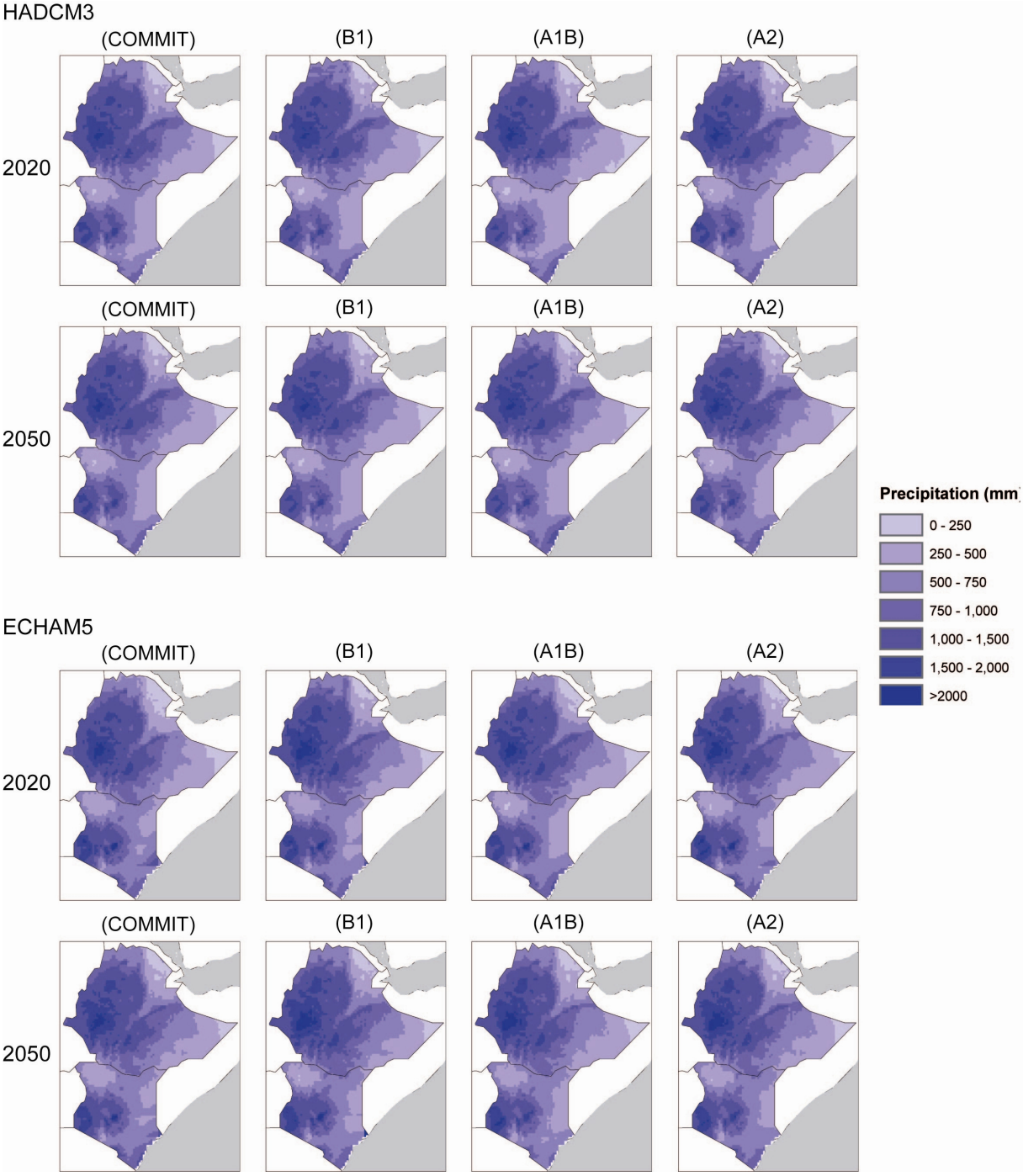

Appendix 1b Spatially distributed mean annual temperature (°C)

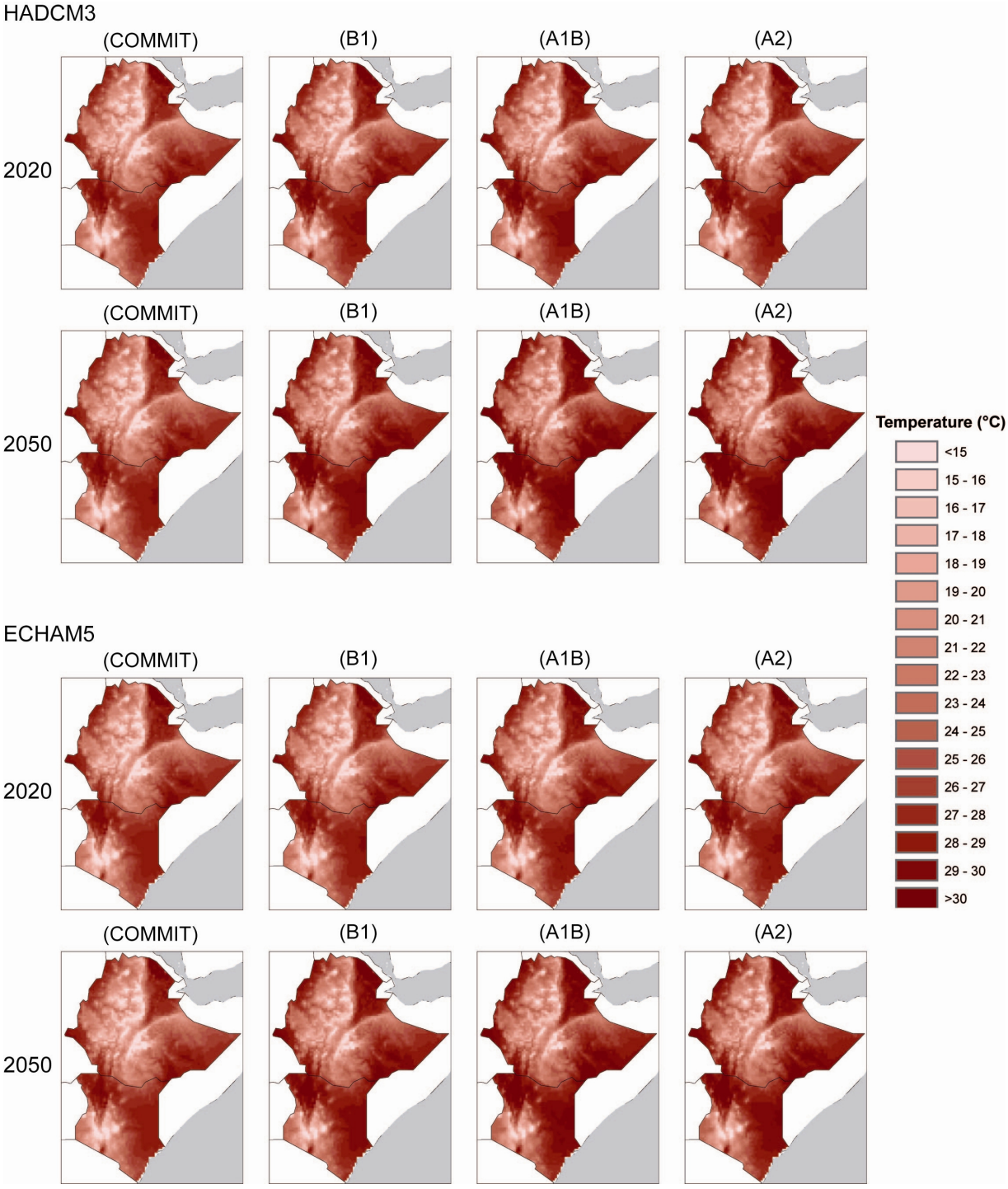

Appendix 2: Maps showing the spatial anomalies in mean annual precipitation and temperature between the baseline period, and the future scenarios (scenario - baseline)

Appendix 2a Anomaly of mean annual precipitation (scenario - baseline period 1961-1990)

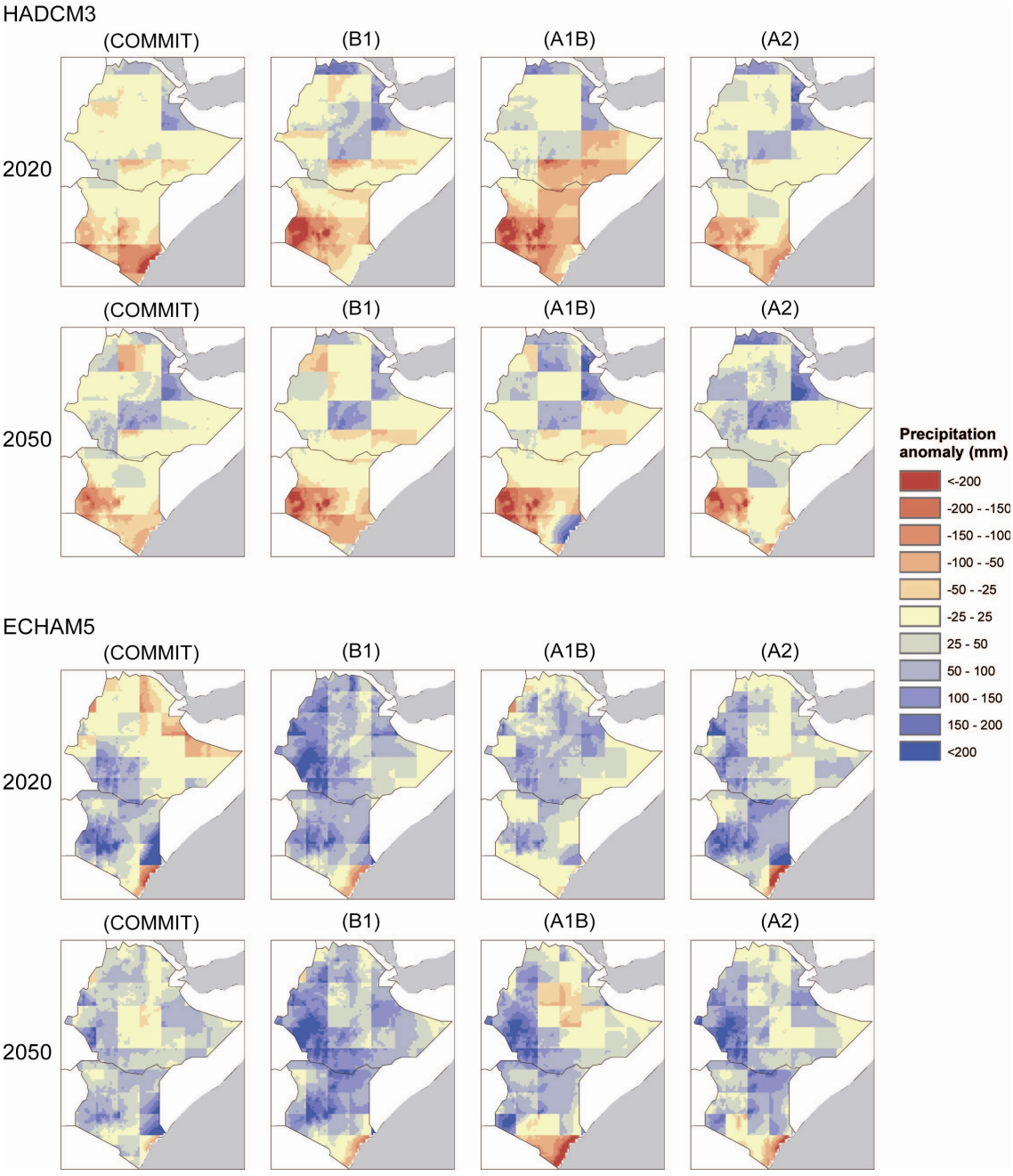

Appendix 2b Anomaly of mean annual temperature (scenario – baseline period 1961-1990)

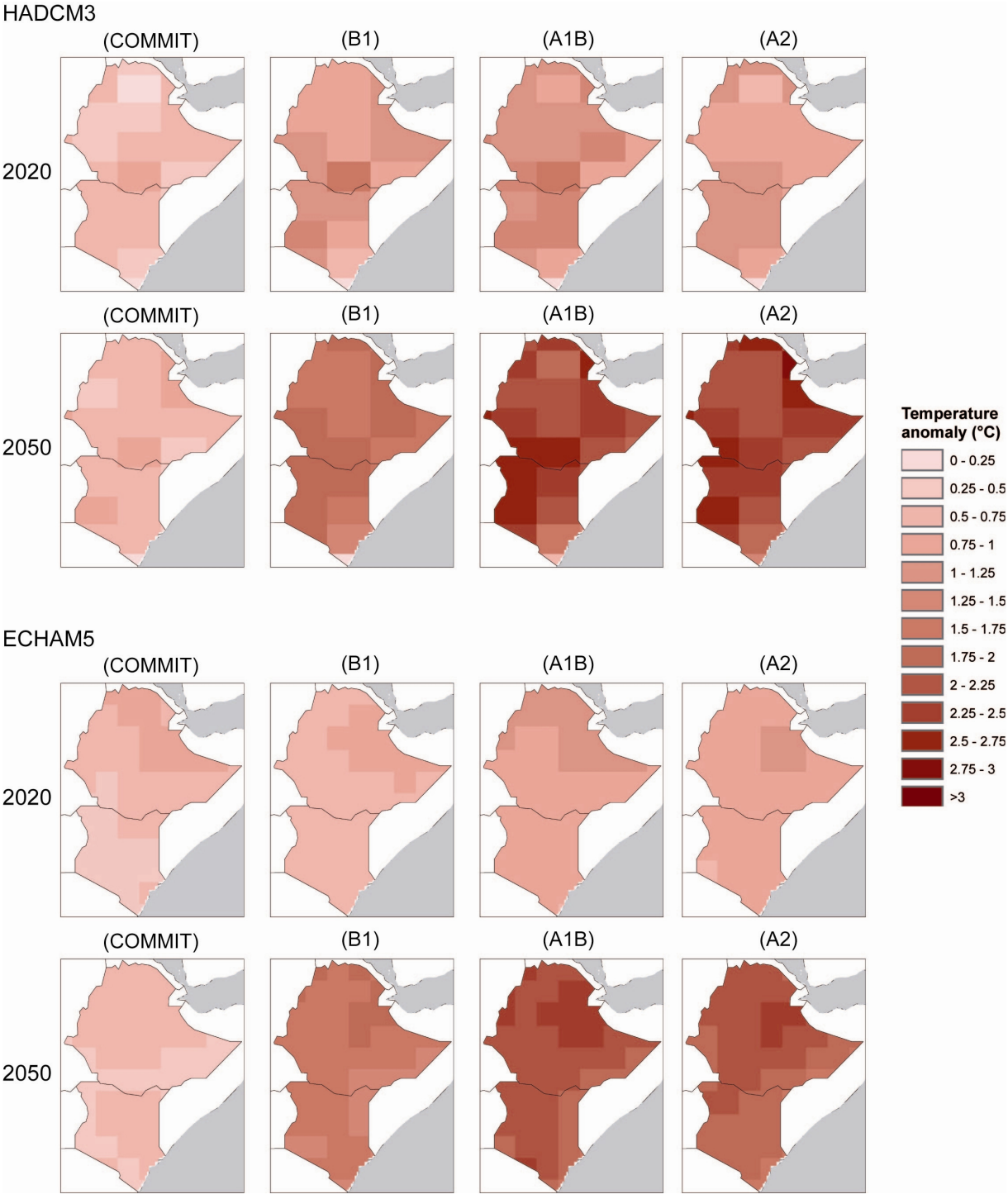

Appendix 3: Graphs showing change in precipitation between the baseline period, 2020, and 2050, and trends in precipitation over the period 1900-2100

Appendix 3.1 HADCM3 – Moyale - Precipitation

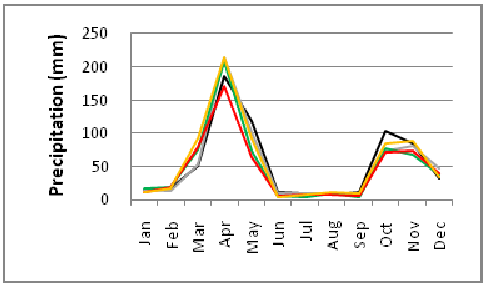

3.1a Mean monthly precipitation - 2020

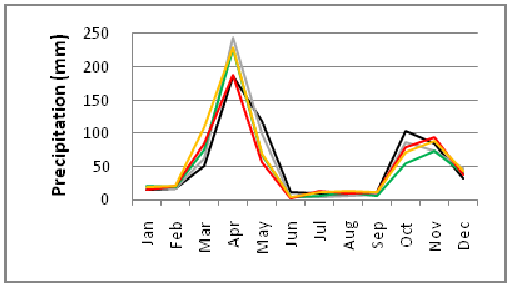

3.1b Mean monthly precipitation - 2050

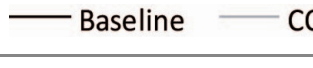

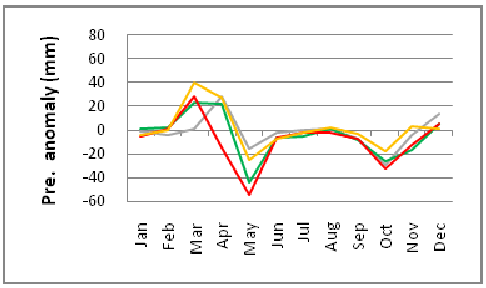

3.1c Precipitation anomaly (2020 – baseline)

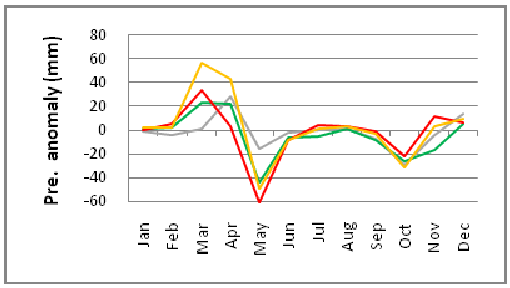

3.1d Precipitation anomaly (2050 – baseline)

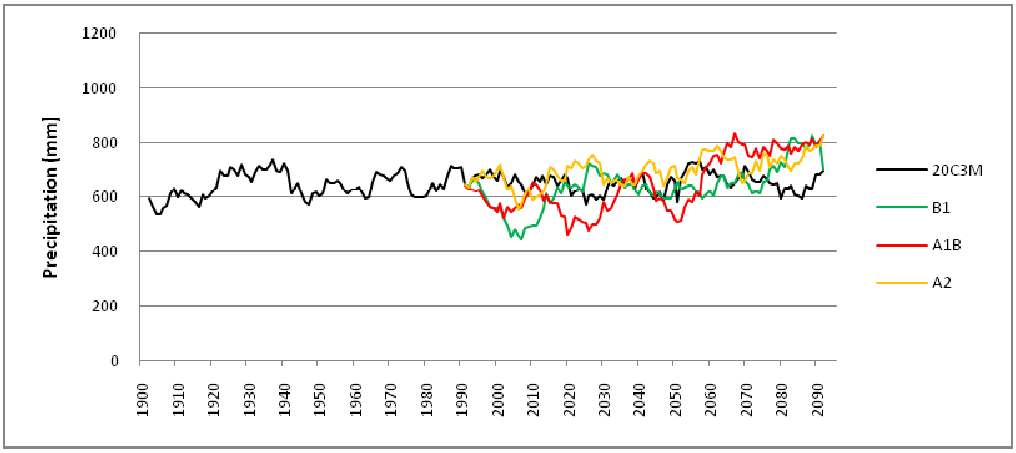

3.1e Mean annual precipitation, 1901-2100 (10-yr running mean)

Appendix 3.2 ECHAM5 – Moyale - Precipitation

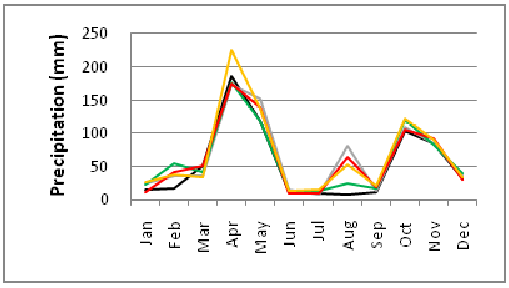

3.2a Mean monthly precipitation - 2020

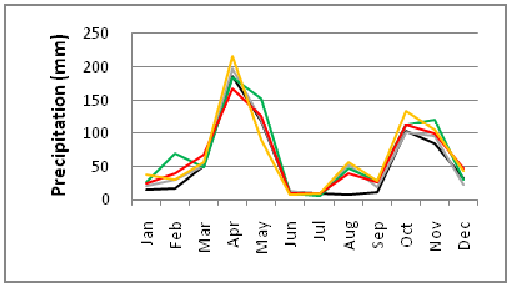

3.2b Mean monthly precipitation - 2050

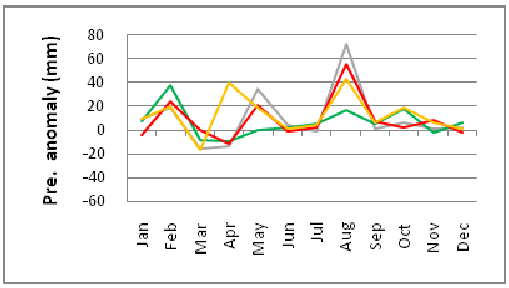

3.2c Precipitation anomaly (2020 – baseline)

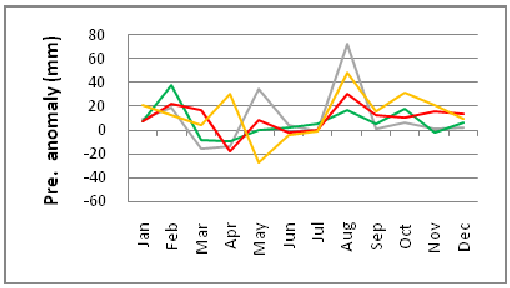

3.2d Precipitation anomaly (2050 – baseline)

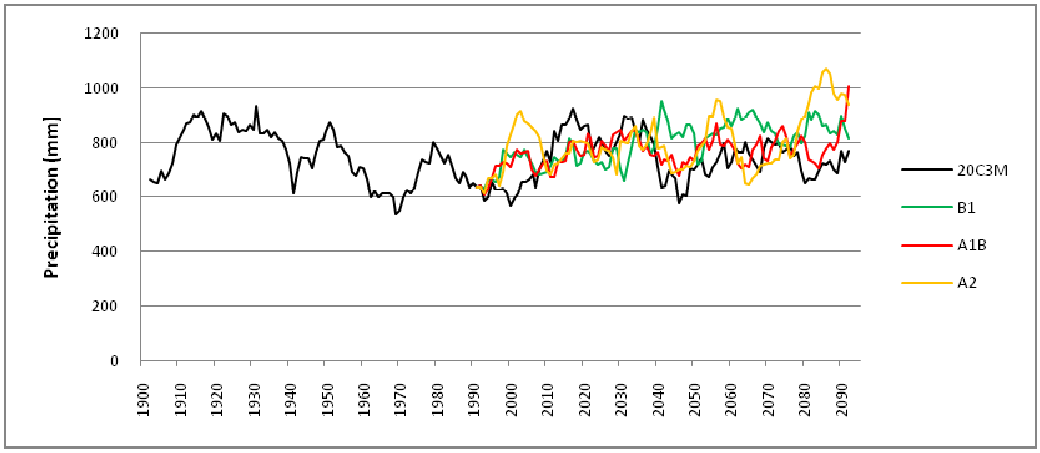

3.2e Mean annual precipitation, 1901-2100 (10-yr running mean)

Appendix 3.3 HADCM3 – Mandera - Precipitation

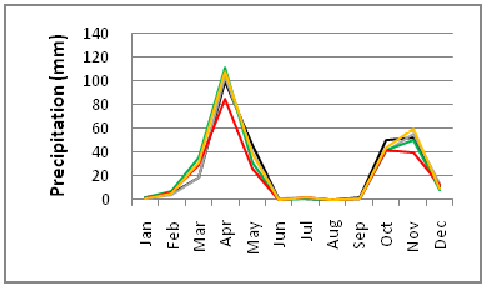

3.3a Mean monthly precipitation - 2020

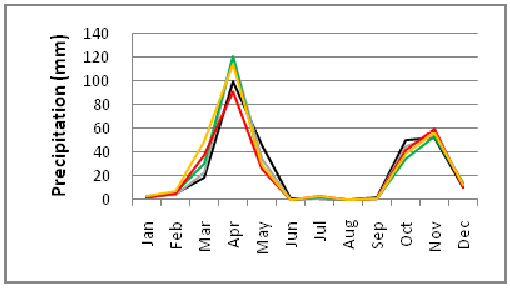

3.3b Mean monthly precipitation - 2050

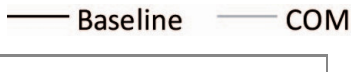

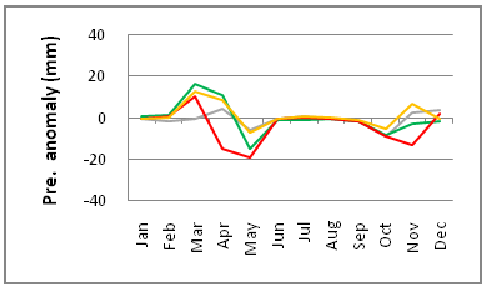

3.3c Precipitation anomaly (2020 – baseline)

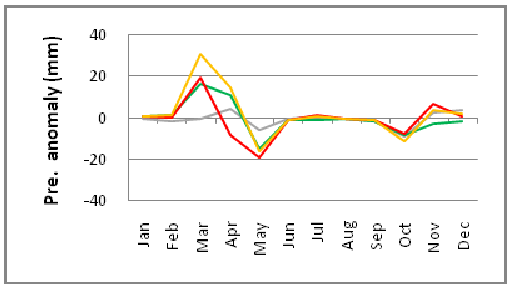

3.3d Precipitation anomaly (2050 – baseline)

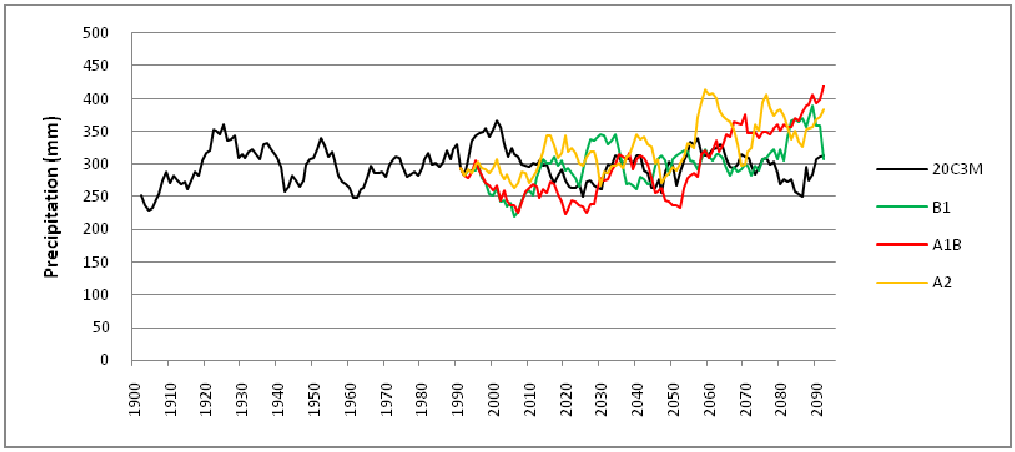

3.3e Mean annual precipitation, 1901-2100 (10-yr running mean)

Appendix 3.4 ECHAM5 – Mandera - Precipitation

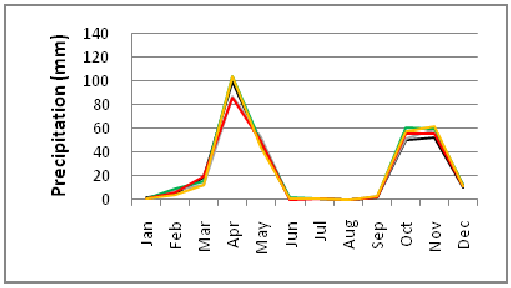

3.4a Mean monthly precipitation - 2020

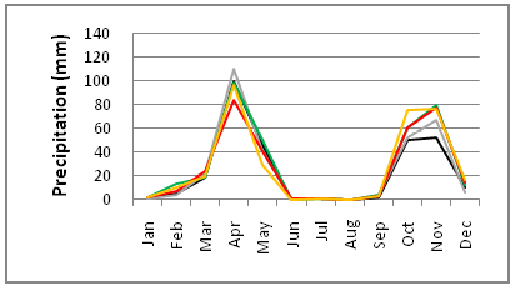

3.4b Mean monthly precipitation - 2050

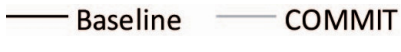

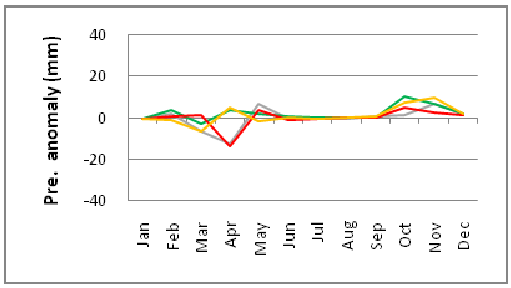

3.4c Precipitation anomaly (2020 – baseline)

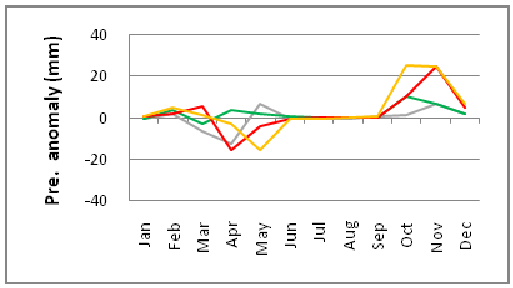

3.4d Precipitation anomaly (2050 – baseline)

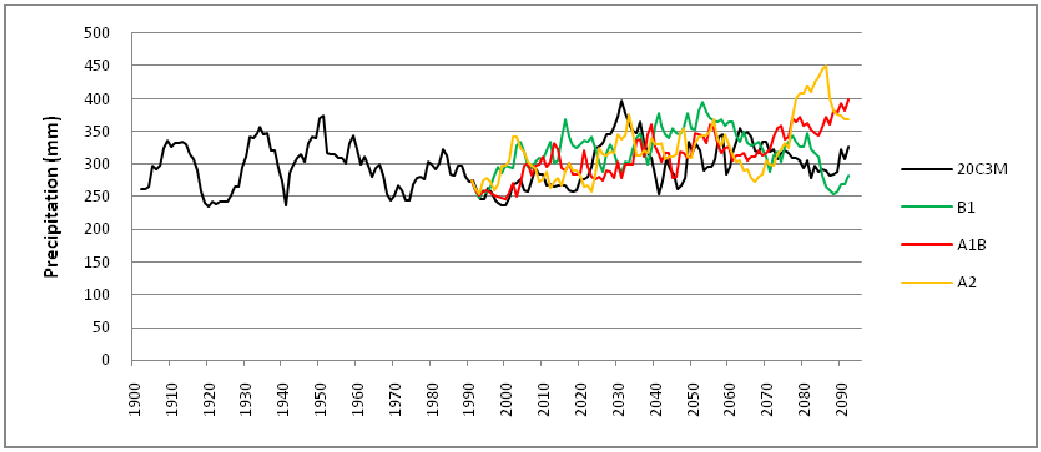

3.4e Mean annual precipitation, 1901-2100 (10-yr running mean)

Appendix 3.5 HADCM3 – Marsabit - Precipitation

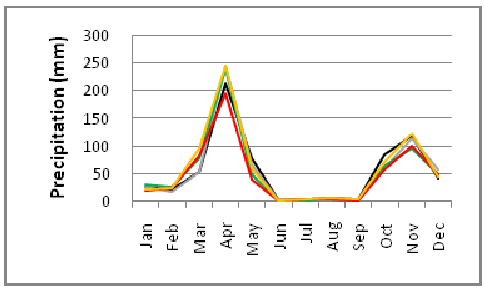

3.5a Mean monthly precipitation - 2020

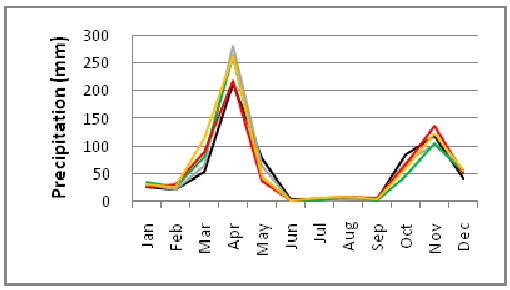

3.5b Mean monthly precipitation - 2050

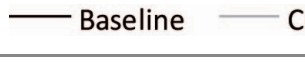

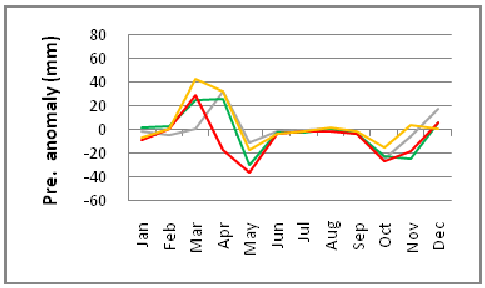

3.5c Precipitation anomaly (2020 – baseline)

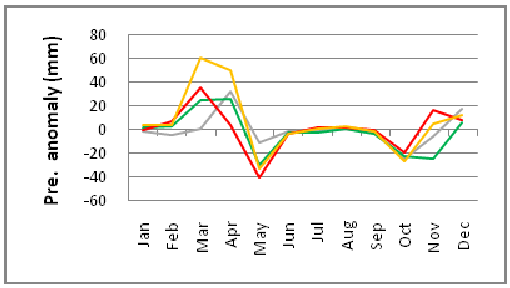

3.5d Precipitation anomaly (2050 – baseline)

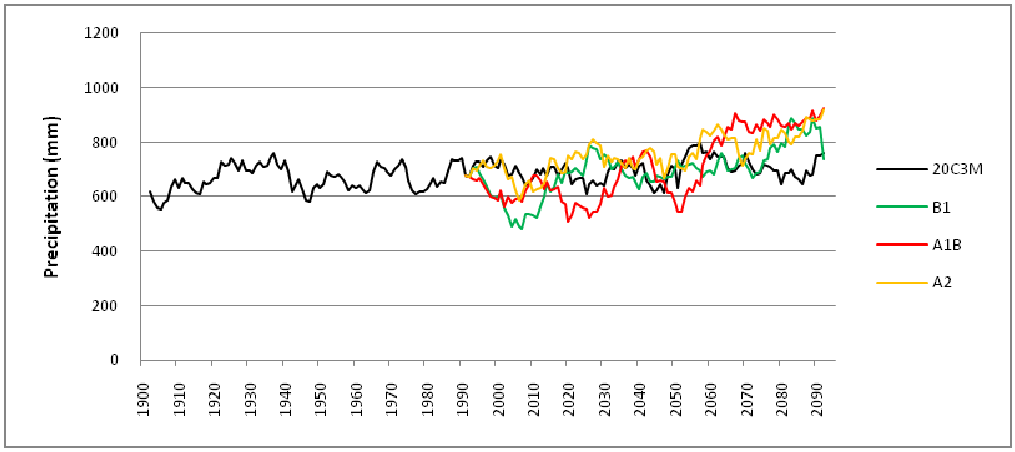

3.5e Mean annual precipitation, 1901-2100 (10-yr running mean)

Appendix 3.6 ECHAM5 – Marsabit - Precipitation

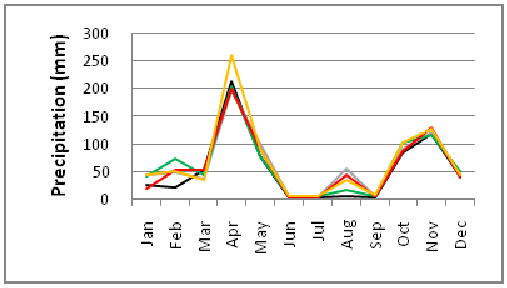

3.6a Mean monthly precipitation - 2020

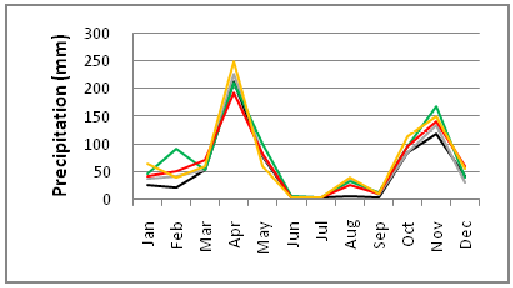

3.6b Mean monthly precipitation - 2050

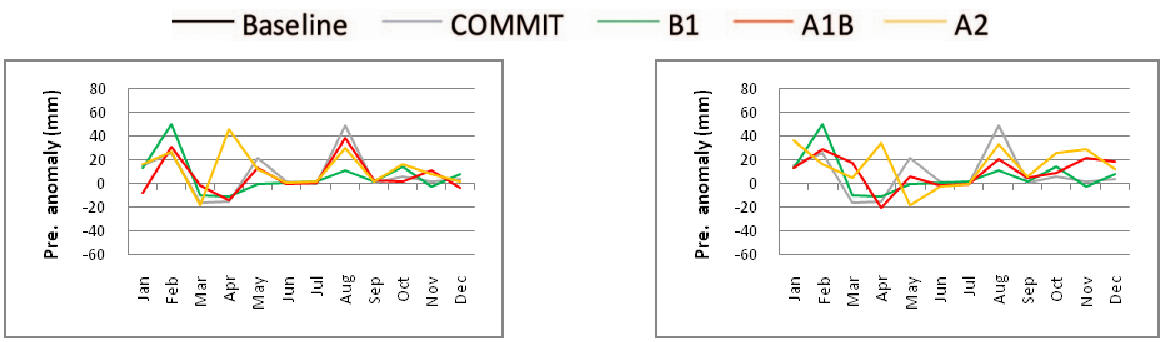

3.6c Precipitation anomaly (2020 – baseline)

3.6d Precipitation anomaly (2050 – baseline)

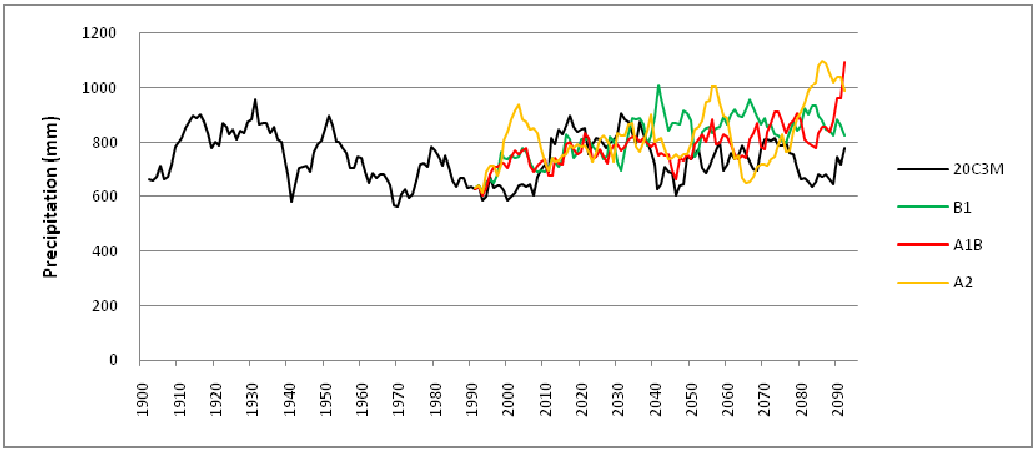

3.6e Mean annual precipitation, 1901-2100 (10-yr running mean)

Appendix 3.7 HADCM3 – Maralal - Precipitation

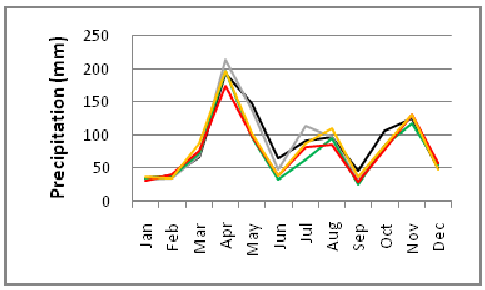

3.7a Mean monthly precipitation - 2020

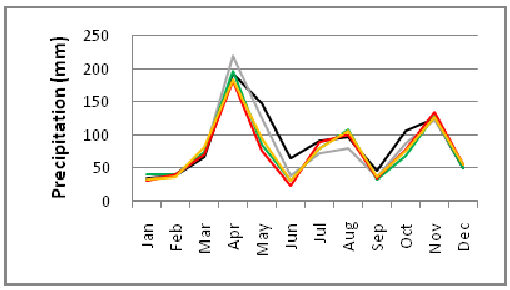

3.7b Mean monthly precipitation - 2050

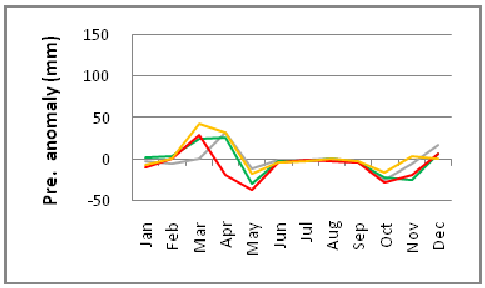

3.7c Precipitation anomaly (2020 – baseline)

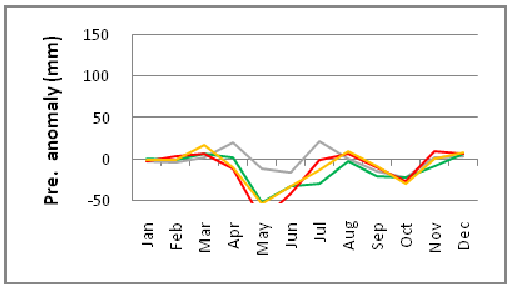

3.7d Precipitation anomaly (2050 – baseline)

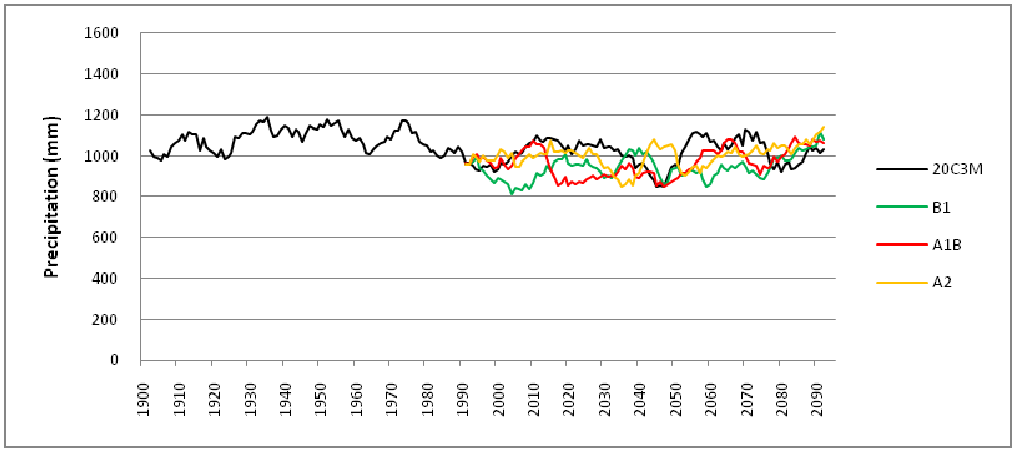

3.7e Mean annual precipitation, 1901-2100 (10-yr running mean)

Appendix 3.8 ECHAM5– Maralal - Precipitation

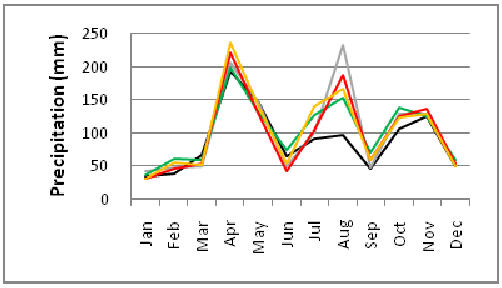

3.8a Mean monthly precipitation - 2020

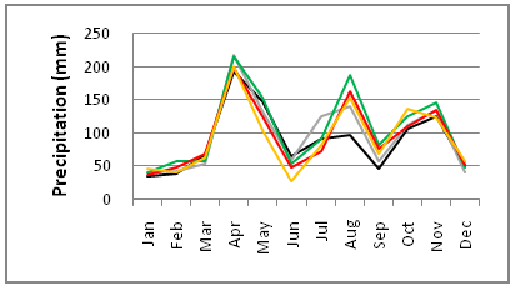

3.8b Mean monthly precipitation - 2050

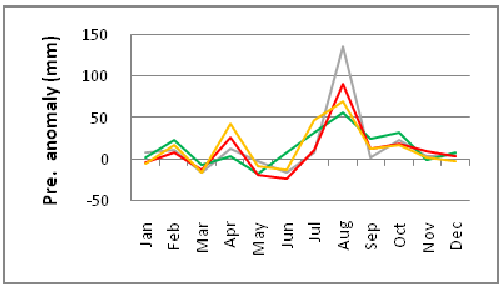

3.8c Precipitation anomaly (2020 – baseline)

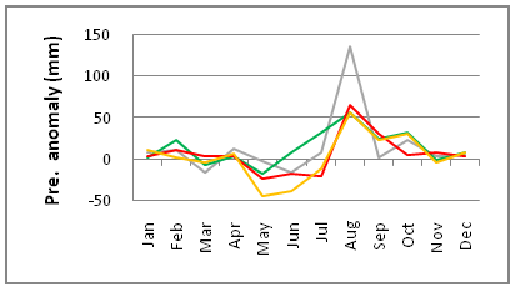

3.8d Precipitation anomaly (2050 – baseline)

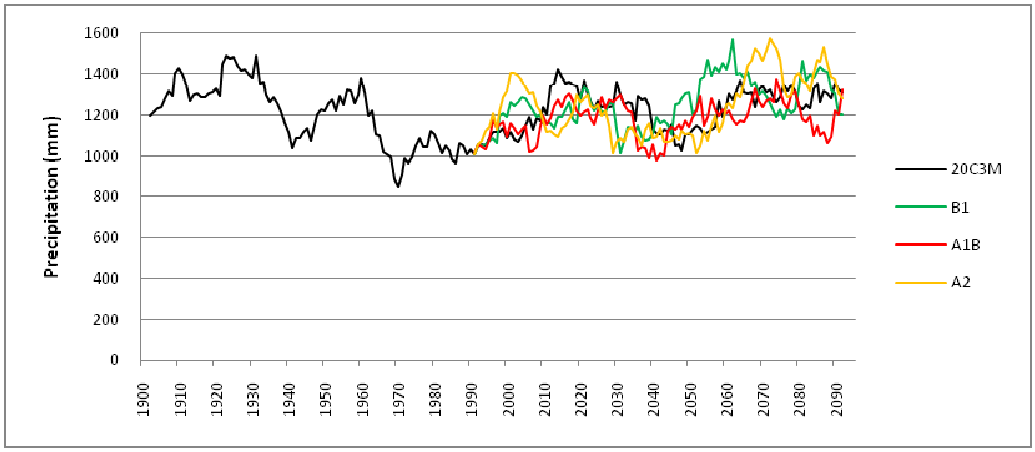

3.8e Mean annual precipitation, 1901-2100 (10-yr running mean)

Appendix 3.9 HADCM3 – Isiolo - Precipitation

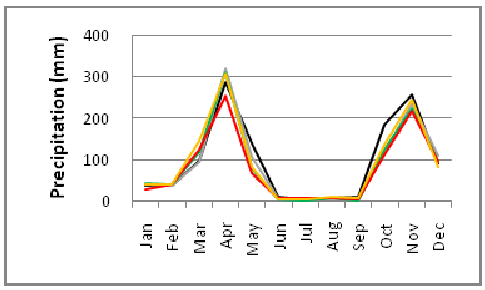

3.9a Mean monthly precipitation - 2020

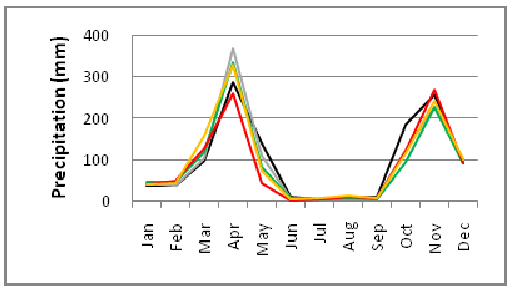

3.9b Mean monthly precipitation - 2050

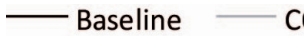

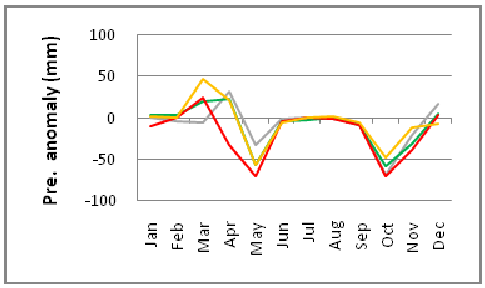

3.9c Precipitation anomaly (2020 – baseline)

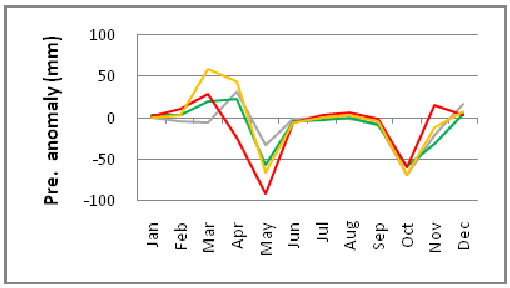

3.9d Precipitation anomaly (2050 – baseline)

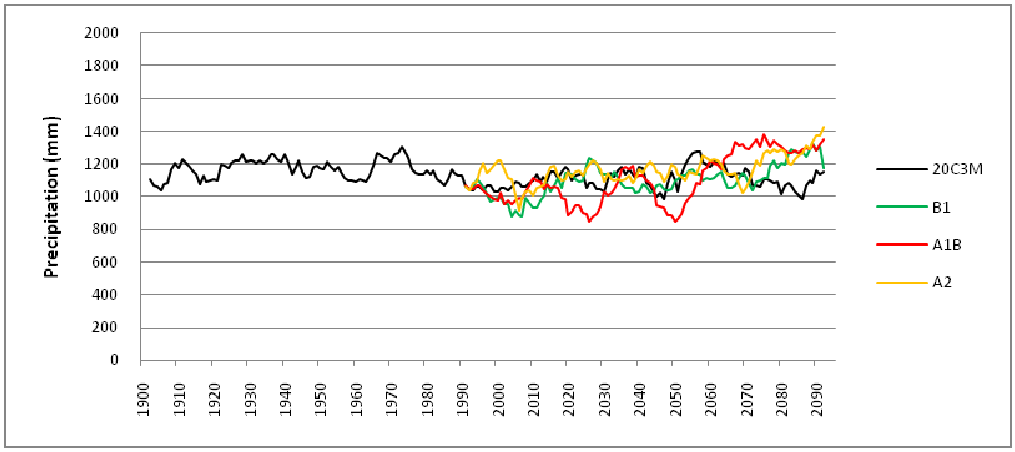

3.9e Mean annual precipitation, 1901-2100 (10-yr running mean)

Appendix 3.1 ECHAM5– Isiolo - Precipitation

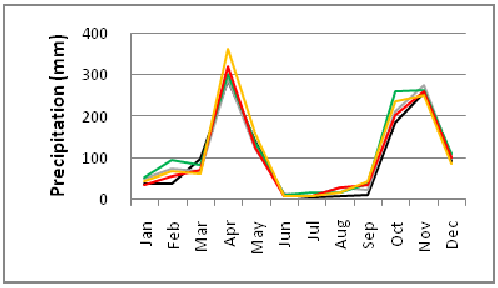

3.10a Mean monthly precipitation - 2020

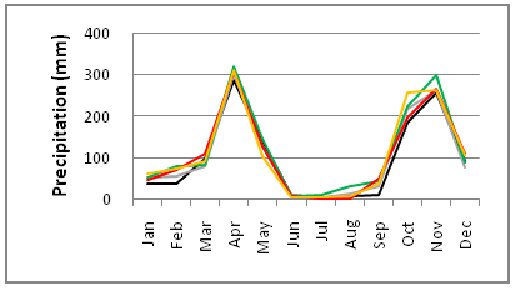

3.10b Mean monthly precipitation - 2050

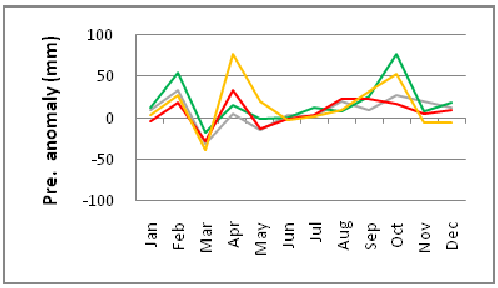

3.10c Precipitation anomaly (2020 – baseline)

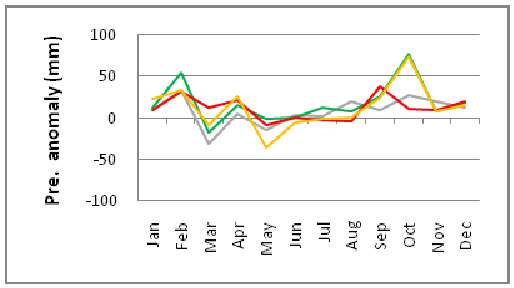

3.10d Precipitation anomaly (2050 – baseline)

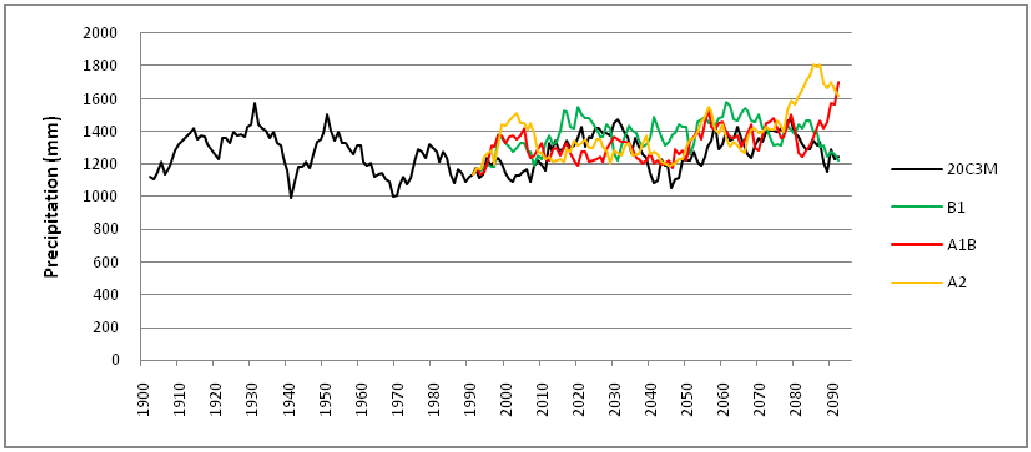

3.10e Mean annual precipitation, 1901-2100 (10-yr running mean)

Appendix 3.11 HADCM3 – Nairobi - Precipitation

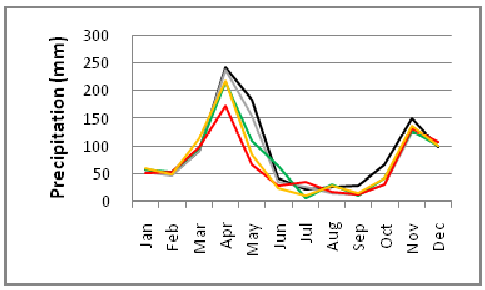

3.11a Mean monthly precipitation - 2020

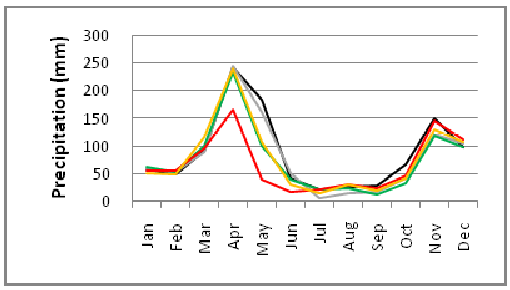

3.11b Mean monthly precipitation - 2050

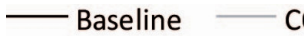

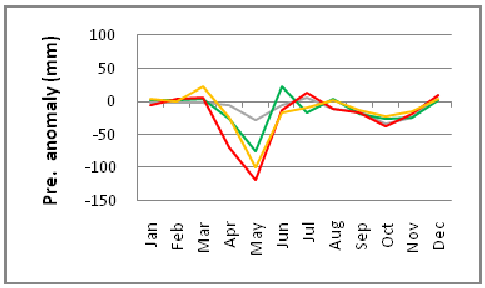

3.11c Precipitation anomaly (2020 – baseline)

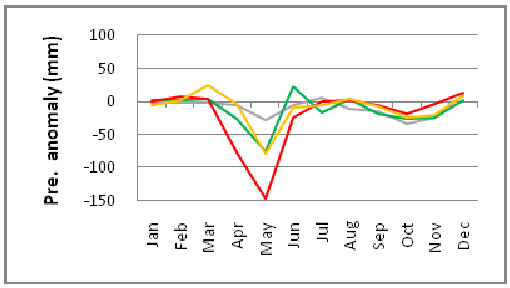

3.11d Precipitation anomaly (2050 – baseline)

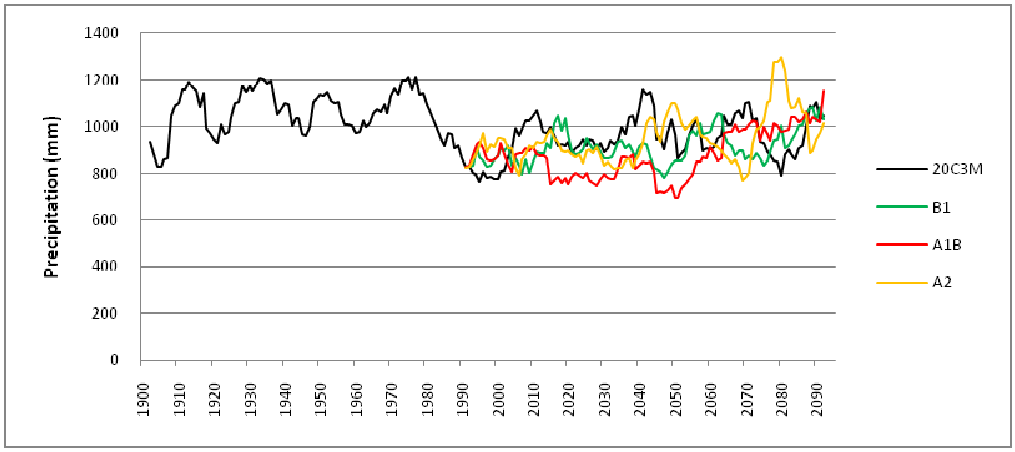

3.11e Mean annual precipitation, 1901-2100 (10-yr running mean)

Appendix 3.12 ECHAM5– Nairobi - Precipitation

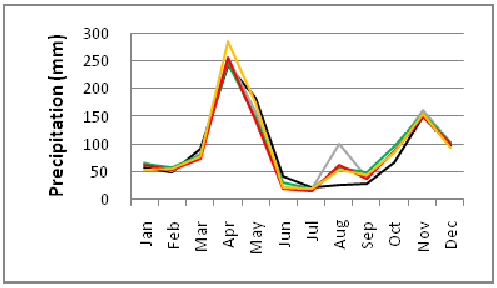

3.12a Mean monthly precipitation - 2020

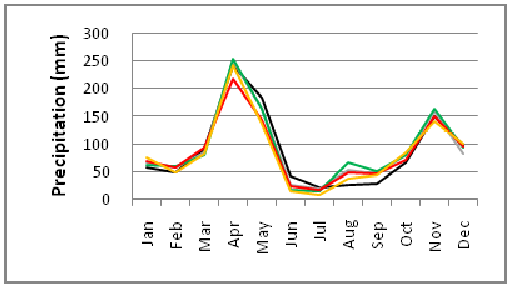

3.12b Mean monthly precipitation - 2050

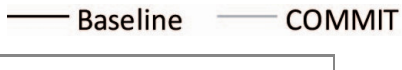

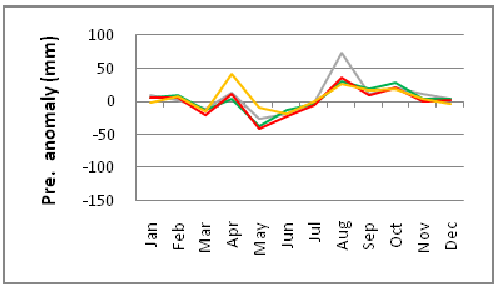

3.12c Precipitation anomaly (2020 – baseline)

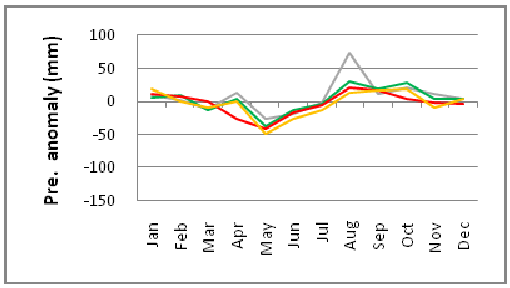

3.12d) Precipitation anomaly (2050 – baseline)

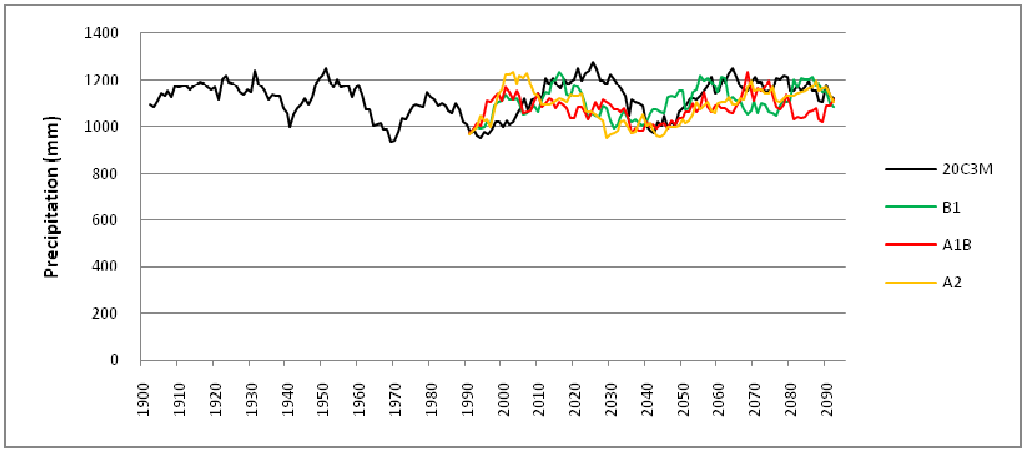

3.12e Mean annual precipitation, 1901-2100 (10-yr running mean)

Appendix 3.13 HADCM3 – Awasa - Precipitation

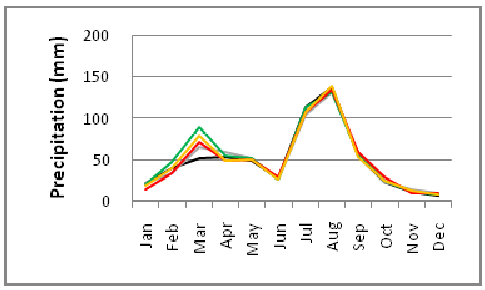

3.13a Mean monthly precipitation - 2020

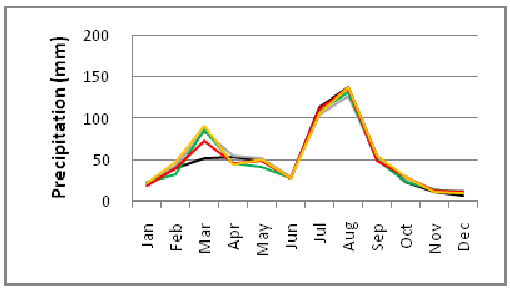

3.13b Mean monthly precipitation - 2050

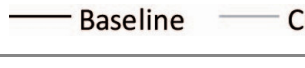

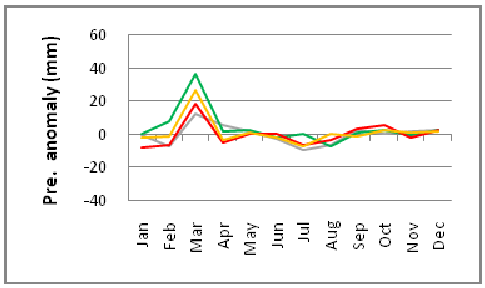

3.13c Precipitation anomaly (2020 – baseline)

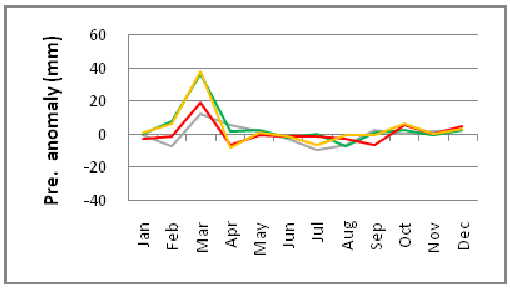

3.13d Precipitation anomaly (2050 – baseline)

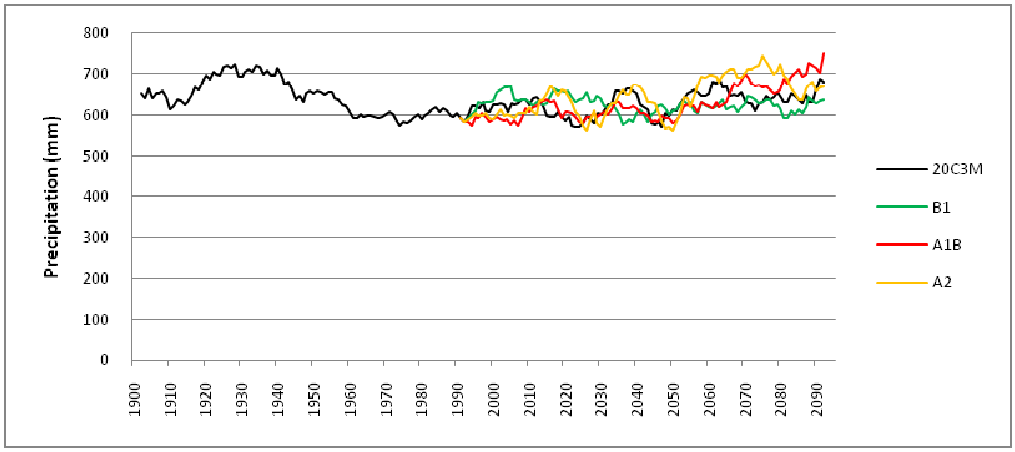

3.13e Mean annual precipitation, 1901-2100 (10-yr running mean)

Appendix 3.14 ECHAM5– Awasa - Precipitation

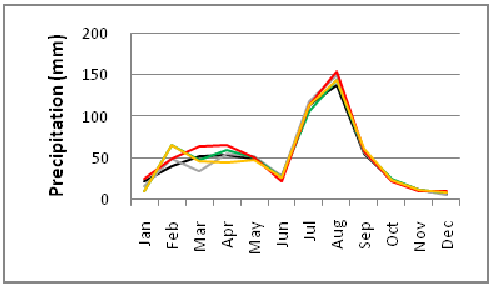

3.14a Mean monthly precipitation - 2020

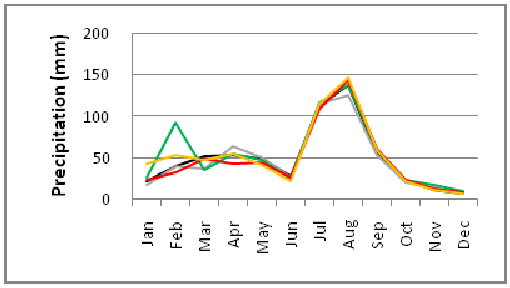

3.14b Mean monthly precipitation - 2050

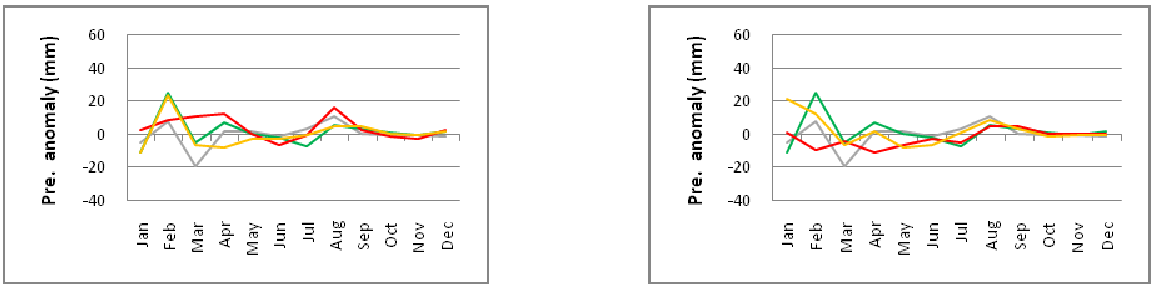

3.14c Precipitation anomaly (2020 – baseline)

3.14d Precipitation anomaly (2050 – baseline)

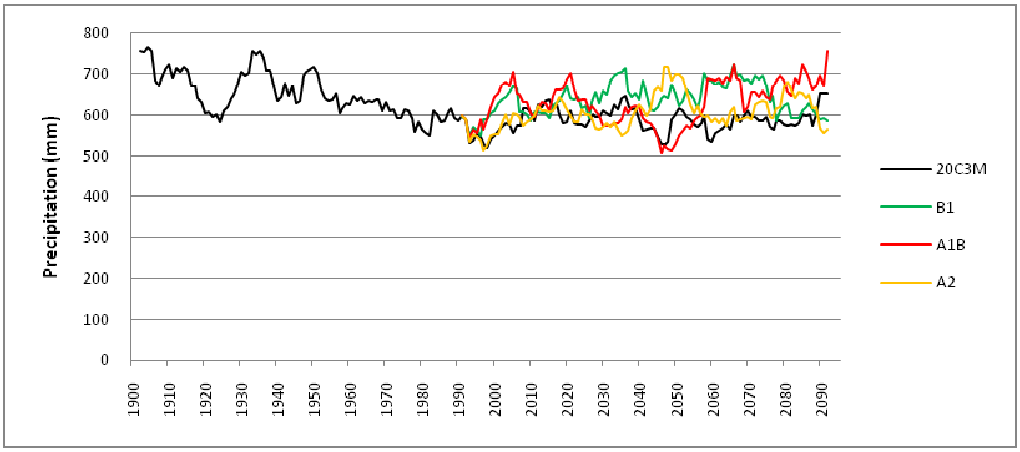

3.14e Mean annual precipitation, 1901-2100 (10-yr running mean)

Appendix 3.15 HADCM3 – Kelem - Precipitation

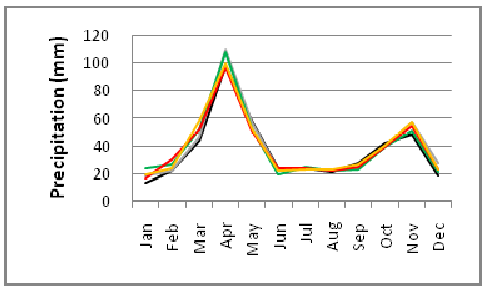

3.15a Mean monthly precipitation - 2020

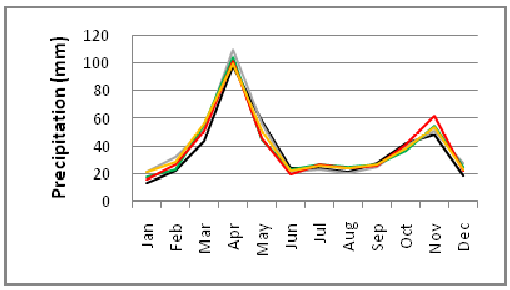

3.15b Mean monthly precipitation - 2050

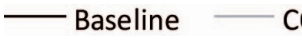

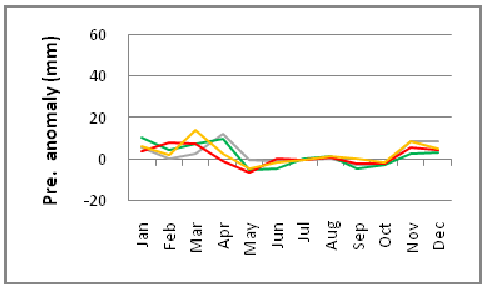

3.15c Precipitation anomaly (2020 – baseline)

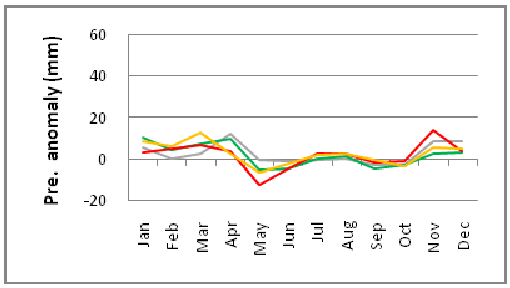

3.15d Precipitation anomaly (2050 – baseline)

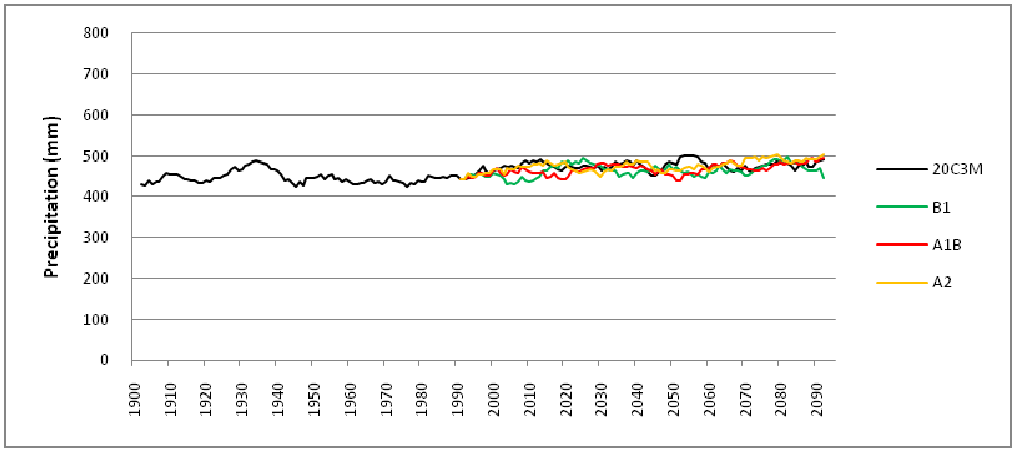

3.15e Mean annual precipitation, 1901-2100 (10-yr running mean)

Appendix 3.16 ECHAM5 – Kelem - Precipitation

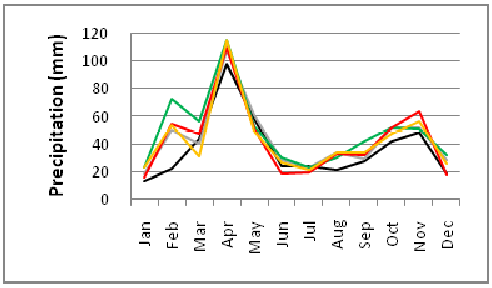

3.16a *Mean monthly precipitation - 2020*

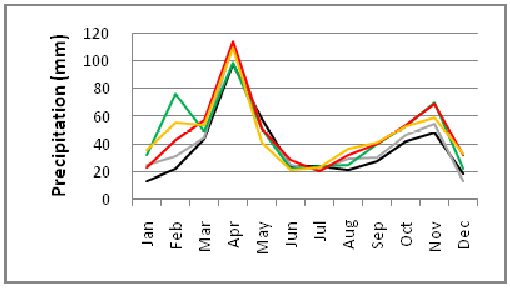

3.16b *Mean monthly precipitation - 2050*

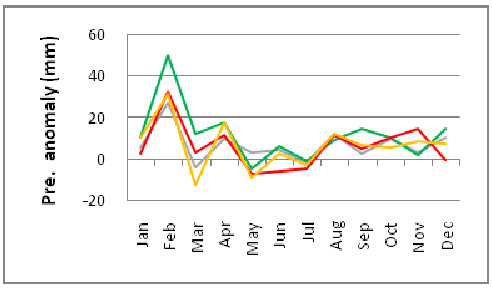

3.16c *Precipitation anomaly (2020 – baseline)*

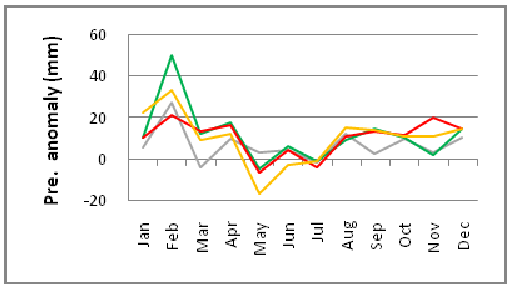

3.16d *Precipitation anomaly (2050 – baseline)*

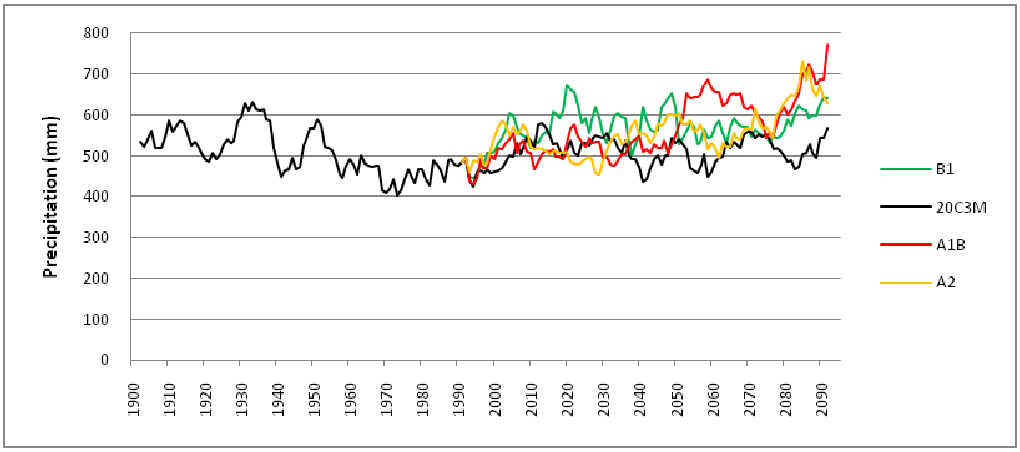

3.16e *Mean annual precipitation, 1901-2100 (10-yr running mean)*

Appendix 3.17 HADCM3 – Asayita - Precipitation

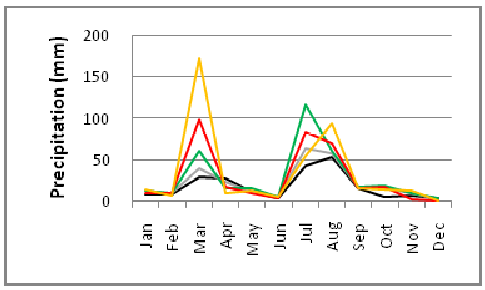

3.17a Mean monthly precipitation - 2020

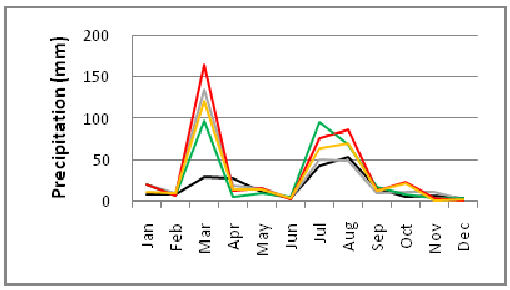

3.17b Mean monthly precipitation - 2050

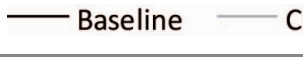

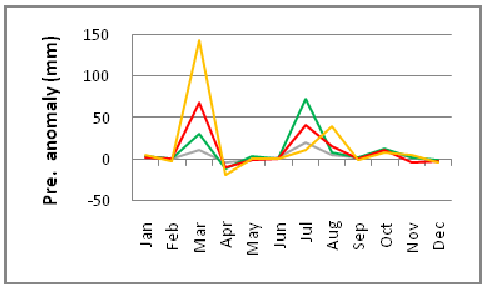

3.17c Precipitation anomaly (2020 – baseline)

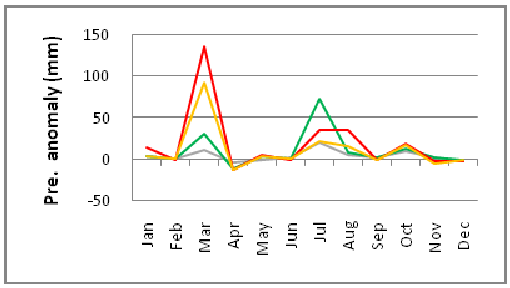

3.17d Precipitation anomaly (2050 – baseline)

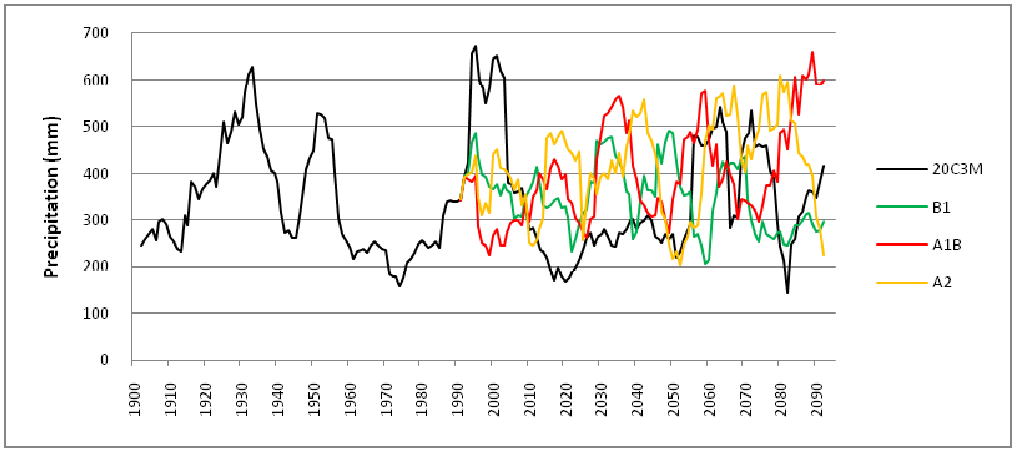

3.17e Mean annual precipitation, 1901-2100 (10-yr running mean)

Appendix 3.18 ECHAM5– Asayita - Precipitation

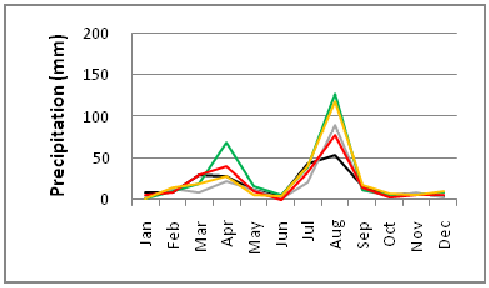

3.18a Mean monthly precipitation - 2020

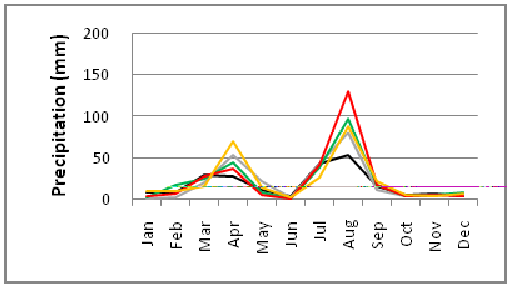

3.18b Mean monthly precipitation - 2050

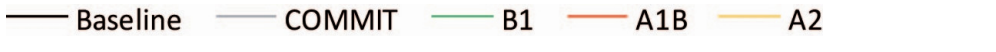

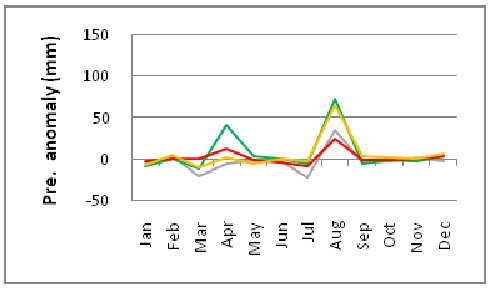

3.18c Precipitation anomaly (2020 – baseline)

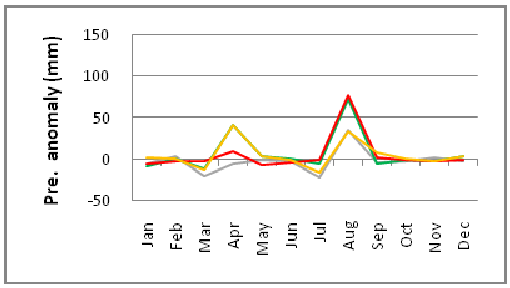

3.18d Precipitation anomaly (2050 – baseline)

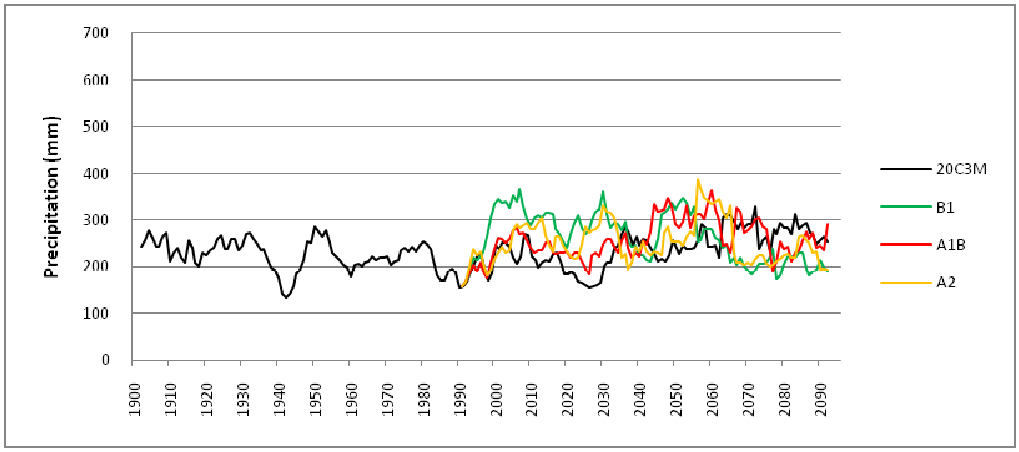

3.18e Mean annual precipitation, 1901-2100 (10-yr running mean)

Appendix 3.19 HADCM3 – Addis Ababa - Precipitation

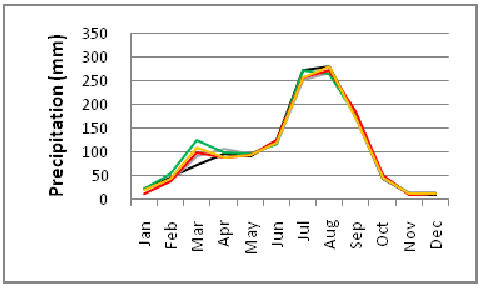

3.19a Mean monthly precipitation - 2020

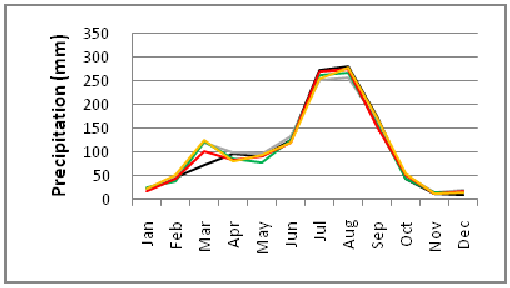

3.19b Mean monthly precipitation - 2050

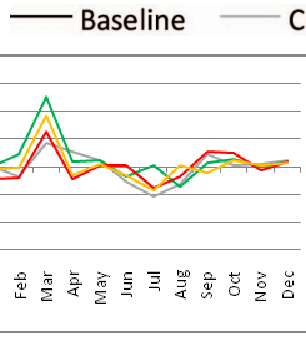

3.19c Precipitation anomaly (2020 – baseline)

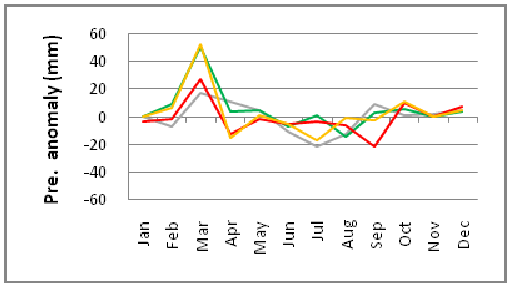

3.19d Precipitation anomaly (2050 – baseline)

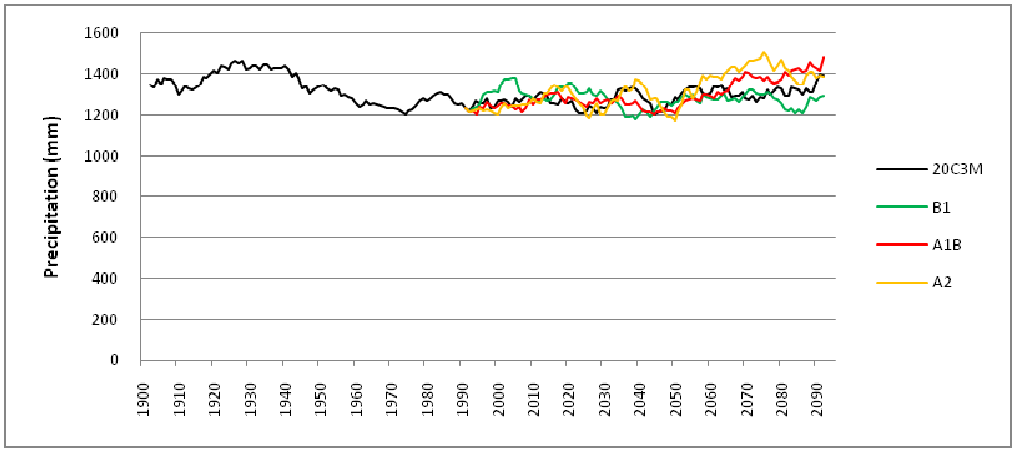

3.19e Mean annual precipitation, 1901-2100 (10-yr running mean)

Appendix 3.20 ECHAM5 – Addis Ababa - Precipitation

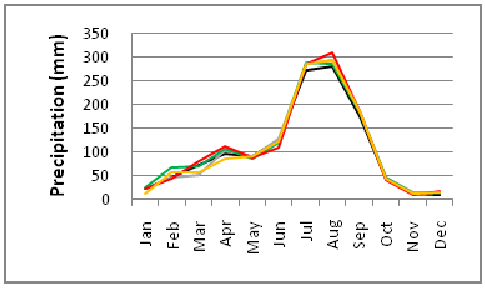

3.20a *Mean monthly precipitation - 2020*

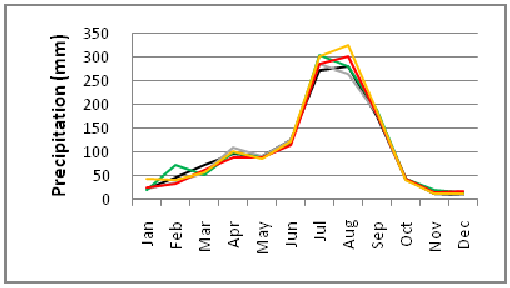

3.20b *Mean monthly precipitation - 2050*

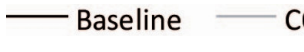

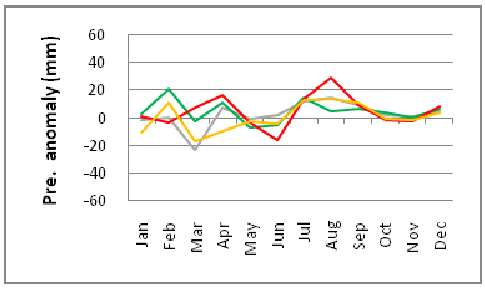

3.20c *Precipitation anomaly (2020 – baseline)*

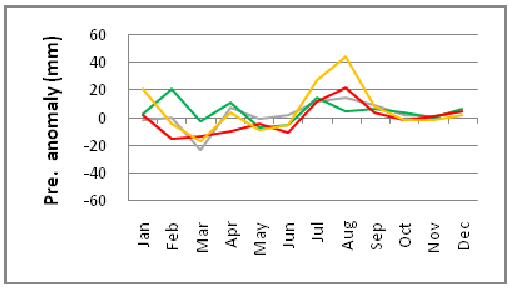

3.20d *Precipitation anomaly (2050 – baseline)*

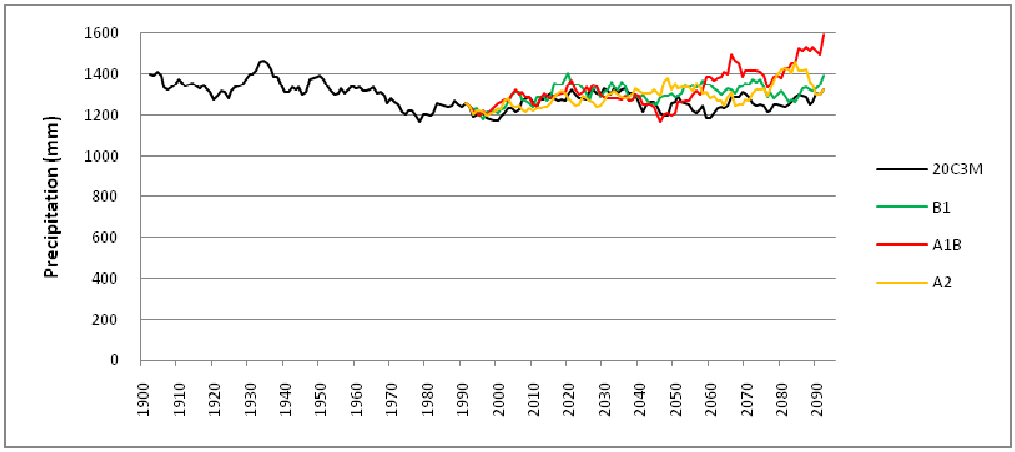

3.20e *Mean annual precipitation, 1901-2100 (10-yr running mean)*

Appendix 4 Graphs showing change in temperature between the baseline period, 2020, and 2050, and trends in temperature over the period 1900-2100

Appendix 4.1 HADCM3 – Moyale - Temperature

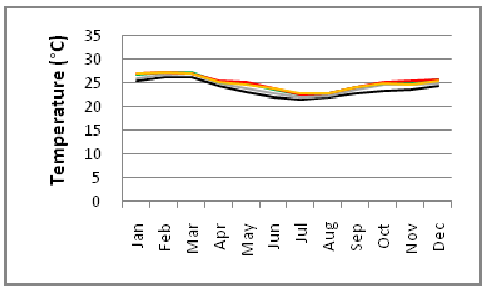

4.1a Mean monthly temperature - 2020

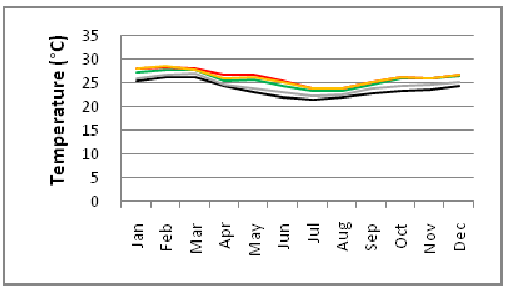

4.1b Mean monthly temperature - 2050

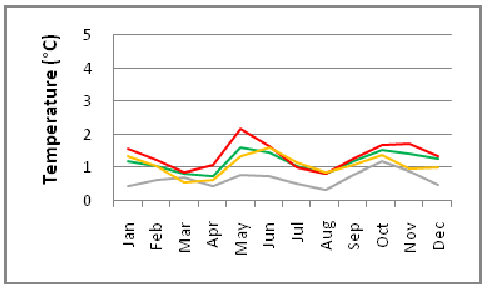

4.1c Temperature anomaly (2020 – baseline)

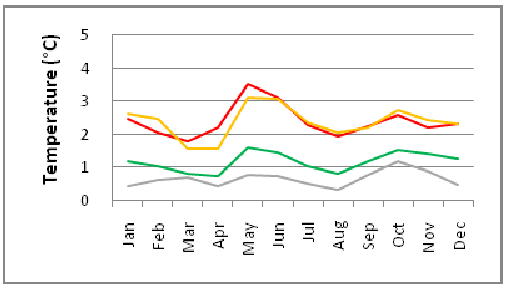

4.1d Temperature anomaly (2050 – baseline)

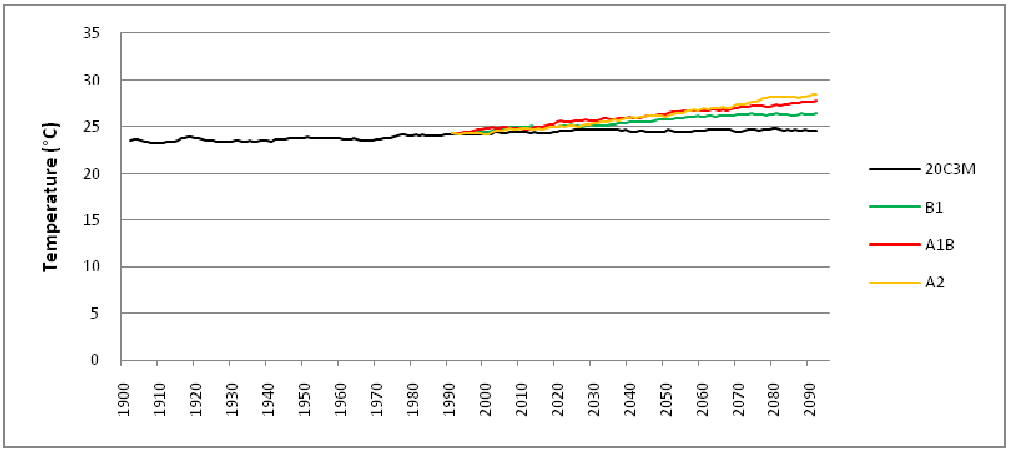

4.1e Mean annual temperature, 1901-2100 (10-yr running mean)

Appendix 4.2 ECHAM5 – Moyale - Temperature

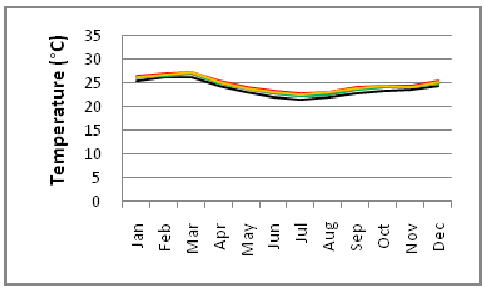

4.2a Mean monthly temperature - 2020

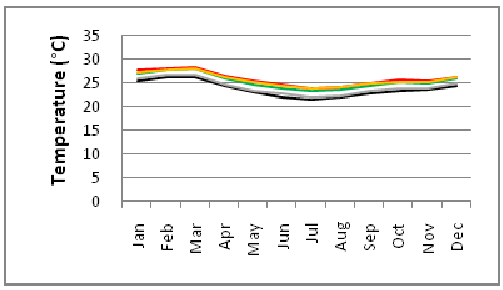

4.2 Mean monthly temperature - 2050

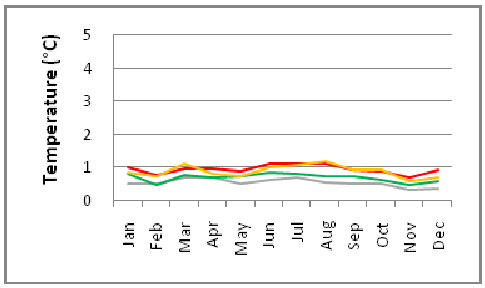

4.2c Temperature anomaly (2020 – baseline)

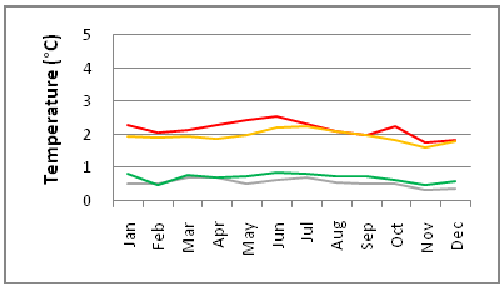

4.2d Temperature anomaly (2050 – baseline)

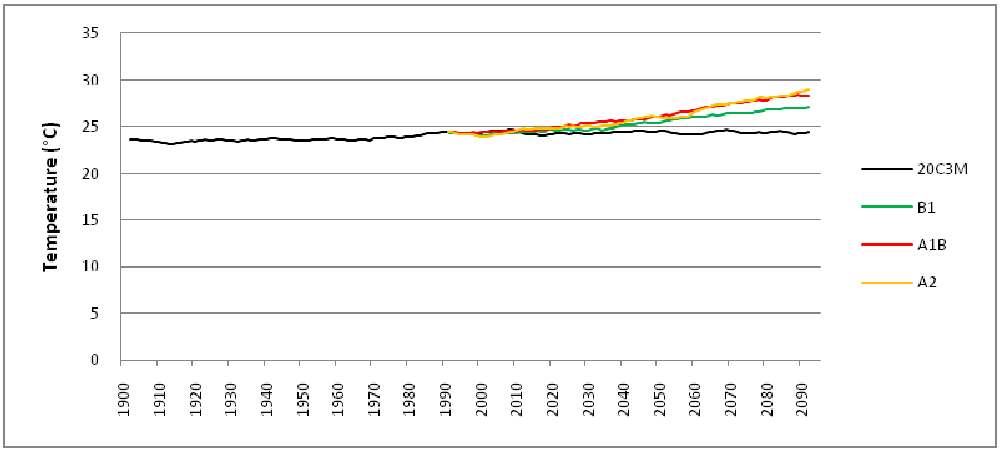

4.2e Mean annual temperature, 1901-2100 (10-yr running mean)

Appendix 4.3 HADCM3 – Mandera - Temperature

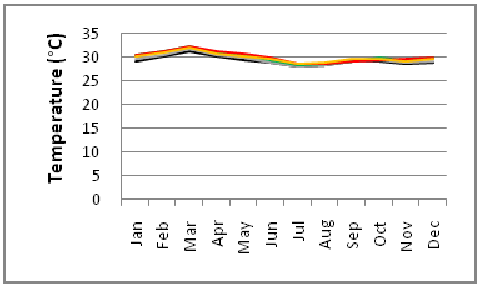

4.3a Mean monthly temperature - 2020

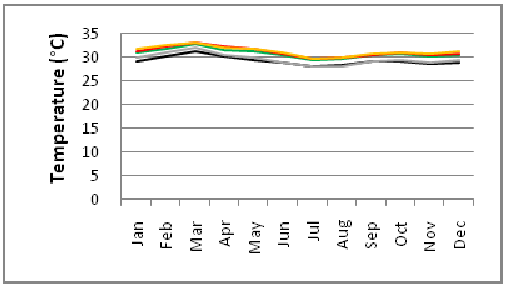

4.3b Mean monthly temperature - 2050

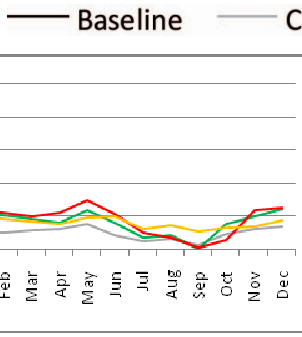

4.3c Temperature anomaly (2020 – baseline)

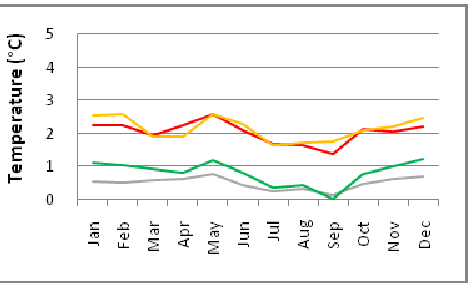

4.3d Temperature anomaly (2050 – baseline)

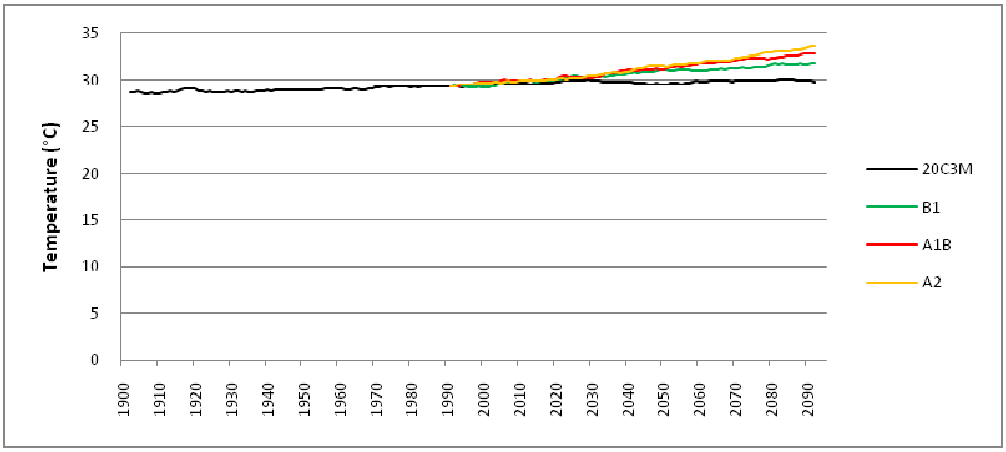

4.3e Mean annual temperature, 1901-2100 (10-yr running mean)

Appendix 4.4 ECHAM5 – Mandera - Temperature

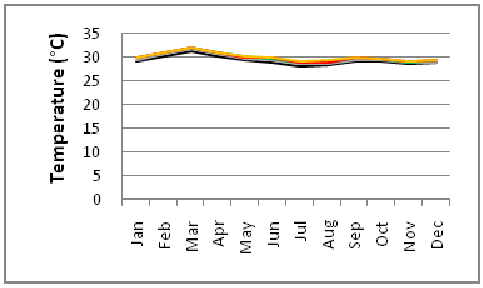

4.4a Mean monthly temperature - 2020

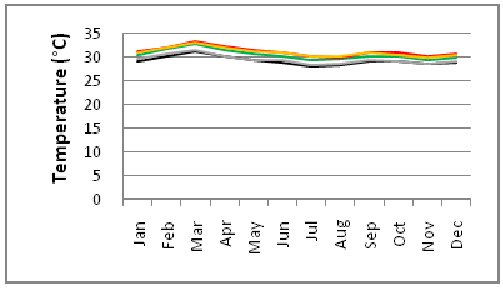

4.4b Mean monthly temperature - 2050

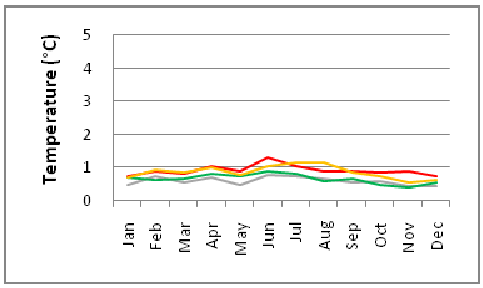

4.4c Temperature anomaly (2020 – baseline)

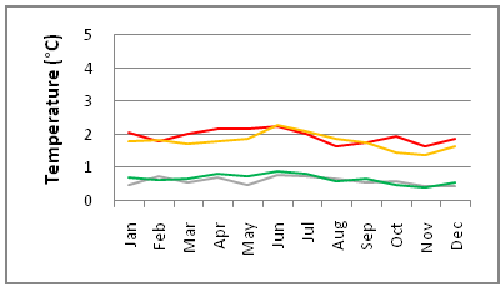

4.4d Temperature anomaly (2050 – baseline)

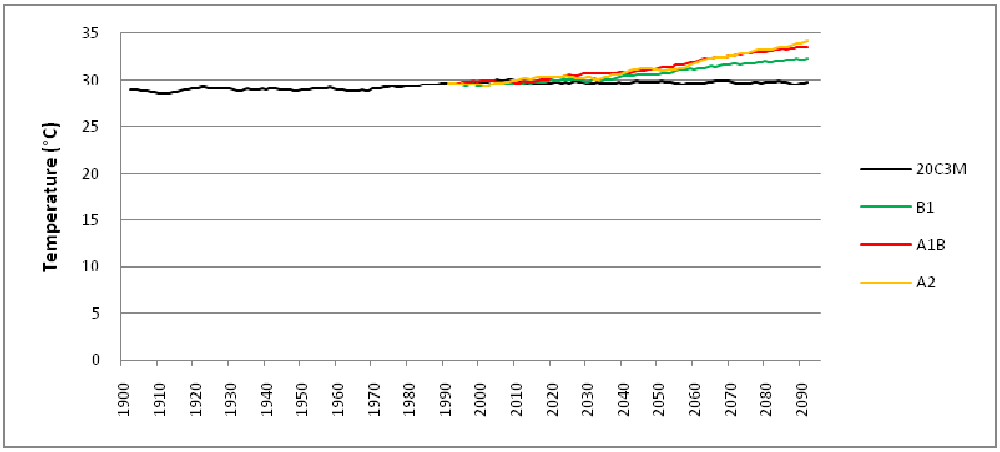

4.4e Mean annual temperature, 1901-2100 (10-yr running mean)

Appendix 4.5 HADCM3 – Marsabit - Temperature

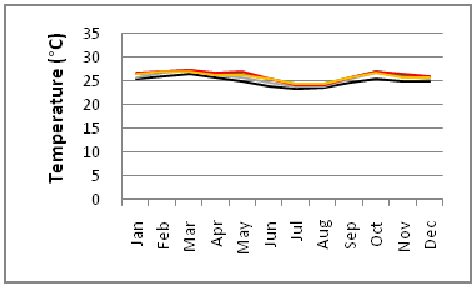

4.5a Mean monthly temperature - 2020

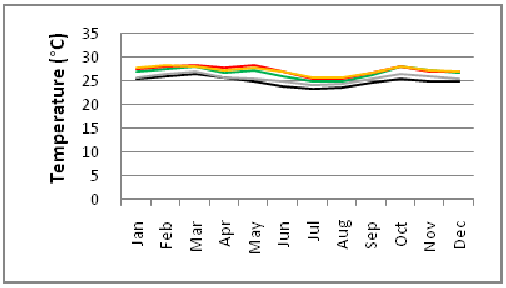

4.5b Mean monthly temperature - 2050

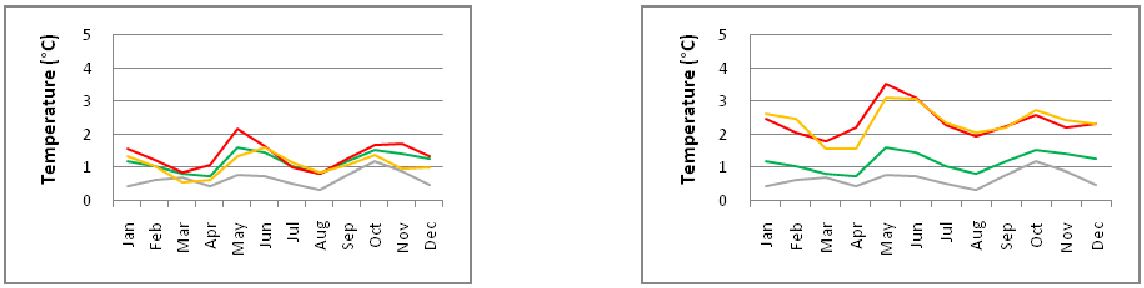

4.5c Temperature anomaly (2020 – baseline)

4.5d Temperature anomaly (2050 – baseline)

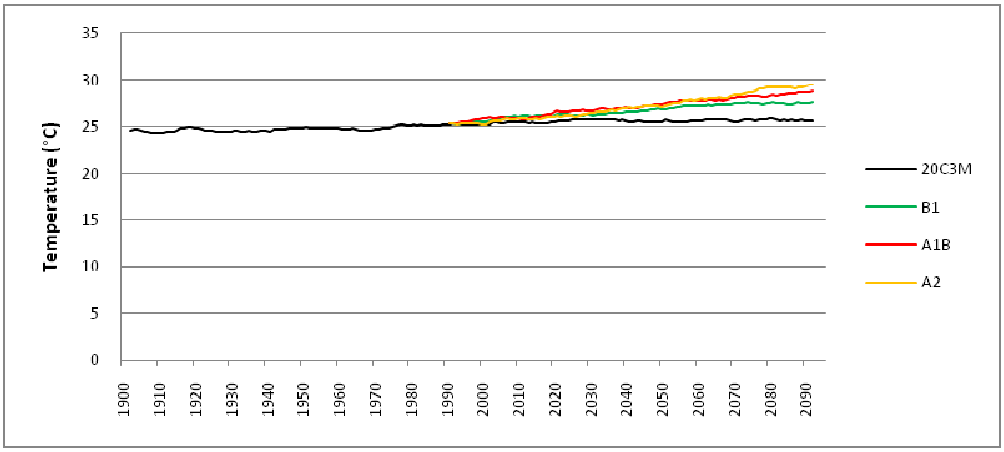

4.5e Mean annual temperature, 1901-2100 (10-yr running mean)

Appendix 4.6 ECHAM5 – Marsabit - Temperature

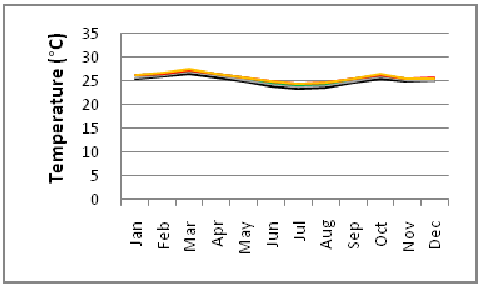

4.6a Mean monthly temperature - 2020

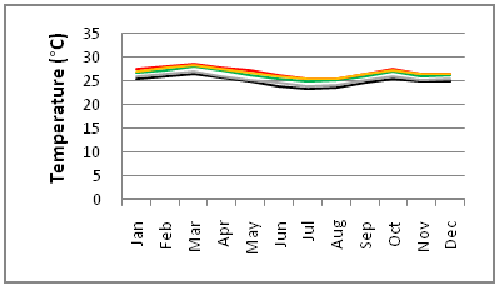

4.6b Mean monthly temperature - 2050

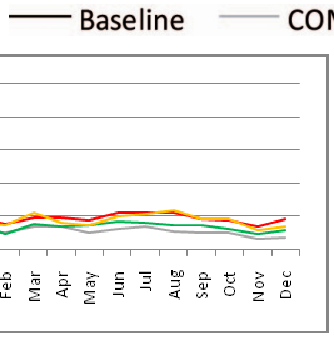

4.6c Temperature anomaly (2020 – baseline)

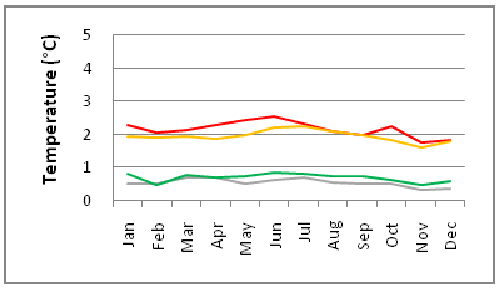

4.6d Temperature anomaly (2050 – baseline)

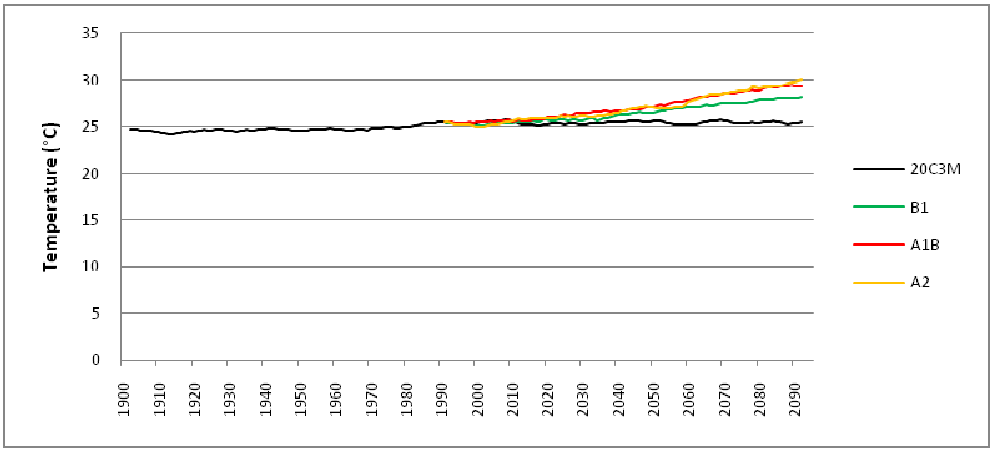

4.6e Mean annual temperature, 1901-2100 (10-yr running mean)

Appendix 4.7 HADCM3 – Maralal - Temperature

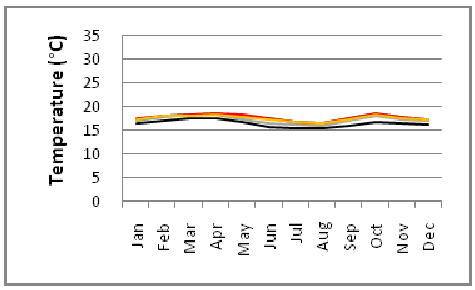

4.7a Mean monthly temperature - 2020

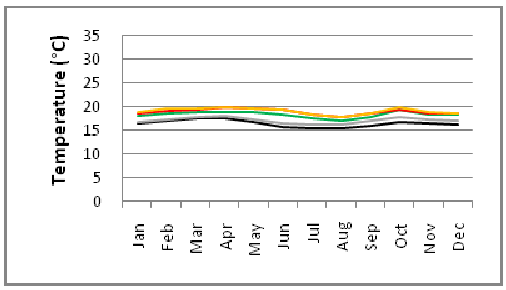

4.7b Mean monthly temperature - 2050

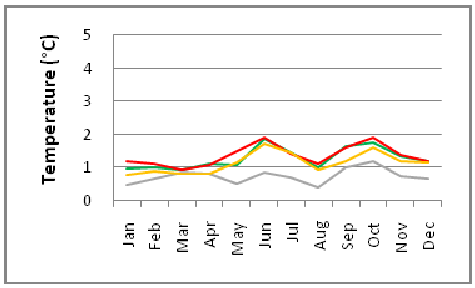

4.7c Temperature anomaly (2020 – baseline)

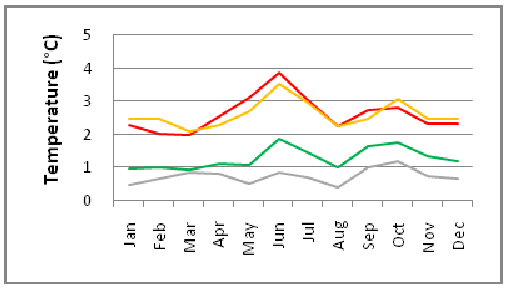

4.7d Temperature anomaly (2050 – baseline)

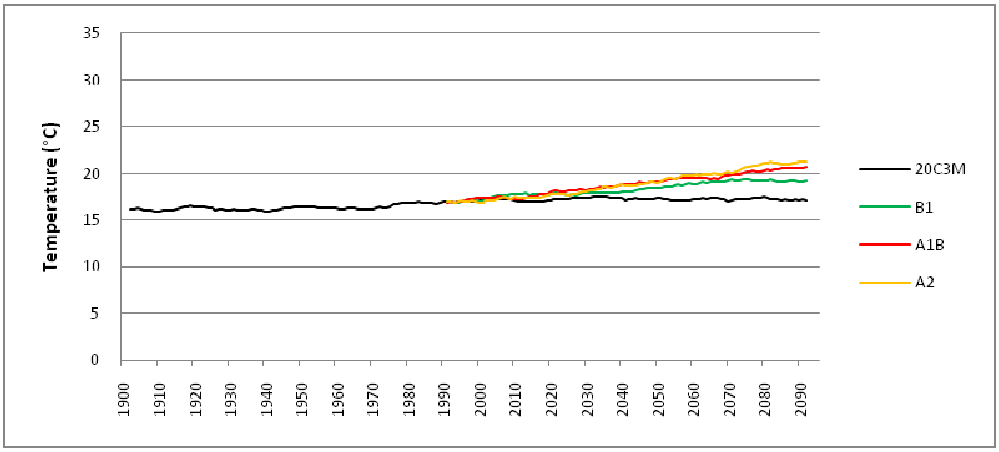

4.7e Mean annual temperature, 1901-2100 (10-yr running mean)

Appendix 4.8 ECHAM5– Maralal - Temperature

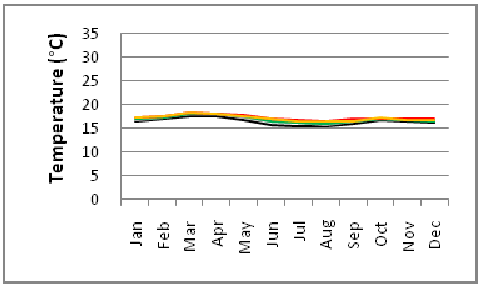

4.8a Mean monthly temperature - 2020

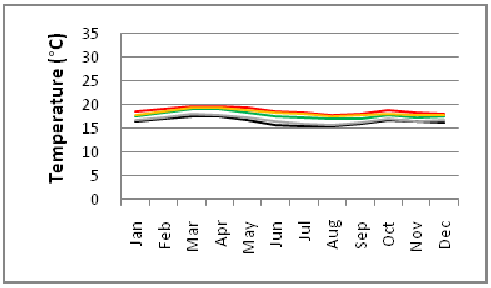

4.8b Mean monthly temperature - 2050

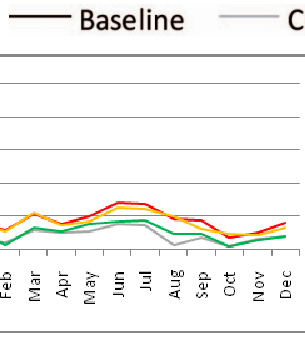

4.8c Temperature anomaly (2020 – baseline)

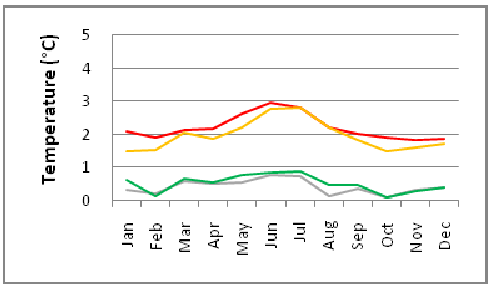

4.8d Temperature anomaly (2050 – baseline)

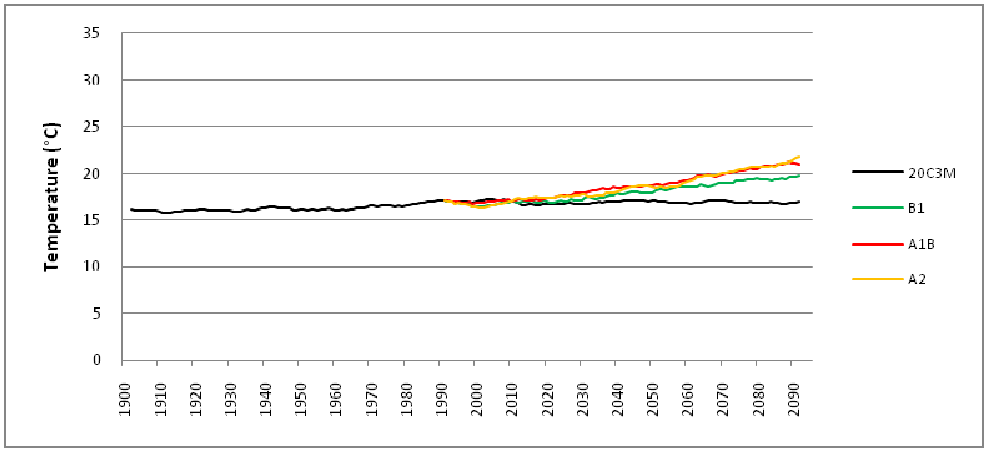

4.8e Mean annual temperature, 1901-2100 (10-yr running mean)

Appendix 4.9 HADCM3 – Isiolo - Temperature

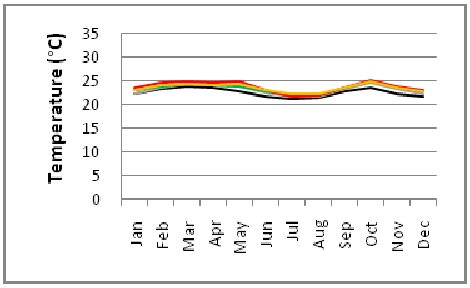

4.9a Mean monthly temperature - 2020

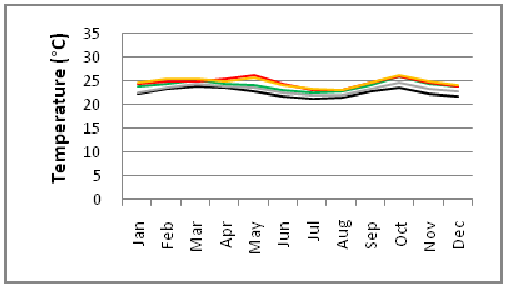

4.9b Mean monthly temperature - 2050

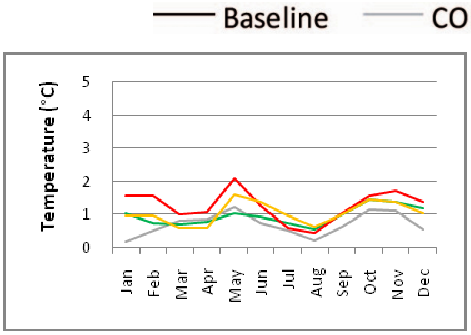

4.9c Temperature anomaly (2020 – baseline)

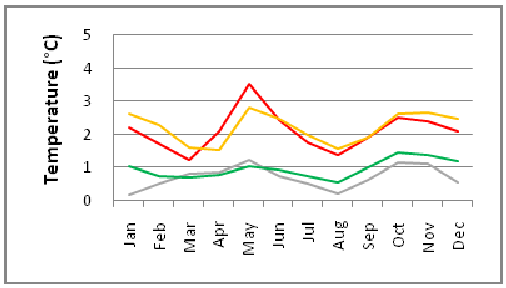

4.9d Temperature anomaly (2050 – baseline)

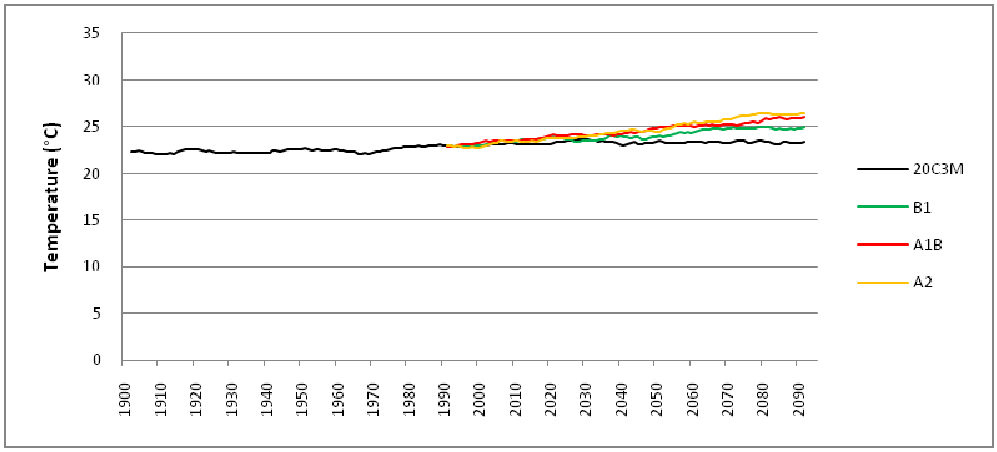

4.9e Mean annual temperature, 1901-2100 (10-yr running mean)

Appendix 4.10 ECHAM5– Isiolo - Temperature

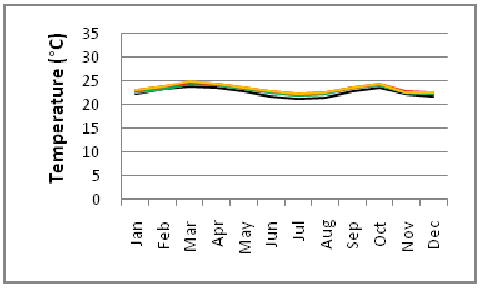

4.10a Mean monthly temperature - 2020

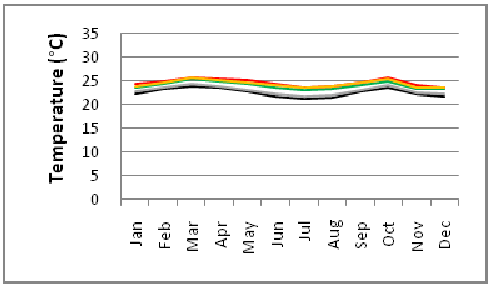

4.10b Mean monthly temperature - 2050

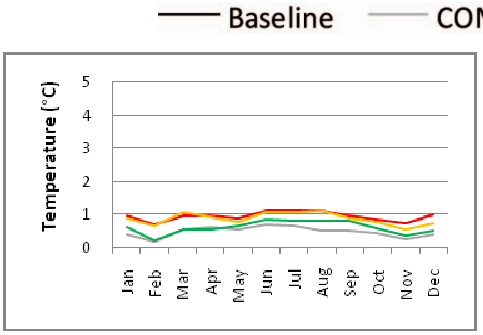

4.10c Temperature anomaly (2020 – baseline)

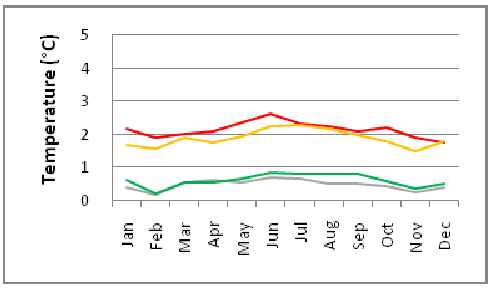

4.10d Temperature anomaly (2050 – baseline)

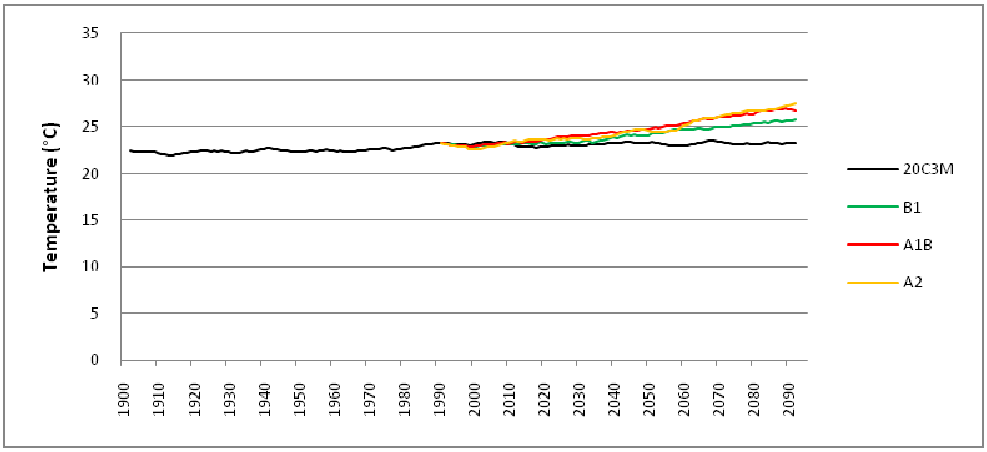

4.10e Mean annual temperature, 1901-2100 (10-yr running mean)

Appendix 4.11 HADCM3 – Nairobi - Temperature

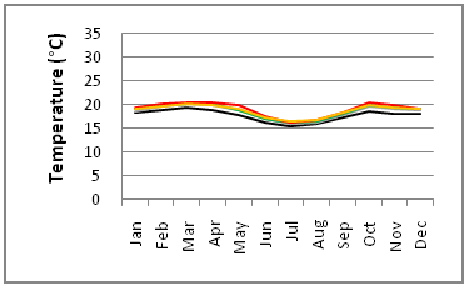

4.11a Mean monthly temperature - 2020

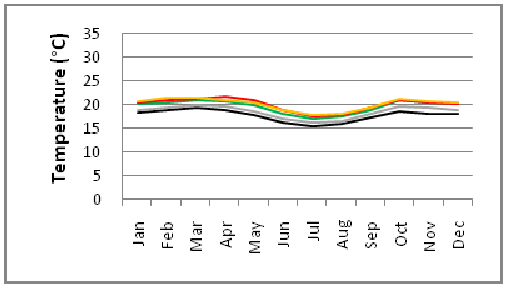

4.11b Mean monthly temperature - 2050

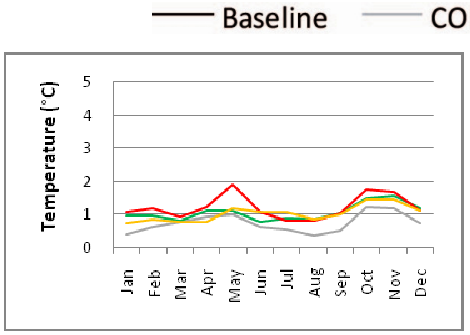

4.11c Temperature anomaly (2020 – baseline)

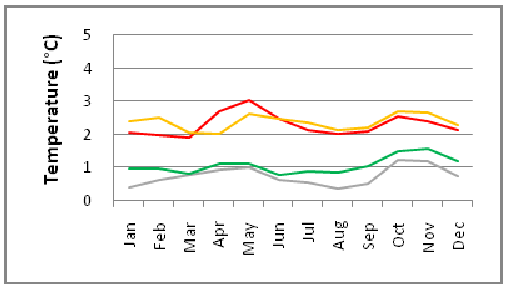

4.11d Temperature anomaly (2050 – baseline)

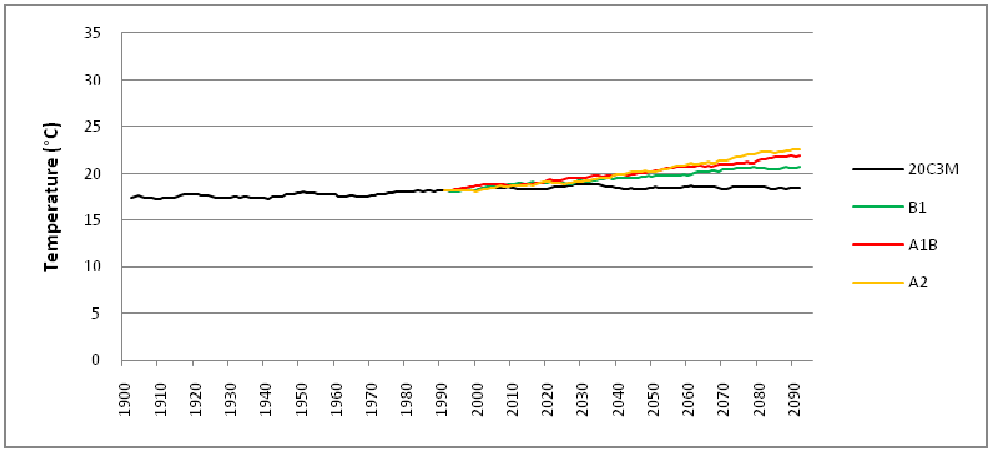

4.11e Mean annual temperature, 1901-2100 (10-yr running mean)

Appendix 4.12 ECHAM5– Nairobi - Temperature

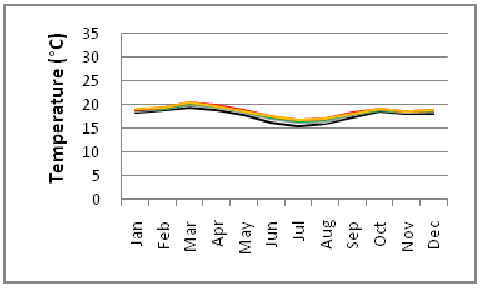

4.12a Mean monthly temperature - 2020

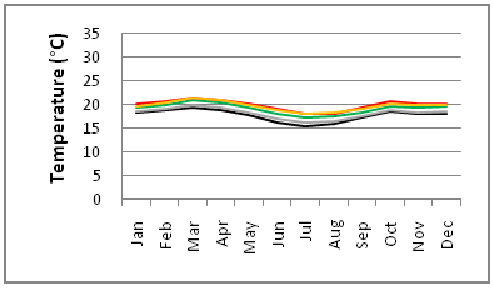

4.12b Mean monthly temperature - 2050

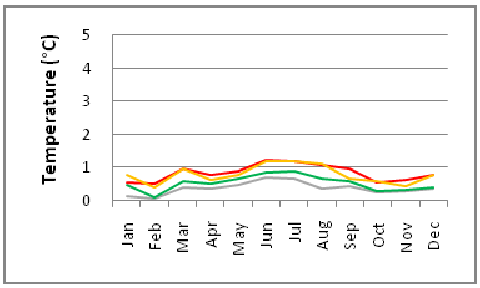

4.12c Temperature anomaly (2020 – baseline)

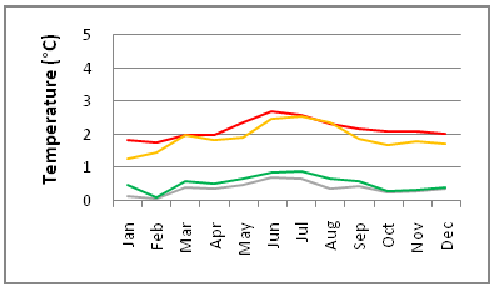

4.12d Temperature anomaly (2050 – baseline)

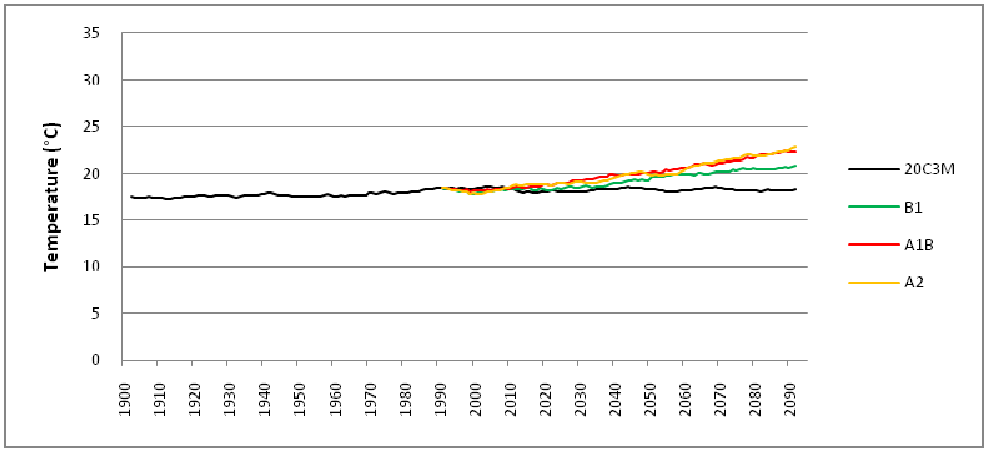

4.12e Mean annual temperature, 1901-2100 (10-yr running mean)

Appendix 4.13 HADCM3 – Awasa - Temperature

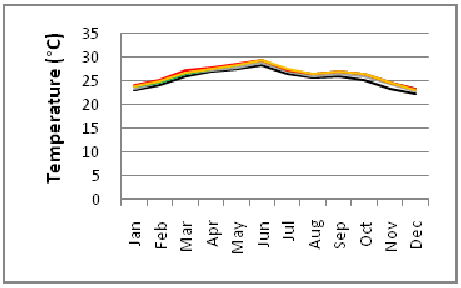

4.13a Mean monthly temperature - 2020

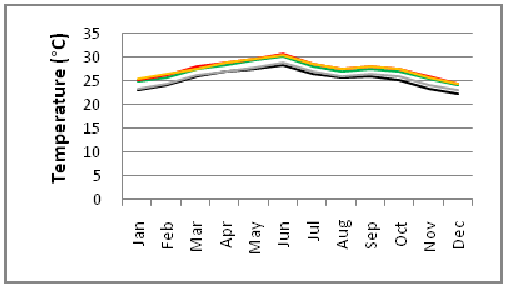

4.13b Mean monthly temperature - 2050

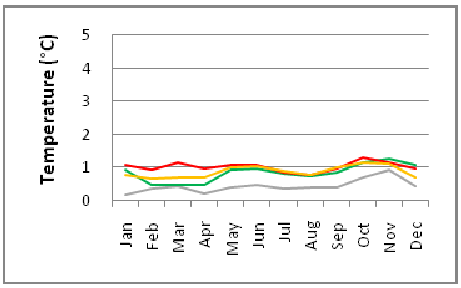

4.13c Temperature anomaly (2020 – baseline)

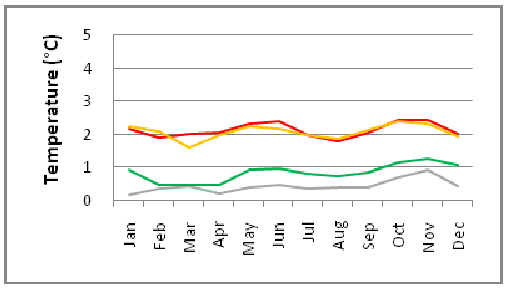

4.13d Temperature anomaly (2050 – baseline)

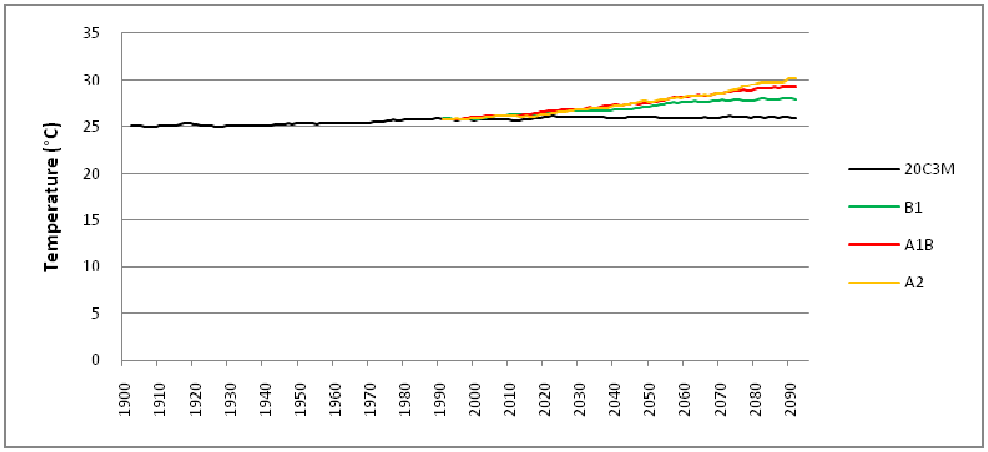

4.13e Mean annual temperature, 1901-2100 (10-yr running mean)

Appendix 4.14 ECHAM5– Awasa - Temperature

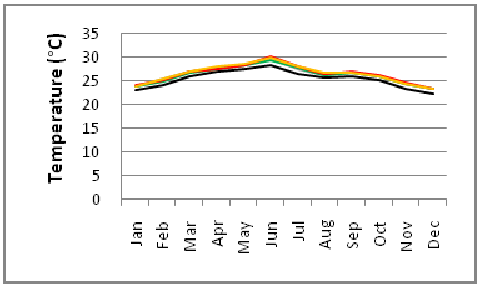

4.14a Mean monthly temperature - 2020

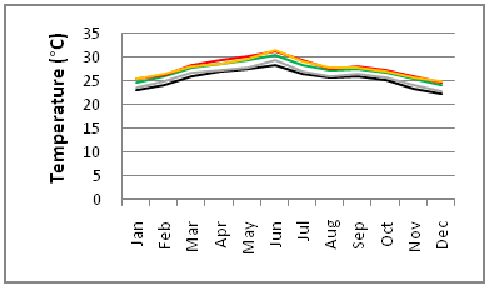

4.14b Mean monthly temperature - 2050

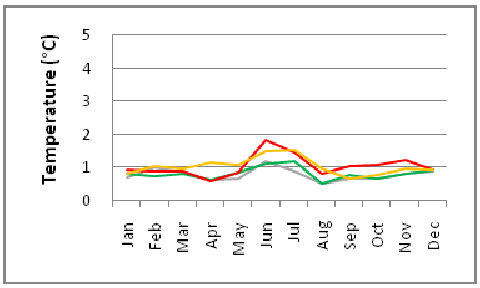

4.14c Temperature anomaly (2020 – baseline)

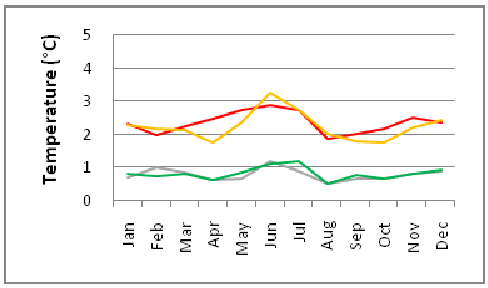

4.14d Temperature anomaly (2050 – baseline)

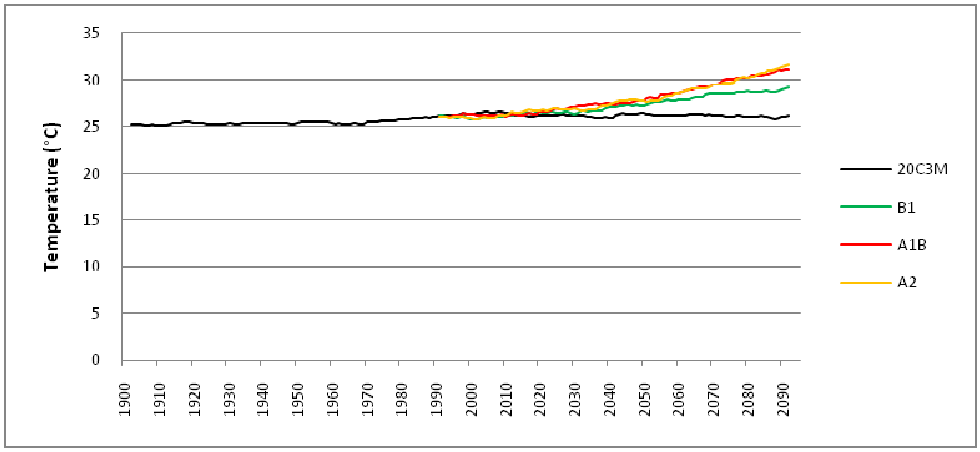

4.14e Mean annual temperature, 1901-2100 (10-yr running mean)

Appendix 4.15 HADCM3 – Kelem - Temperature

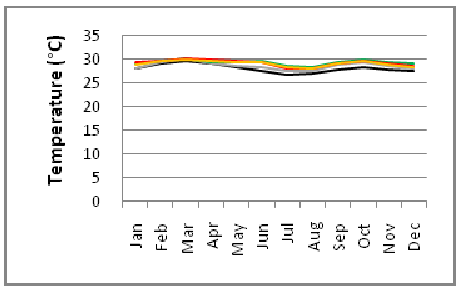

4.15a Mean monthly temperature - 2020

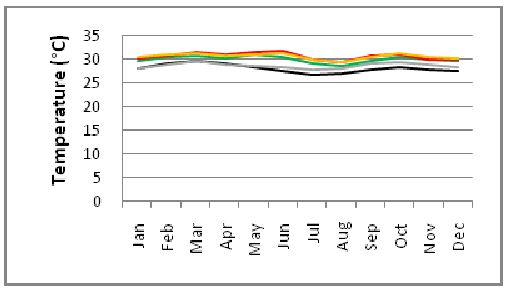

4.15b Mean monthly temperature - 2050

4.15c Temperature anomaly (2020 – baseline)

4.15d Temperature anomaly (2050 – baseline)

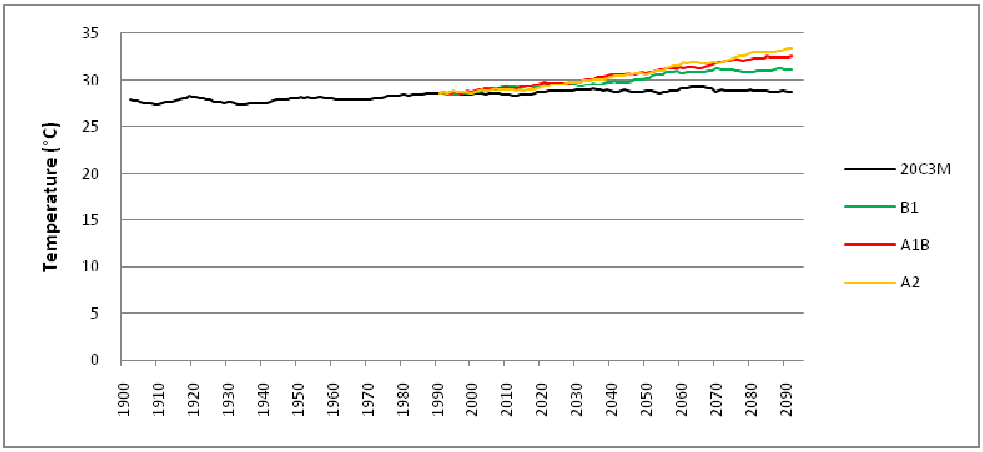

4.15e Mean annual temperature, 1901-2100 (10-yr running mean)

Appendix 4.16 ECHAM5 – Kelem - Temperature

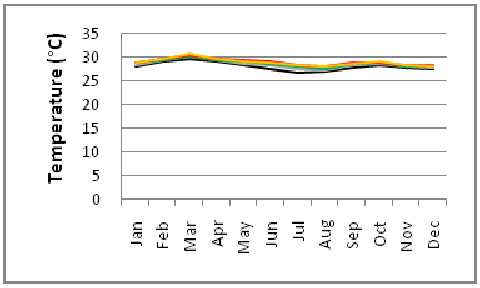

4.16a Mean monthly temperature - 2020

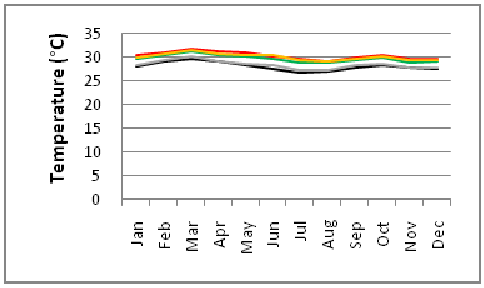

4.16b Mean monthly temperature - 2050

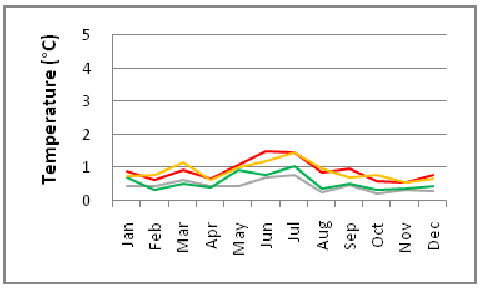

4.16c Temperature anomaly (2020 – baseline)

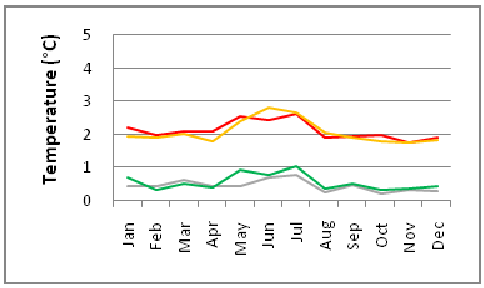

4.16d Temperature anomaly (2050 – baseline)

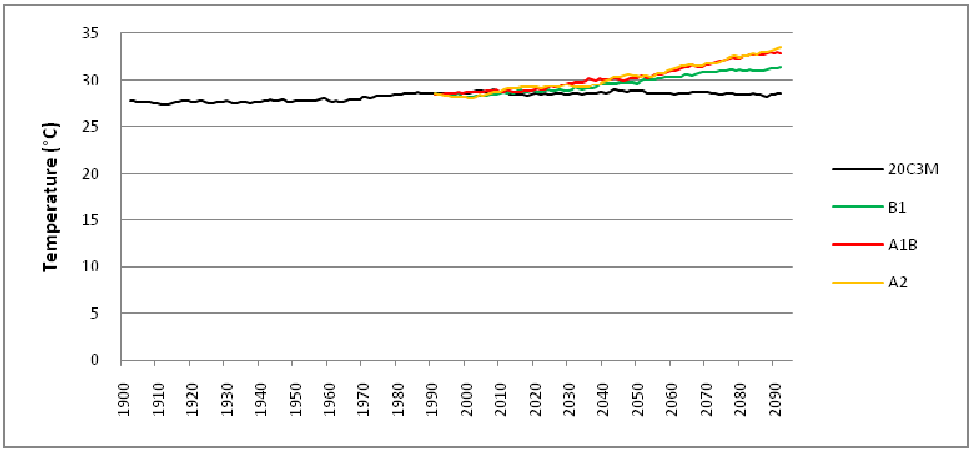

4.16e Mean annual temperature, 1901-2100 (10-yr running mean)

Appendix 4.17 HADCM3 – Asayita - Temperature

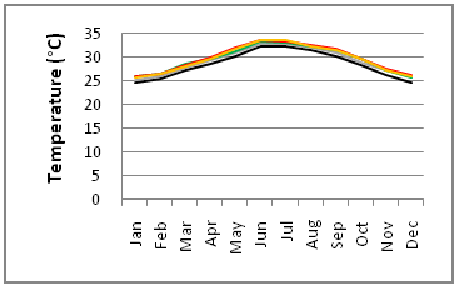

4.17a Mean monthly temperature - 2020

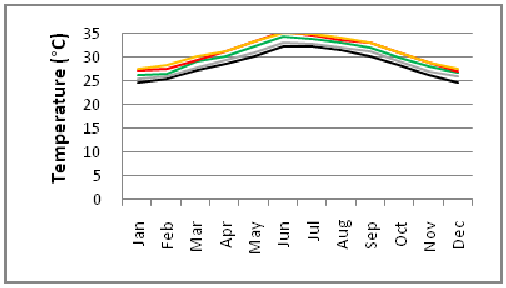

4.17b Mean monthly temperature - 2050

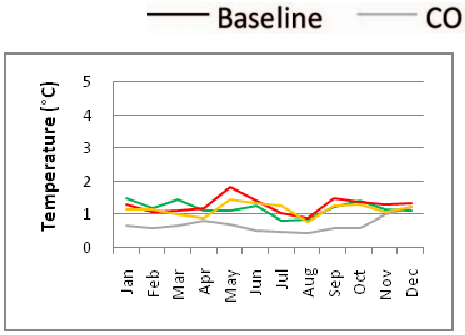

4.17c Temperature anomaly (2020 – baseline)

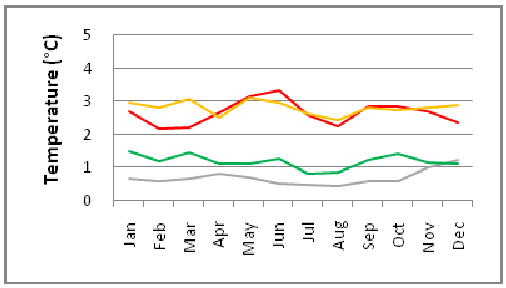

4.17d Temperature anomaly (2050 – baseline)

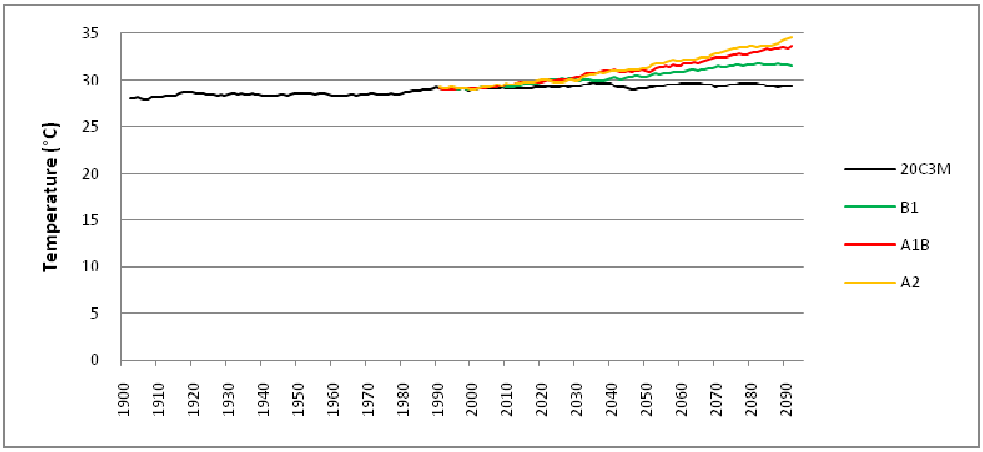

4.17e Mean annual temperature, 1901-2100 (10-yr running mean)

Appendix 4.18 ECHAM5– Asayita - Temperature

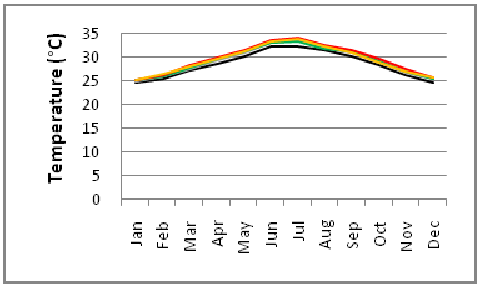

4.18a Mean monthly temperature - 2020

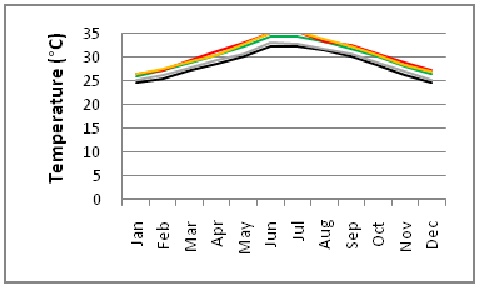

4.18b Mean monthly temperature - 2050

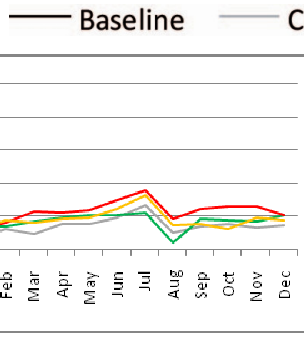

4.18c Temperature anomaly (2020 – baseline)

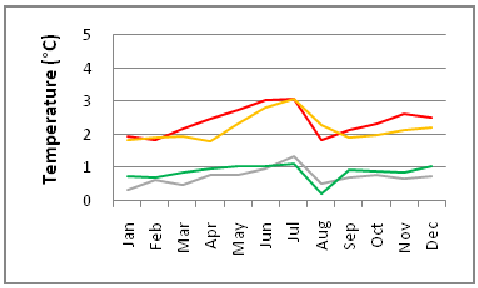

4.18d Temperature anomaly (2050 – baseline)

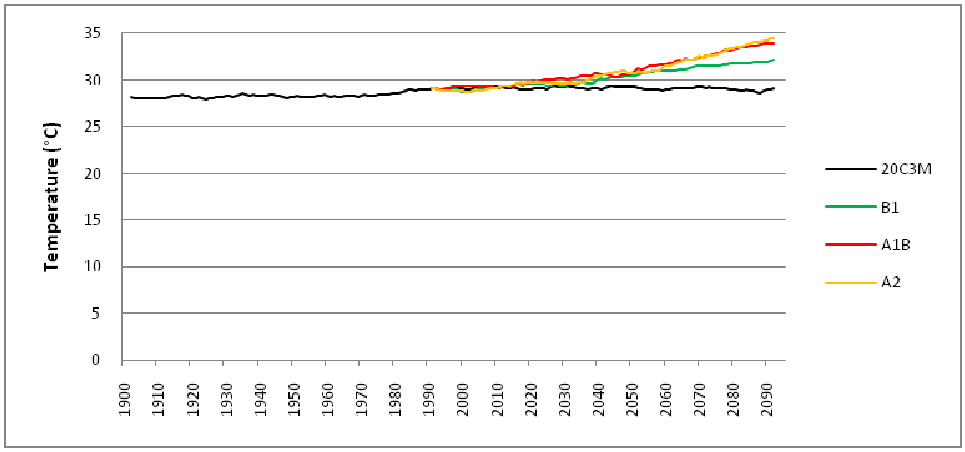

4.18e Mean annual temperature, 1901-2100 (10-yr running mean)

Appendix 4.19 HADCM3 – Addis Ababa - Temperature

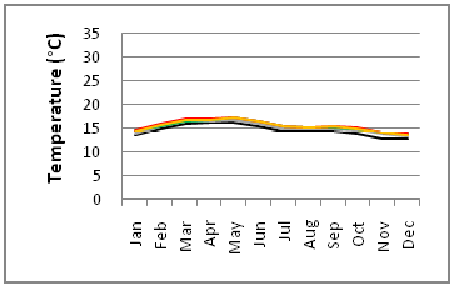

4.19a Mean monthly temperature - 2020

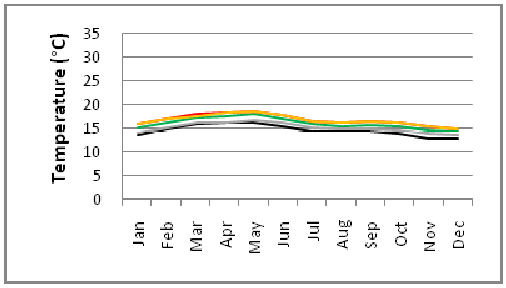

4.19b Mean monthly temperature - 2050

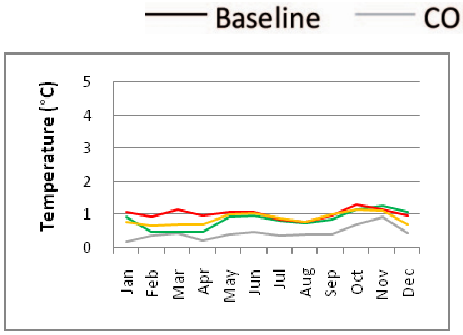

4.19c Temperature anomaly (2020 – baseline)

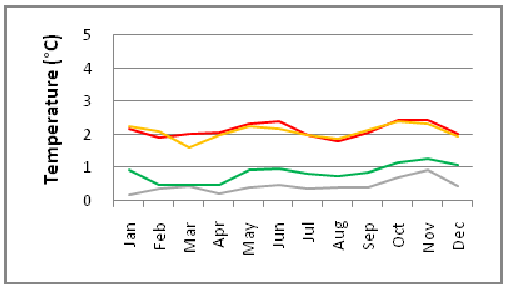

4.19d Temperature anomaly (2050 – baseline)

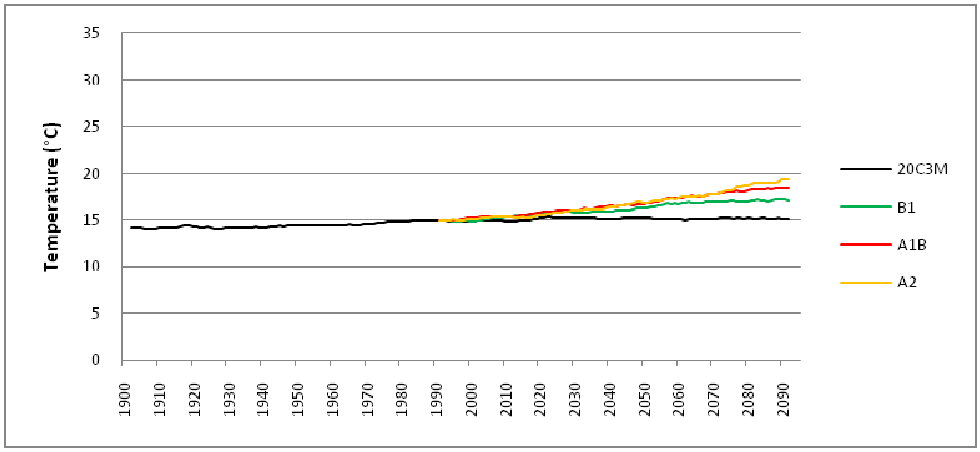

4.19e Mean annual temperature, 1901-2100 (10-yr running mean)

Appendix 4.20 ECHAM5 – Addis Ababa - Temperature

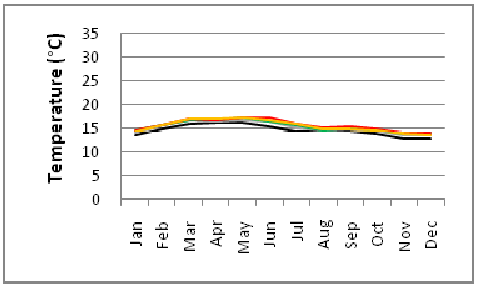

4.20a Mean monthly temperature - 2020

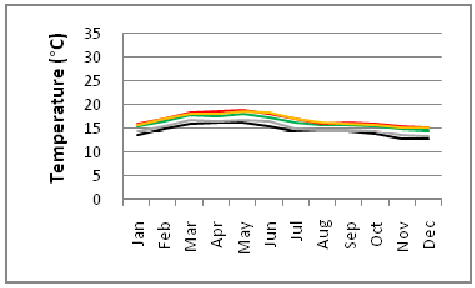

4.20b Mean monthly temperature - 2050

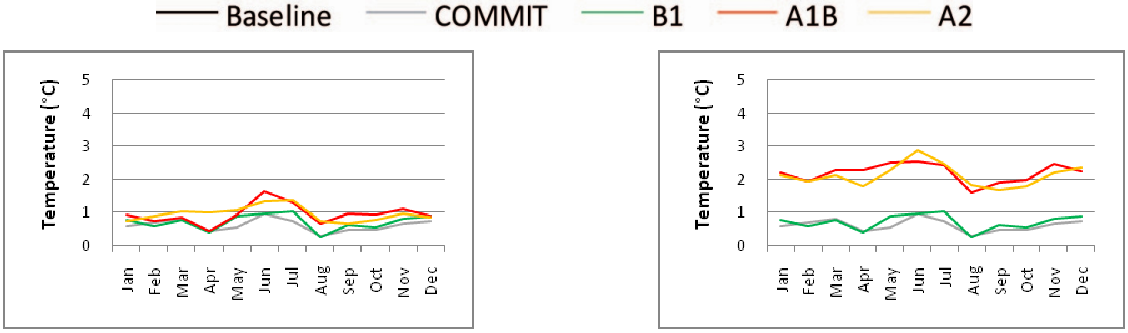

4.20c Temperature anomaly (2020 – baseline)

4.20d Temperature anomaly (2050 – baseline)

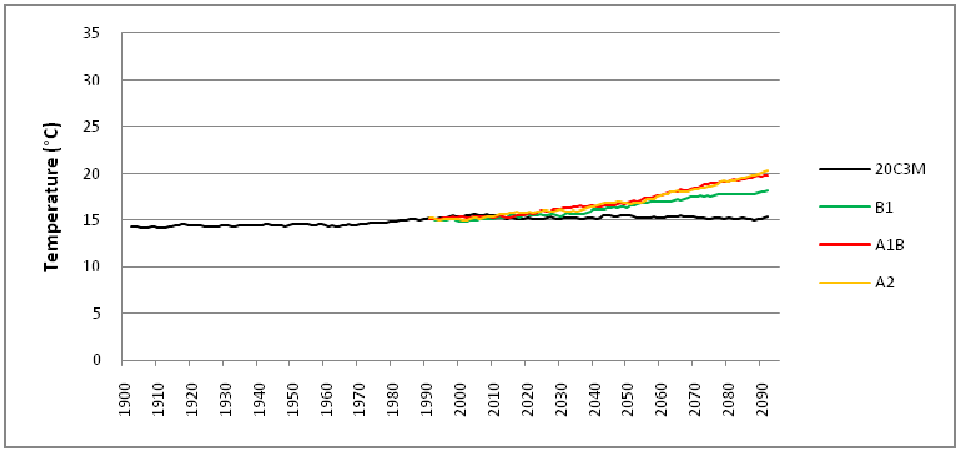

4.20e Mean annual temperature, 1901-2100 (10-yr running mean)

Appendix 5 Tables showing the percentage of months above or below given thresholds for precipitation, and above given thresholds for temperature.

For each parameter the data are shown for the following 10 locations indicated on the map in Figure 1.1: Moyale, Mandera, Marsabit, Maralal, Isiolo, Nairobi, Awasa, Kelem, Asayita, and Addis Ababa.

Appendix 5.1 Percentage of months in the downscaled HADCM3 climate data in which precipitation below the thresholds given in the first column. Note that the baseline data are derived from HADCM3, and are thus different to the baseline data for ECHAM5.

Station	1961-	2020				2050			
Threshold (mm)	1990	COMMIT	B1	A1B	A2	COMMIT	B1	A1B	A2
Moyale									
1	12.8	13.3	16.7	19.4	13.1	16.1	11.9	14.7	12.8
5	24.2	26.1	29.2	31.9	23.9	29.2	25.8	25.0	25.3
10	34.2	36.9	37.8	39.7	34.7	37.2	37.2	32.5	35.0
20	50.0	46.9	49.4	50.6	49.2	49.4	48.1	47.2	46.9
Mandera									
1	35.3	35.8	38.1	40.0	37.2	36.1	37.8	37.5	37.2
5	53.3	51.4	53.1	51.4	51.1	50.6	51.4	51.9	49.7
10	59.2	57.2	58.3	57.8	57.2	56.1	57.5	58.9	55.6
20	65.3	65.8	66.1	66.1	65.3	65.6	66.4	68.1	65.8
Marsabit									
1	14.4	16.1	18.6	21.9	14.2	19.2	14.2	16.1	15.3
5	29.2	31.4	32.8	35.3	28.3	33.3	31.7	28.6	29.4
10	39.7	39.7	40.3	42.8	37.8	40.6	39.2	37.2	38.9
20	50.6	48.1	49.2	51.1	50.3	49.4	50.8	48.1	48.1
Maralal									
1	0.3	0.0	1.1	1.1	0.3	0.3	1.4	1.1	0.8
5	0.8	1.7	3.9	3.6	2.2	0.8	4.2	3.3	2.8
10	1.7	6.4	8.3	5.3	5.3	1.1	7.2	6.7	6.7
20	8.6	12.5	15.3	13.9	10.0	10.6	13.3	12.2	11.1
Isiolo									
1	6.9	9.7	10.8	13.9	8.9	7.5	9.4	11.7	9.7
5	17.5	21.4	23.9	24.4	21.7	21.4	21.1	22.2	23.1
10	27.2	27.8	31.4	30.3	28.9	29.2	29.2	26.1	28.9
20	36.1	38.6	38.3	38.1	35.8	37.2	38.6	35.6	35.8
Nairobi									
1	9.7	10.3	13.1	13.1	12.5	12.2	13.1	13.6	12.8
5	15.3	17.5	20.8	19.7	20.8	21.1	20.8	22.5	19.2
10	20.3	21.7	25.6	26.1	23.9	25.0	24.2	27.5	24.2
50	25.0	31.1	31.9	33.3	30.3	29.2	31.9	34.7	29.4
Awasa									
1	8.1	6.7	4.4	7.2	7.2	4.2	4.2	9.2	6.7
5	12.8	13.1	11.4	14.2	12.2	10.0	9.4	14.4	11.1
10	18.6	19.2	17.2	18.1	17.2	15.0	16.9	18.3	15.0
50	29.2	28.3	25.3	28.6	26.9	24.7	29.2	26.9	26.4
Kelem									
1	1.4	0.8	0.3	0.6	0.8	0.8	0.3	1.1	0.8
5	4.4	3.9	2.5	1.9	2.5	1.9	3.6	4.4	2.8
10	8.6	6.7	5.3	5.8	5.3	4.2	7.8	6.7	5.0
50	23.6	22.5	23.9	20.6	19.7	21.9	21.9	20.0	17.2
Asayita									
1	35.8	35.3	35.8	34.4	34.7	31.1	35.6	34.2	35.8
5	54.2	53.6	54.2	52.5	52.5	50.8	50.6	50.6	53.3
10	65.8	61.7	63.3	60.8	63.6	65.3	61.9	60.8	64.2
50	76.4	72.2	72.8	70.8	73.6	73.1	73.9	72.2	75.3
Addis Ababa									
1	7.2	6.4	4.2	6.1	7.2	3.9	4.2	7.8	5.8
5	11.7	12.2	10.3	12.5	11.4	6.9	8.9	14.2	10.8
10	16.4	17.2	14.4	16.9	15.6	12.8	14.7	16.9	14.2
50									

Appendix 5.2 Percentage of months in the downscaled ECHAM5 climate data in which precipitation is below the thresholds given in the first column. Note that the baseline data are derived from ECHAM5, and are thus different to the baseline data for HADCM3.

Appendix	1961-	2020				2050			
Threshold (mm)	1990	COMMIT	B1	A1B	A2	COMMIT	B1	A1B	A2
Moyale									
1	30.0	26.7	21.4	28.1	25.6	29.7	25.6	24.2	27.5
5	40.6	36.1	33.9	37.2	35.6	37.2	34.2	32.8	36.1
10	46.7	42.2	38.6	41.9	41.4	41.1	39.4	37.8	40.0
20	52.5	49.7	45.6	47.5	47.8	48.3	45.0	45.6	45.6
Mandera									
1	43.1	44.2	41.1	43.3	47.8	43.6	39.7	41.7	42.5
5	53.6	54.2	53.6	55.6	55.6	55.0	50.6	54.2	52.2
10	61.1	60.0	60.3	60.6	61.7	60.0	57.2	58.6	57.2
20	67.5	67.8	67.2	64.4	66.1	65.8	64.4	66.1	63.9
Marsabit									
1	31.4	27.5	24.4	30.6	27.5	31.1	26.7	25.6	29.4
5	42.8	39.7	34.7	38.6	38.6	38.6	37.2	35.6	38.3
10	49.2	43.6	40.0	42.8	43.1	43.6	40.8	41.4	41.9
20	56.4	49.2	46.4	50.0	48.9	50.0	45.8	46.1	46.4
Maralal									
1	8.9	4.7	6.1	6.7	6.4	9.2	6.9	6.9	8.1
5	13.9	9.2	10.8	10.6	11.1	13.9	11.4	9.7	14.4
10	16.4	11.9	13.1	15.3	14.4	16.7	13.9	13.9	18.1
20	23.3	19.4	18.6	21.7	19.4	23.1	19.7	21.4	21.9
Isiolo									
1	22.5	18.1	16.9	18.6	20.6	21.1	17.8	20.6	20.8
5	32.8	26.4	27.2	29.4	29.7	31.7	26.7	31.1	32.2
10	38.1	30.6	29.4	33.1	33.9	36.9	32.2	35.0	35.0
20	41.9	35.8	36.9	38.3	37.8	41.1	35.8	37.5	38.3
Nairobi									
1	2.5	2.8	2.2	3.3	3.6	2.5	2.8	3.1	4.4
5	9.2	7.5	8.3	10.8	7.8	8.6	10.3	11.1	13.6
10	16.1	13.6	13.3	15.8	12.5	15.6	15.6	16.9	19.2
50	23.6	19.4	20.3	23.9	22.2	20.6	22.2	23.9	26.1
Awasa									
1	14.2	14.4	12.8	14.4	13.9	15.8	13.3	14.7	14.2
5	20.8	21.1	19.7	21.7	20.8	23.3	18.3	23.1	20.0
10	25.6	26.1	26.1	25.8	28.1	26.9	26.1	28.3	24.2
50	35.0	36.7	35.0	36.1	37.8	37.8	35.8	38.9	40.3
Kelem									
1	15.6	10.6	10.8	15.6	13.9	15.8	13.1	10.8	11.4
5	21.7	16.9	16.1	21.4	18.3	21.4	20.3	16.9	16.4
10	28.3	21.1	20.3	26.7	23.6	27.5	23.9	23.3	21.9
50	42.5	34.2	30.6	38.6	33.1	38.1	35.3	34.4	33.1
Asayita									
1	48.1	53.6	45.8	49.7	51.1	48.3	45.6	53.9	47.5
5	59.4	65.0	60.0	62.5	60.6	58.1	61.1	63.6	58.6
10	65.0	73.1	67.2	70.6	66.9	66.7	67.5	71.1	64.7
50	74.4	79.7	75.8	77.5	75.0	77.8	75.0	80.8	74.2
Addis Ababa									
1	9.2	7.8	8.6	11.4	11.9	10.8	9.4	11.1	9.2
5	16.1	14.4	13.6	17.5	14.7	15.6	15.0	16.4	15.0
10	20.0	18.6	17.8	20.8	19.4	20.0	18.3	20.6	20.3
50	25.8	25.3	23.3	25.8	28.3	26.7	25.8	27.8	25.3

Appendix 5.3 Percentages of months in the downscaled HADCM3 climate data in which precipitation is above the thresholds given in the first column. Note that the baseline data are derived from HADCM3, and are thus different to the baseline data for ECHAM5.

Appendix Threshold (mm)	1961-1990	2020 COMMIT	2020 B1	2020 A1B	2020 A2	2050 COMMIT	2050 B1	2050 A1B	2050 A2
Moyale									
100	18.9	19.2	15.6	15.0	20.6	18.6	14.7	16.9	19.7
200	5.3	5.0	4.4	3.6	5.0	6.4	6.9	3.9	7.2
300	1.7	1.4	2.5	1.1	1.7	3.1	1.9	2.5	2.2
350	0.8	1.1	1.1	0.3	0.6	1.7	1.1	1.1	1.1
Mandera									
100	5.0	5.6	6.1	2.8	6.1	4.7	6.1	5.3	7.5
200	1.1	0.8	1.1	0.3	0.3	1.9	0.3	0.6	1.1
300	0.0	0.0	0.0	0.0	0.0	0.0	0.0	0.0	0.0
350	0.0	0.0	0.0	0.0	0.0	0.0	0.0	0.0	0.0
Marsabit									
100	19.4	19.4	16.7	16.7	21.1	19.7	17.2	18.9	21.7
200	5.0	5.3	5.6	3.9	7.5	5.6	7.2	6.1	9.4
300	2.5	2.8	2.8	1.9	2.5	3.9	3.1	3.1	3.6
350	1.7	1.4	2.2	1.1	1.4	2.8	1.4	2.5	2.2
Maralal									
100	32.8	35.3	28.6	29.2	31.4	28.3	26.9	27.2	28.3
200	8.1	7.2	5.0	4.7	6.1	6.1	6.1	5.8	5.8
300	1.4	1.4	1.4	0.3	1.1	1.1	1.4	0.3	0.8
350	0.3	0.6	0.3	0.3	0.3	0.3	0.0	0.3	0.3
Isiolo									
100	34.7	31.9	32.2	31.1	34.4	33.1	29.7	28.1	28.1
200	17.8	14.2	13.3	12.5	16.7	15.3	12.8	14.7	18.3
300	6.1	6.7	5.8	3.6	6.4	7.2	8.3	7.8	8.3
350	3.9	4.2	4.2	2.5	3.9	4.4	4.7	4.7	5.8
Nairobi									
100	28.9	28.1	23.9	23.1	28.6	27.8	24.2	24.2	30.6
200	7.8	7.8	7.2	4.7	6.7	6.9	7.5	5.6	7.2
300	4.7	3.9	4.2	2.2	1.7	4.7	3.9	0.8	3.3
350	4.2	3.3	3.3	1.4	1.1	3.6	3.3	0.8	2.5
Awasa									
100	15.6	16.7	18.6	16.7	16.7	17.2	16.4	16.9	18.3
200	0.0	0.0	0.0	0.0	0.0	0.0	0.3	0.0	0.3
300	0.0	0.0	0.0	0.0	0.0	0.0	0.0	0.0	0.0
350	0.0	0.0	0.0	0.0	0.0	0.0	0.0	0.0	0.0
Kelem									
100	3.9	5.8	6.1	3.9	4.4	6.1	5.3	5.8	4.2
200	0.0	0.0	0.0	0.0	0.0	0.0	0.0	0.0	0.0
300	0.0	0.0	0.0	0.0	0.0	0.0	0.0	0.0	0.0
350	0.0	0.0	0.0	0.0	0.0	0.0	0.0	0.0	0.0
Asayita									
100	5.0	6.1	8.6	6.9	8.1	6.1	8.3	8.6	7.2
200	0.6	0.8	2.8	3.3	3.1	1.9	3.1	3.9	2.8
300	0.0	0.6	1.1	1.9	2.2	1.4	2.2	2.5	1.9
350	0.0	0.3	0.6	0.6	1.9	0.8	1.1	2.2	1.4
Addis Ababa									
100	41.4	45.0	45.8	43.9	42.8	47.8	40.8	43.6	44.4
200	19.4	18.9	18.9	19.4	17.8	18.6	18.6	19.2	19.4
300	5.6	3.1	5.3	3.6	5.0	2.5	4.4	3.9	3.6
350									

Appendix 5.4 Percentage of months in the downscaled ECHAM5 climate data in which precipitation is above the thresholds given in the first column. Note that the baseline data are derived from ECHAM5, and are thus different to the baseline data for HADCM3.

Appendix	1961-	2020				2050			
Threshold (mm)	1990	COMMIT	B1	A1B	A2	COMMIT	B1	A1B	A2
Moyale									
100	20.0	21.9	21.4	23.6	23.1	21.9	23.9	24.2	25.6
200	7.2	8.6	8.1	8.6	10.8	8.1	10.8	7.8	10.0
300	2.8	5.0	2.2	3.1	3.9	3.3	3.1	2.8	3.6
350	0.8	1.9	1.1	1.1	1.1	1.9	2.2	0.6	1.9
Mandera									
100	5.6	5.8	6.4	6.1	6.4	6.4	10.6	7.8	7.8
200	0.8	0.8	0.6	0.6	1.4	1.9	0.3	0.8	1.1
300	0.0	0.0	0.0	0.0	0.0	0.0	0.0	0.0	0.0
350	0.0	0.0	0.0	0.0	0.0	0.0	0.0	0.0	0.0
Marsabit									
100	20.6	23.9	24.4	22.5	26.4	22.5	26.4	25.6	25.6
200	7.2	9.7	8.3	8.9	9.2	8.9	10.0	8.1	12.2
300	2.2	3.3	2.8	1.9	4.4	3.3	3.3	2.5	3.6
350	1.7	1.7	1.4	1.4	2.5	1.7	2.2	2.2	2.2
Maralal									
100	34.2	38.3	41.1	38.6	38.6	37.2	40.0	36.1	36.1
200	12.2	13.3	13.6	12.2	16.4	14.4	15.0	11.9	9.7
300	3.6	5.8	4.7	3.9	6.9	4.2	5.0	3.9	3.9
350	1.4	3.6	2.8	3.3	3.6	1.9	3.6	2.5	2.2
Isiolo									
100	35.3	37.2	38.9	37.5	35.3	35.3	38.6	36.7	39.4
200	18.1	19.2	22.8	19.4	21.4	21.1	21.4	20.8	20.8
300	9.4	9.7	12.2	9.2	11.9	10.3	12.8	9.7	10.8
350	6.1	6.4	7.2	6.1	7.8	6.9	8.1	6.9	6.9
Nairobi									
100	33.1	37.2	35.6	32.5	32.8	34.4	35.8	33.9	34.4
200	9.7	12.8	8.3	10.0	11.7	11.9	11.7	8.3	9.2
300	5.0	4.4	3.3	3.9	5.6	3.9	5.0	3.6	3.1
350	2.2	2.2	2.5	2.8	3.1	2.5	3.1	1.9	1.4
Awasa									
100	18.3	18.9	17.5	19.7	16.9	17.2	20.0	16.7	17.2
200	0.6	0.8	1.7	1.4	1.4	1.4	2.2	1.7	2.8
300	0.0	0.0	0.0	0.0	0.6	0.3	0.3	0.0	0.6
350	0.0	0.0	0.0	0.0	0.3	0.0	0.3	0.0	0.3
Kelem									
100	7.2	9.2	10.6	10.0	10.0	9.7	12.2	11.4	11.1
200	0.3	0.8	2.2	1.1	0.6	0.8	1.7	1.1	1.4
300	0.0	0.0	0.3	0.0	0.0	0.0	0.6	0.3	0.6
350	0.0	0.0	0.0	0.0	0.0	0.0	0.3	0.3	0.3
Asayita									
100	5.0	5.0	8.3	6.1	7.2	7.2	6.1	8.6	6.1
200	0.3	0.8	2.5	1.7	2.2	1.7	0.8	3.3	2.2
300	0.0	0.3	1.7	0.6	0.3	0.0	0.6	1.4	0.6
350	0.0	0.3	1.1	0.3	0.0	0.0	0.6	0.6	0.6
Addis Ababa									
100	43.6	42.5	42.2	43.6	41.7	41.9	41.4	40.8	43.3
200	17.5	18.6	21.1	20.8	21.1	18.6	18.9	19.4	21.1
300	7.2	6.9	5.8	8.3	6.1	6.1	8.9	7.5	9.2
350	2.2	2.5	2.8	3.3	2.5	1.9	4.2	3.1	5.3

Appendix 5.5 Percentage of months in the downscaled HADCM3 climate data in which temperature is above the thresholds given in the first column. Note that the baseline data are derived from HADCM3, and are thus different to the baseline data for ECHAM5.

Appendix	1961-	2020				2050			
Threshold (°C)	1990	COMMIT	B1	A1B	A2	COMMIT	B1	A1B	A2
Moyale									
27	6.4	10.8	15.8	18.3	16.4	10.8	25.8	37.8	37.2
28	0.6	2.5	3.6	6.7	2.5	1.4	12.5	19.4	21.1
29	0.0	0.0	0.6	1.1	0.0	0.0	4.4	5.0	9.4
30	0.0	0.0	0.0	0.0	0.0	0.0	0.3	0.6	2.8
Mandera									
27	99.4	98.9	97.5	98.1	98.6	99.2	100.0	99.2	99.7
28	84.4	93.6	94.4	93.3	93.6	90.6	99.7	98.9	99.2
29	50.0	70.3	78.9	80.8	81.9	68.6	93.9	95.6	96.4
30	22.8	35.6	48.9	53.6	48.6	36.1	74.7	82.2	83.3
Marsabit									
27	6.9	20.3	27.5	34.7	25.0	20.0	47.8	60.6	53.9
28	1.7	4.2	9.2	12.2	6.1	3.6	21.1	36.9	33.1
29	0.3	0.0	1.4	2.2	0.6	0.0	6.7	11.7	17.8
30	0.0	0.0	0.0	0.0	0.0	0.0	0.6	2.2	3.3
Maralal									
27	0.0	0.0	0.0	0.0	0.0	0.0	0.0	0.0	0.0
28	0.0	0.0	0.0	0.0	0.0	0.0	0.0	0.0	0.0
29	0.0	0.0	0.0	0.0	0.0	0.0	0.0	0.0	0.0
30	0.0	0.0	0.0	0.0	0.0	0.0	0.0	0.0	0.0
Isiolo									
27	0.3	0.0	1.4	1.4	0.0	0.0	3.1	6.9	9.2
28	0.0	0.0	0.0	0.0	0.0	0.0	0.0	0.8	1.1
29	0.0	0.0	0.0	0.0	0.0	0.0	0.0	0.0	0.0
30	0.0	0.0	0.0	0.0	0.0	0.0	0.0	0.0	0.0
Nairobi									
27	0.0	0.0	0.0	0.0	0.0	0.0	0.0	0.0	0.0
28	0.0	0.0	0.0	0.0	0.0	0.0	0.0	0.0	0.0
29	0.0	0.0	0.0	0.0	0.0	0.0	0.0	0.0	0.0
30	0.0	0.0	0.0	0.0	0.0	0.0	0.0	0.0	0.0
Awasa									
27	21.9	30.6	39.4	43.6	42.2	33.3	56.9	65.3	65.0
28	10.3	13.6	18.3	21.1	20.0	13.3	31.1	43.9	43.6
29	0.8	4.4	7.2	9.7	10.3	5.0	16.4	27.5	25.3
30	0.0	0.0	1.4	1.4	1.4	0.0	7.8	13.9	11.4
Kelem									
27	0.0	0.0	0.0	0.0	0.0	0.0	0.0	0.0	0.0
28	0.0	0.0	0.0	0.0	0.0	0.0	0.0	0.0	0.0
29	0.0	0.0	0.0	0.0	0.0	0.0	0.0	0.0	0.0
30	0.0	0.0	0.0	0.0	0.0	0.0	0.0	0.0	0.0
Asayita									
27	0.0	0.0	0.0	0.0	0.0	0.0	0.0	0.0	0.0
28	0.0	0.0	0.0	0.0	0.0	0.0	0.0	0.0	0.0
29	0.0	0.0	0.0	0.0	0.0	0.0	0.0	0.0	0.0
30	0.0	0.0	0.0	0.0	0.0	0.0	0.0	0.0	0.0
Addis Ababa									
27	0.0	0.0	0.0	0.0	0.0	0.0	0.0	0.0	0.0
28	0.0	0.0	0.0	0.0	0.0	0.0	0.0	0.0	0.0
29	0.0	0.0	0.0	0.0	0.0	0.0	0.0	0.0	0.0
30	0.0	0.0	0.0	0.0	0.0	0.0	0.0	0.0	0.0

Appendix 5.6 Percentage of months in the downscaled ECHAM5 climate data in which temperature is above the thresholds given in the first column. Note that the baseline data are derived from ECHAM5, and are thus different to the baseline data for HADCM3.

Appendix	1961-	2020				2050			
Threshold (°C)	1990	COMMIT	B1	A1B	A2	COMMIT	B1	A1B	A2
Moyale									
27	2.8	8.3	10.6	12.8	13.3	6.7	18.6	29.4	26.9
28	0.3	0.6	1.1	2.8	2.5	0.8	8.3	14.7	11.7
29	0.0	0.0	0.0	0.0	0.0	0.0	3.9	5.3	3.3
30	0.0	0.0	0.0	0.0	0.0	0.0	0.6	0.3	0.6
Mandera									
27	97.2	99.4	99.2	100.0	100.0	99.7	100.0	99.7	99.7
28	83.9	93.6	94.4	96.9	96.1	91.1	96.4	98.9	99.4
29	55.8	74.7	73.3	79.7	80.0	68.1	87.8	95.3	95.6
30	23.6	38.6	44.7	50.6	48.6	37.8	65.3	78.6	76.4
Marsabit									
27	3.9	10.6	13.3	18.9	15.3	8.3	35.0	52.8	44.4
28	0.6	0.8	1.7	3.9	4.4	1.1	11.9	26.7	18.1
29	0.0	0.0	0.3	0.0	0.0	0.0	3.9	7.2	3.6
30	0.0	0.0	0.0	0.0	0.0	0.0	1.1	0.8	0.6
Maralal									
27	0.0	0.0	0.0	0.0	0.0	0.0	0.0	0.0	0.0
28	0.0	0.0	0.0	0.0	0.0	0.0	0.0	0.0	0.0
29	0.0	0.0	0.0	0.0	0.0	0.0	0.0	0.0	0.0
30	0.0	0.0	0.0	0.0	0.0	0.0	0.0	0.0	0.0
Isiolo									
27	0.0	0.0	0.0	0.0	0.0	0.0	2.5	3.3	1.4
28	0.0	0.0	0.0	0.0	0.0	0.0	0.3	0.6	0.0
29	0.0	0.0	0.0	0.0	0.0	0.0	0.0	0.0	0.0
30	0.0	0.0	0.0	0.0	0.0	0.0	0.0	0.0	0.0
Nairobi									
27	0.0	0.0	0.0	0.0	0.0	0.0	0.0	0.0	0.0
28	0.0	0.0	0.0	0.0	0.0	0.0	0.0	0.0	0.0
29	0.0	0.0	0.0	0.0	0.0	0.0	0.0	0.0	0.0
30	0.0	0.0	0.0	0.0	0.0	0.0	0.0	0.0	0.0
Awasa									
27	23.9	34.4	38.3	39.7	40.6	31.7	52.8	61.7	60.6
28	10.0	17.8	19.7	23.9	25.0	17.5	32.5	45.0	43.1
29	2.8	8.3	11.1	12.5	12.5	8.9	21.1	30.3	28.3
30	1.4	4.4	5.6	5.6	6.4	2.8	10.3	17.2	16.1
Kelem									
27	82.2	90.8	88.6	95.3	94.2	89.7	96.1	99.4	98.9
28	53.9	64.2	68.9	76.4	81.9	68.9	88.3	94.2	93.6
29	23.6	36.1	38.6	49.4	49.2	38.3	68.3	78.3	80.8
30	5.8	14.7	19.7	24.7	20.6	12.2	39.2	54.7	57.8
Asayita									
27	64.7	69.2	72.8	75.6	72.8	71.1	81.7	86.7	85.3
28	54.2	60.6	63.3	65.3	63.1	60.3	73.1	76.9	73.1
29	46.1	53.6	53.1	57.2	55.3	52.8	63.1	67.8	63.6
30	34.4	44.4	42.5	48.1	43.1	41.1	53.6	56.9	53.3
Addis Ababa									
27	0.0	0.0	0.0	0.0	0.0	0.0	0.0	0.0	0.0
28	0.0	0.0	0.0	0.0	0.0	0.0	0.0	0.0	0.0
29	0.0	0.0	0.0	0.0	0.0	0.0	0.0	0.0	0.0
30	0.0	0.0	0.0	0.0	0.0	0.0	0.0	0.0	0.0